Clemson University
TigerPrints

All Theses | Theses

12-2007

A PILOT STUDY ON THE EFFECTS OF TEMPERATURE ON THE MATERIAL PROPERTIES OF PRESTRESSED CONCRETE AND THE USE OF THERMOGRAVIMETRIC ANALYSIS IN THE ASSESSMENT OF HEAT-AFFECTED CONCRETE

Kacie Caple
Clemson University, kacie32884@aol.com

Follow this and additional works at: https://tigerprints.clemson.edu/all_theses

 Part of the Civil Engineering Commons

Recommended Citation
Caple, Kacie, "A PILOT STUDY ON THE EFFECTS OF TEMPERATURE ON THE MATERIAL PROPERTIES OF PRESTRESSED CONCRETE AND THE USE OF THERMOGRAVIMETRIC ANALYSIS IN THE ASSESSMENT OF HEAT-AFFECTED CONCRETE" (2007). *All Theses*. 251.
https://tigerprints.clemson.edu/all_theses/251

This Thesis is brought to you for free and open access by the Theses at TigerPrints. It has been accepted for inclusion in All Theses by an authorized administrator of TigerPrints. For more information, please contact kokeefe@clemson.edu.

A PILOT STUDY ON THE EFFECTS OF TEMPERATURE ON THE MATERIAL PROPERTIES OF PRESTRESSED CONCRETE AND THE USE OF THERMOGRAVIMETRIC ANALYSIS IN THE ASSESSMENT OF HEAT-AFFECTED CONCRETE

A Thesis
Presented to
the Graduate School of
Clemson University

In Partial Fulfillment
of the Requirements for the Degree
Master of Science
Civil Engineering

---

by
Kacie Danielle Caple
December 2007

Accepted by:
Dr. Scott D. Schiff, Committee Chair
Dr. Prasad R. Rangaraju
Dr. Patrick J. Fortney

ABSTRACT

An understanding of the material property changes in building materials due to exposure to a fire is needed for accurate damage assessment of a structure. Discussion pertaining to material property changes and the bond between concrete and prestressing steel following elevated temperature exposures is presented. Evaluation of the use of thermogravimetric analysis (TGA) as a post-fire analysis tool to determine the maximum temperature exposure of concrete is also included.

Heated concrete cylinders were tested to determine the compressive strength and modulus of elasticity changes of concrete. Heated steel prestressing strands were tested in tension to determine changes in the ultimate stress and modulus of elasticity. Changes in the bond performance were investigated by conducting pull-out tests on prestressing steel embedded in concrete specimens. Using mortar and cement paste samples, TGA was evaluated as a possible option for determining the temperature exposure of cementitious materials. TGA was also performed on concrete samples extracted from heated cylinders to determine if the temperature profile could be predicted.

The results from this project are intended to serve as the basis for the development of useful tools in the forensic investigations of prestressed concrete members after fire exposure. Using TGA to determine the exposure of an element could provide information on the history of a fire, identifying the maximum temperature exposure within an element and a general evaluation of the duration of the heat exposure. Based on this information, changes in the material properties can be predicted, resulting in more reliable investigations of prestressed concrete members exposed to fire.

DEDICATION

I dedicate this thesis to my parents, Duane and Annette Caple, for their unending love and support.

ACKNOWLEDGEMENTS

I would first like to acknowledge my professors, Dr. Scott Schiff, Dr. Patrick Fortney, and Dr. Prasad Rangaraju. Without them, the opportunity to take part in this pilot study would not have been possible. Next, I want to thank Adam D'Alessandro for being a loving and calming influence throughout the writing of this document and my family for their continual support.

This research would not have been possible without the financial support of the Precast/Prestressed Concrete Institute (PCI) through the award of a Daniel P. Jenny Research Fellowship. Metromont Corporation supplied the concrete, prestressing steel, and chucks for use in this project. Tindall Corporation allowed the use of their equipment to determine the material properties of the concrete cylinders. The Clemson University National Brick Research Center allowed the use of their oven and kiln to pre-heat and heat the test specimens.

TABLE OF CONTENTS

Table of Contents (continued)

Page

Table of Contents (continued)

Page

LIST OF TABLES

List of Tables (continued)

Table Page

List of Tables (continued)

Table Page

List of Tables (continued)

Table Page

LIST OF FIGURES

List of Figures (continued)

Figure Page

List of Figures (continued)

Figure Page

List of Figures (continued)

Figure Page

List of Figures (continued)

Figure Page

List of Figures (continued)

Figure Page

List of Figures (continued)

Figure Page

CHAPTER ONE

INTRODUCTION

Understanding the behavior of structural materials is an important element in the forensic investigations of fire-exposed structures. By advancing this knowledge, improved predictions can be established for determining the post-fire capacity of structures.

Historically, concrete has been known for its desirable thermal properties, possessing a relatively low thermal conductivity and a high specific heat (Ramachandran 2002). These material properties allow for a lower heat transfer throughout the material, making it more ideal for fire conditions as compared to other materials. However, as concrete is heated it undergoes physical and chemical changes leading to strength degradations. Dependant on the maximum temperature and duration at which this temperature is sustained, concrete can be changed with exposure to elevated temperature. The rate of heating and cooling also play a role in this degradation (St John et al. 1998).

1.1 Problem Statement

It is crucial to understand how to assess fire damage in structures. However, many investigators still express uncertainty when evaluating fire-damaged structures. Because of this uncertainty, actions may be taken in order to replace structures or structural members exposed to fire.

For instance, the Puyallup River Bridge in Washington was damaged by a fire in 2002. This structure was a three-span precast concrete bridge. A 7000-psi compressive strength concrete was used in the girders, and a 5000-psi compressive strength concrete was used in both the deck and columns. A railroad tanker caught fire beneath the bridge, creating a large heat source. Visual observations gave indications of the damage. Spalling occurred on several members, revealing the reinforcement beneath the concrete. Also, the flanges on the girders directly above the fire were shown to experience a color change to a whitish gray. Despite these visual signs of fire damage, the bridge was reopened the next day. Investigators stated that they "found no significant loss of capacity" in the bridge, but they planned to replace one span of the bridge to protect the exposed reinforcement as a long-term precautionary action (Shutt 2006).

In 2005, a fire caused by a tanker truck resulted in damage to the 50-year-old, precast concrete Norwalk River Bridge in Connecticut. The chief engineer, Arthur Gruhn, was unsure how strong the bridge was following the fire. He said, "We couldn't really gauge how much damage the fire had done, but we could see the bridge was in reasonably good shape." This bridge was repaired for temporary use, and the construction of a new bridge soon followed (Shutt 2006).

Because of this uncertainty, it is crucial to understand the behavior of concrete following fire exposure. It is also important to have quick and reliable methods for evaluating concrete following a fire. With a better understanding of the affects of fire on concrete and improved investigative techniques, more reliable investigations may take

place on structures following a fire, perhaps saving money and time for all those involved.

1.2 Project Objectives

In this research project, an experimental research program was established to determine the basic material property changes of the concrete and prestressing steel in a prestressed concrete member when exposed to elevated temperatures. The first objective of the project was to evaluate changes in the material properties of both normal strength concrete and prestressing steel with respect to temperature. Specifically, the influence of duration of exposure to elevated temperatures and the peak temperature achieved on selected material properties were studied. Changes in the compressive strength and modulus of elasticity of concrete were evaluated using cylindrical concrete specimens. Changes in the tensile strength and the modulus of elasticity of prestressing steel strands were investigated using half-inch special prestressing strands. The bond interaction between concrete and prestressing steel strand was investigated by performing pull-out tests on cylindrical concrete specimens with embedded prestressing steel strands.

The second objective of the project was to investigate the use of thermogravimetric analysis (TGA) as a reliable tool to determine the maximum temperature of exposure in a concrete sample during a fire. TGA was first verified as a maximum temperature predictor using cement paste and mortar samples in a controlled

laboratory environment. After verification, TGA was used to predict a temperature profile in samples from heat-affected concrete.

1.3 Project Significance

Results from this pilot project could serve as a stepping stone for establishing new tools for forensic investigators in the evaluation of heat-affected concrete members. For instance, the capacity of a heat-affected prestressed concrete beam could be predicted based on knowing the changes in the material properties of concrete, steel prestressing strand, and bond as a result of heat exposure. By understanding the material property changes, more accurate investigations could be performed with more reliable predictions on the capacity of prestressed concrete members. These efforts could potentially help to eliminate unneeded expenses for the replacement of structural members that are still capable of withstanding design conditions.

TGA could potentially serve as a useful tool in initially predicting the maximum temperature of exposure of a concrete member or in establishing temperature contours within a concrete section. By examining heat contours, forensic engineers could have a better understanding of the history of a fire. For instance, a concrete section with a defined contour containing multiple layers of heat exposure (step gradient) could indicate a short burn occurred. On the contrary, if the concrete contains multiple layers of a single heat exposure, a long burn at that temperature likely took place.

The results could also aid in the design of structures for fire resistance. By knowing the changes in material properties, a designer can better assess the capacity of a design for certain fire scenarios.

CHAPTER TWO

LITERATURE REVIEW

A review assessing the fundamentals of prestressed concrete, heat effects on both concrete and steel properties, and the use of thermogravimetric analysis for evaluating cementitious materials was performed to provide an adequate background to conduct the research presented in this thesis. The information presented in this Chapter reflects information, results, and methodologies that are significant to the project.

2.1 Fundamentals of Prestressed Concrete

The idea of prestressed concrete takes advantage of the strong compressive strength of concrete, while also accounting for the weak tensile strength of the material. Since the weak tensile strength of concrete allows cracks to form when subjected to flexural stresses, prestressing concrete counteracts this tendency by adding a concentric or eccentric axial force in a structural concrete section. This force, known as the prestressing force, is applied along the length of a structural concrete member (Nawy 2006).

Historical Development of Prestressing

Early trials with prestressing began in 1872 with P. Jackson in California, when he developed and patented a prestressing system. This first system created a single beam, or arch, by connecting individual blocks using a tie rod. Later in 1888, C. Doehring of Germany patented a system for using metal wire to prestress slabs (Nawy 2006).

Problems with early prestressing resulted from prestressing losses which occurred because of the use of low-strength steel. This steel was unable to account for losses in the concrete over time, including shrinkage and creep. R. Dill of Nebraska was the first to create a reinforcement system to compensate for prestressing losses. Dill developed the idea of post-tensioning unbonded rods in succession to account for the time-dependant losses in concrete, such as creep and shrinkage (Nawy 2006). By doing this, Dill was able to compress the concrete after these time-dependent behaviors occurred.

As prestressing advances continued, circular prestressing became available in the early 1920s by W. Hewett of Minneapolis as a means of creating tanks and pipes. This method was utilized in order to prevent cracking due to the internal pressure applied by the liquids within the tanks. E. Freyssinet proposed the use of high-strength and high-ductility steels for reducing prestressing losses between 1926 and 1928. The Freyssinet system established in 1940 incorporated a conical wedge anchor for 12-wire tendons (Nawy 2006). Although this system was suggested to be used primarily for post-tensioning purposes, it was also utilized in prestressing (Schokker 2005). Today, Freyssinet is considered to be the "engineering visionary" behind prestressed concrete (Marianos, Jr. 2005).

Throughout World War II, bridges were in high demand throughout Europe, and the rush to construct these structures rapidly was imperative. During this time, prestressing became a popular tool by G. Magnel of Belgium and Y. Guyon of Paris for building bridges rapidly. The Magnel system used wedges for anchoring prestressing wires, similar to the Freyssinet system. The main difference between the two systems

was that the wedges in the Magnel system were flat and possessed the ability to anchor two wires at the same time (Nawy 2006). Magnel later became known as the chief design engineer of the Walnut Lane Bridge in Pennsylvania, the first prestressed concrete girder bridge in the United States. With the construction of this bridge, the American bridge designers became more intrigued by the possibilities of prestressed concrete (Marianos, Jr. 2005).

The idea of partial prestressing came about in the 1930s and 1960s by P. Abeles of England (Nawy 2006). This method incorporated the use of untensioned reinforcement in beams. The purpose of this technique was to increase the ultimate moment capacity of a beam, while reducing the crack widths of a member without completely eliminating crack formation. Controversy over this system arose after it was incorporated into the construction of railway bridges. At the time, other engineers claimed that this system did not take advantage of the positive attributes of both concrete and steel. This controversy is still present today (Marianos, Jr. 2005)

Other pioneers in the pursuit of advancing prestressed concrete design include F. Leonhardt of Germany, V. Mikhailov of Russia, and T. Y. Lin of the United States. The design process behind prestressing became considerably simplified by Lin's load-balancing method, making prestressing even more attractive to designers. Lin's load-balancing method incorporated basic principles of engineering mechanics, such as statics, to design prestressed concrete members. For instance, Lin simplifies design of prestressed concrete by using the vertical force created by draped or harped prestressing tendons to counteract the gravity load on the beam (Nawy 2006).

Principles of Prestressed Concrete

The addition of a prestressing force in a structural concrete member reduces the amount of tensile stress and tensile cracks that can possibly occur during loading. For example, without a prestressing force, a typical reinforced concrete beam deflects in such a way that tensile stresses result in cracks along the tension side of the beam, as shown in Figure 2.1. However, by adding a prestressing force, the beam is initially at a slight camber as shown in Figure 2.2, bending in the opposite direction of transverse loading. Upon loading a prestressed beam, it deflects in such a way that tensile forces are reduced in comparison to the generic reinforced concrete beam, resulting in fewer cracks along the tension face as shown in Figure 2.2.

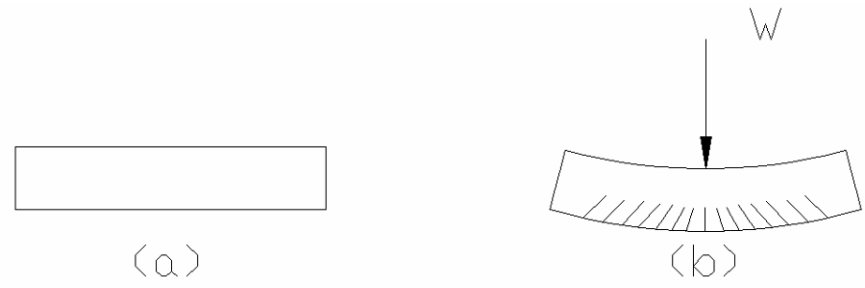

Figure 2.1: Reinforced concrete beam (a) unloaded and (b) loaded.

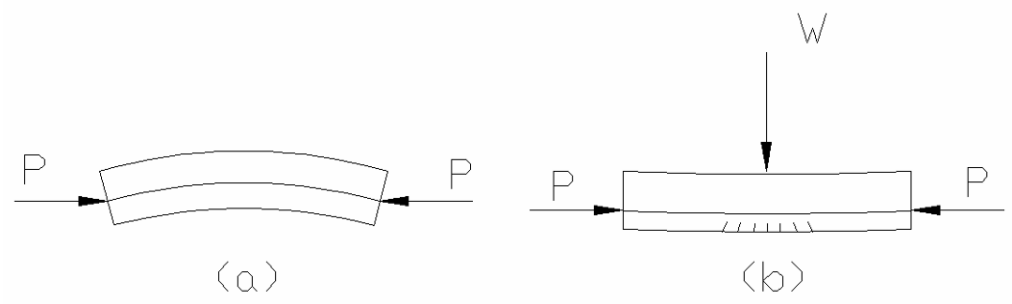

Figure 2.2: Concrete beam with prestressing force, P. (a) unloaded and (b) loaded.

2.2 Heat Effects on Concrete Appearance

As concrete is heated, physical changes often occur, such as discoloration, cracking, and spalling. By initially assessing these physical features on the surface, engineers can evaluate the extent of damage and establish replacement or repair procedures (St John et al. 1998).

Discoloration

Concrete has been shown to experience a variety of color changes as it is heated, generally dependant on the maximum temperature of exposure. A variety of sources link color changes with specific temperature ranges of exposure. A color change from grey to pink or red is often noticed when reaching temperatures as low as 250 and 300°C[1] (480 and 570°F) (St John et al. 1998). This color change is thought to occur because of iron compounds in the aggregate, causing dehydration and oxidization (St John et al. 1998, Geogali et al. 2004). The intensity of the coloration usually depends upon the aggregate type, and flint aggregate usually creates the most prominent color change in concrete. At temperatures reaching between 500 and 600°C (930 and 1110°F), another color change occurs from pink/red to purple/grey (St John et al. 1998). When exposed to temperatures above 900°C (1650°F), concrete may often change color to a whitish gray or buff (Geogali et al. 2004). Based on these findings, color changes can serve as one of the first indicators of an approximate temperature range of exposure in heat affected concrete.

---

[1] The first temperature listed is that using the primary unit within the particular reference and the second listing within parenthesis is a rough estimate of a converted value to either Celsius or Fahrenheit.

Cracking

Cracking in non-tension zones is another indication that concrete may have been exposed to elevated temperatures. Cracking can occur in both the cement paste and the aggregate within the concrete. The extent of cracking is generally dependant on the maximum temperature of exposure, and long exposures at high temperatures can result in wide cracks and the expansion of crack networks (St John et al. 1998).

The majority of cracking is attributed to the differing thermal expansions of cement and aggregate (St John et al. 1998). Aggregate initially expands as temperatures increase, causing the cement to compress. This causes the concrete to weaken and crack (Chang et al. 2006). For temperatures below 250℃ (480°F), the stresses created by the cement and aggregate result in minimal damage, although microcracks have been noticed in concrete heated to temperatures as low as 180℃ (360°F) (St John et al. 1998). As temperatures increase, cracking becomes more severe.

In a study by Matesová et al. (2006), mosaic cracking was noticed in mortars subjected to high temperatures. The extent of cracking was noticeably different as temperatures were increased from 500 to 800°C (930 to 1470°F), as crack widths increased and the crack network expanded. Additionally, different aggregates produced notably different cracking, indicating that the type of aggregate plays a role in the extent of damage. For instance, mortar containing dolomite aggregate produced similar cracking patterns when heated to 800°C (1470°F) as compared to quartz aggregate heated to 600°C (1110°F). However, when reaching 1000°C (1832°F), both aggregates produced similar cracking patterns (Matesová et al. 2006). Another study by Y.F. Chang

et al. (2006) sites that visible crack networks appeared in concrete cylinder samples at 300°C (570°F). Cracks increased in size at 500°C (930°F), and crack networks expanded to create additional cracks when reaching 700°C (1290°F) (Chang et al. 2006). These two studies further depict the crack propagation as concrete is heated to elevated temperatures.

Spalling

Spalling, characterized as the violent or non-violent breaking off of layers of concrete, is a possible occurrence when subjected to high temperatures. Spalling is influenced not only by the maximum temperature, but also by the rate at which temperature rises. Since noticeable section loss results from spalling, it is perhaps one of the most influential physical indications that repair or replacement is needed in heat affected concrete. Although several types of spalling can occur during a fire (Khoury 2000), the two most common types of spalling are explosive spalling and corner spalling, or the sloughing off of concrete layers. Generally, explosive spalling is a violent loss of concrete sections and occurs quickly, within the first 30 minutes of fire exposure. Corner spalling, however, is a gradual process that occurs in a non-violent manner (Georgali et al. 2005).

Long T. Phan et al. (2002) found that explosive spalling occurred between 200 and 350°C (390 and 660°F) when testing high-strength concrete. The time at which it occurred tended to coincide with a point in which the exterior and interior of the concrete reached a point of maximum temperature difference. Phan et al. (2002) suggests that thermally induced stresses may play a secondary role in explosive spalling, while the

primary reason is due to internal vapor pressures as a result of the moisture content. It was also found that explosive spalling was reduced in specimens loaded while heated, and decreasing water-to-cement ratios increased the chances of spalling (Phan et al. 2002).

2.3 Heat Effects on Concrete Compressive Strength

Since structural concrete members are designed based on their compressive strength, an essential factor in determining whether or not a concrete structure is structurally reliable following a fire is based on the loss reduction of compressive strength. As concrete is heated, chemical and physical changes occur as reactions and expansions take place. Due to these changes, the compressive strength is expected to change based on the maximum temperature the concrete reaches as, well as the exposure time (St John et al. 1998).

Testing conditions are a significant component in how compressive strength is characterized. Generally three testing conditions are considered: stressed tests, unstressed tests, and residual strength tests (Abrams 1971). In stressed tests, concrete is loaded throughout the heating process and tested while continuously heated at a desired maximum air temperature. Unstressed tests are classified as those in which concrete is heated to a desired maximum air temperature under no loading and then tested at the desired maximum air temperature. Residual strength tests are those in which concrete specimens are heated, cooled, and tested at room temperature. Depending on the type of

residual strength desired, the concrete may or may not be loaded during the heating process for residual strength tests. Other comparisons of compressive strengths can be made based on aggregate type, concrete strength grades, and the length of exposure to high temperatures (Abrams 1971).

M. S. Abrams (1971) performed a study on the compressive strength changes in concrete as it was subjected to increasing temperatures up to 1600°F (870°C). In this study, Abrams considered several variables, including aggregate type, loading conditions, testing temperatures, and compressive concrete strengths. The aggregate type was shown to play a role in strength reductions. Carbonate aggregate concrete and sanded lightweight concrete held 75 percent of their original strength up to 1200°F (650°C). Siliceous aggregate concrete retained the same percentage of strength up to only 800°F (430°C) for stressed tests (Abrams 1971).

Testing conditions also affected the compressive strength changes of concrete. The stressed test specimens recorded strengths up to 25 percent higher than unstressed test specimens (Abrams 1971). This difference was attributed to a delay in the formation of cracks in the concrete caused by loading the cylinder throughout the heating process, thus increasing the overall compressive strength (Castillo 1990). The original strength of the concrete had little impact on the percentage of strength loss due to high temperatures, as well (Abrams 1971).

C. Castillo et al. (1990) compared normal strength concrete (NSC) and high strength concrete (HSC) strength reductions resulting from high temperature exposure. A normal strength concrete of 4000 psi was compared to a high strength concrete of 9000

psi. Both sets were tested while heated to their maximum desired temperature. In this study, it was found that NSC experienced lower relative strength losses compared to HSC. For example, between 100 and 200°C (210 and 390°F), NSC experienced a 6- to 10-percent strength loss, and HSC experienced a 15- to 20-percent strength loss under similar testing conditions. The higher strength losses in HSC were attributed to the porosity differences between HSC and NSC, since NSC has a higher porosity allowing moisture to escape more easily. For both NSC and HSC, a strength recovery period occurred when heated between 100 and 400°C (210 and 750°F) (Castillo et al. 1990). In a strength recovery period, concrete increases in strength, sometimes above the original value. The peak strengths within the recovery range were approximately 10 to 20 percent above the unheated, control strengths. The reason for this phenomenon is thought to be due to the stiffening of cement paste or an increase in surface forces between the cement particles due to a loss in moisture. When heated above 400°C (750°F), approximately a 70-percent strength loss occurred in both NSC and HSC at temperatures of 800°C (1470°F) (Castillo et al. 1990).

Castillo et al. (1990) also experimented with various testing conditions and found that specimens that were loaded during the heating process experienced relatively smaller strength reductions compared to those unloaded during the heating process. Castillo noted that by pre-loading a specimen prior to the heating process, cracks are unable to freely form, causing a delay in the failure for these specimens (Castillo et al. 1990).

Chang et al. (2006) performed a study to determine residual stress-strain relationships by testing heated concrete samples after cooling to ambient temperature. In

this study, residual compressive strengths showed that as temperature increased, the strengths continued to decrease. At 200°C (390°F), a 10-percent loss in strength was noted. As temperatures increased to 400, 600, and 800°C (750, 1110, and 1470°F), strength losses of 35, 60, and 85 percent respectively occurred (Chang et al. 2006). The primary difference between the study by Chang and Castillo was that Chang tested specimens after allowing them to cool to room temperature.

It is evident from these studies that two general responses are possible when evaluating the compressive strength changes of heat-affected concrete and that these responses are dependent on the testing conditions. A strength recovery has been known to occur when testing cylinders while they are still heated at a maximum desired temperature, as that noted by Castillo (Castillo et al. 1990). A continual loss in compressive strength with no strength recovery was noted in residual strength tests, as noted by Chang (Chang et al. 2006). A plot to represent the two general scenarios of compressive strength responses with increasing temperature is represented in Figure 2.3.

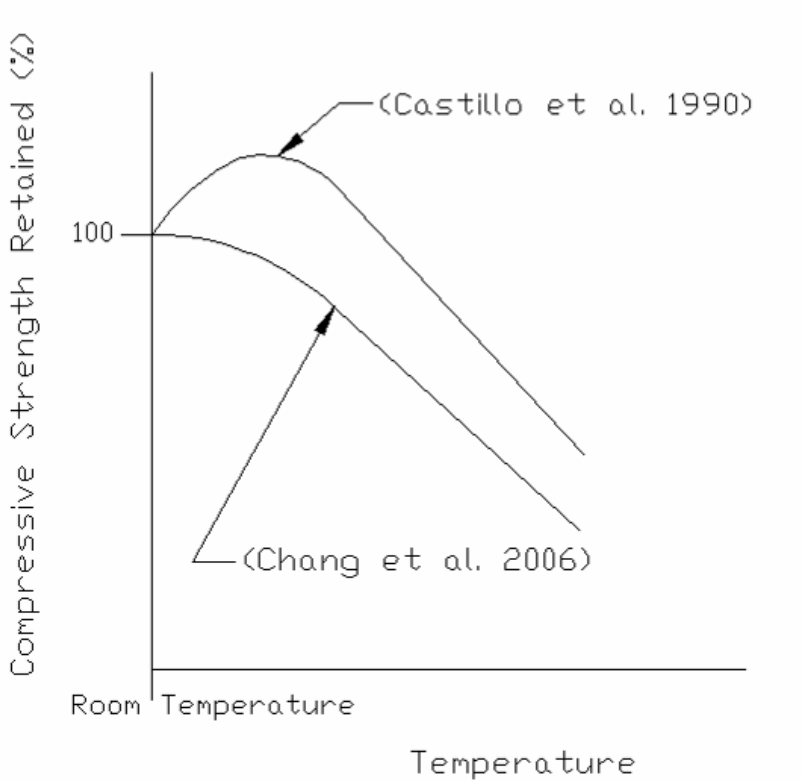

Figure 2.3: Representative trends for the compressive strength of concrete with increasing temperature.

2.4 Heat Effects on the Static Modulus of Elasticity of Concrete

The influence of elevated temperatures on the static modulus of elasticity of concrete is an important issue, especially for areas prone to seismic effects where a structure should be capable of withstanding cyclic loading. Various studies have shown that the static modulus of elasticity of concrete decreases progressively with increasing temperature (Phan et al. 2002, Castillo et al. 1990, Chang et al. 2006). Similar to the compressive strength, testing conditions, among other variables, can play a role in the amount of change in the static modulus.

Castillo et al. (1990) noted that both normal strength concrete (NSC) and high strength concrete (HSC) behaved similarly in their change in static modulus of elasticity when subjected to elevated temperatures. The static modulus tended to decrease slightly between temperatures of 100 and 400°C (210 and 750°F). Losses in the static modulus increased when heated above 400°C (750°F) to approximately 75 and 80 percent of the original value. Relatively small changes in the static modulus were noted when the concrete was heated between 600 and 700°C (1110 and 1290°F) (Castillo et al. 1990).

Matesova et al. (2006) tested the static modulus of mortars subjected to high temperatures and found they did not follow the same trend as the compressive strength changes. Results also suggested that the modulus of elasticity may be influenced by cracks in the concrete (Matesova et al. 2006). Chang et al. (2006) performed another study on the influence of elevated temperatures on stress-strain relationships of concrete. In this study, the elastic modulus was shown to experience losses of 20, 60, and 94 percent when subjected to temperatures of 200, 400, and 600°C (390, 750, and 1110°F), respectively. The relative loss in elastic modulus was higher than the loss in compressive strength of specimens subjected to similar temperatures (Chang et al. 2006). A graph depicting the general trend of the change in the modulus of elasticity of concrete is provided in Figure 2.4, showing a steady decline with increasing temperatures.

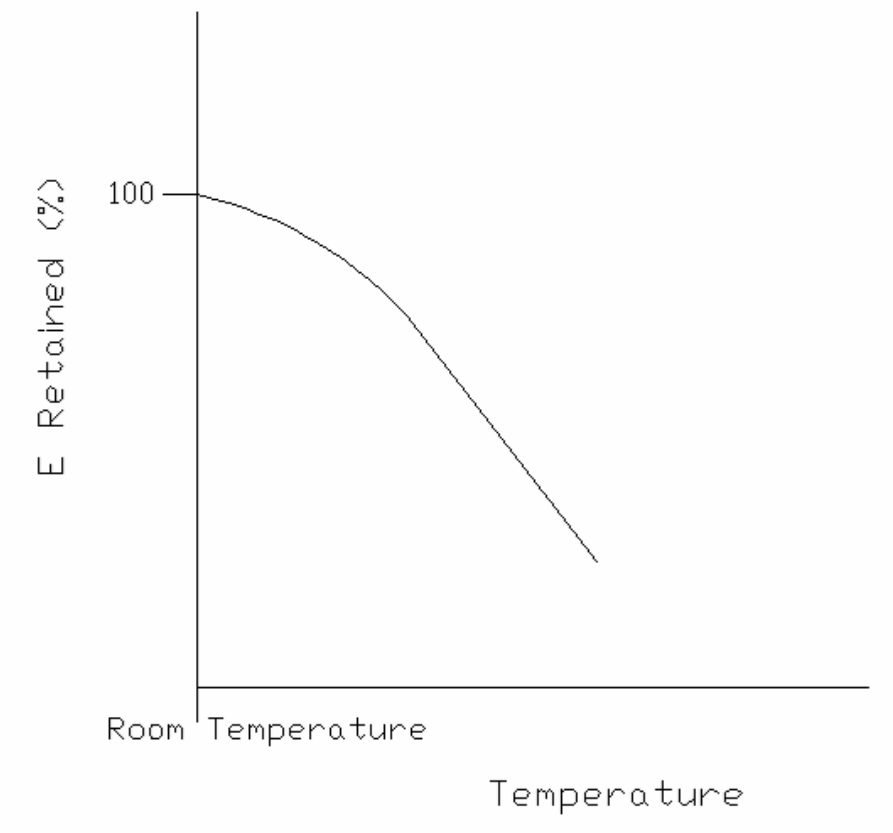

Figure 2.4: Representative response of modulus of elasticity, E, of concrete with increasing temperature exposure.

2.5 Heat Effects on Prestressing Steel

Although concrete provides cover, or insulation, to steel in structural prestressed concrete members, the effects of heat on prestressing steel cannot be disregarded. This information is especially helpful if spalling occurs, possibly resulting in direct exposure of reinforcing steel to high temperatures. However, limited research has been performed on the strength of prestressing steel subjected to elevated temperatures.

Neves et al. (1996) experimented primarily with separate tendons of 5-mm (0.2-inch) diameter that were tested after being cooled to room temperature in order to determine residual tensile strengths. This study showed that the residual tensile strength of these tendons was fairly constant when subjected to temperatures up to 400°C (750°F), followed by a decrease in strength up to 700°C (1290°F). An increase in the residual tensile strength was found to exist when heated to temperatures between 700 and 900°C (1290 and 1650°F). However, the method of cooling played a role in strengths at this temperature level. For instance, the use of a water jet was advantageous for cooling steel specimens at 700 to 800°C (1290 to 1470°F) because it resulted in an increase in the residual tensile strength. However, between temperatures of 800 and 900°C (1470 and 1650°F), the water jet cooling method resulted in extreme tensile strength losses, leading to a loss of all strength at 900°C (1650°F) (Neves et al. 1996).

Holmes et al. (1982) performed a study on the effects of heat on 7-wire prestressing strands. In this study, prestressing strands were heated for 30 minutes at maximum temperatures between 20 and 700°C (70 and 1290°F). Among other testing conditions, tests were performed on the strands to determine residual yield stresses, tensile stresses, and the modulus of elasticity. In these tests, the strands were tested at room temperature after being heated and then cooled; the specimens were not loaded during the heating and cooling processes. It was found in this study that the modulus of elasticity experienced little change as it was heated up to 700°C (1290°F). Losses were noted in the tensile stress of the prestressing strands with exposure above 200°C (390°F).

Beginning at 200°C (390°F), the tensile stress dropped in a fairly linear trend leading to losses of approximately 50 percent at 600°C (1100°F) (Holmes et al. 1982).

2.6 Heat Effects on Prestressing Steel and Concrete Bond

Numerous studies have been performed on the influence of bond changes in reinforced concrete due to high temperature exposure, but fewer studies have primarily focused on the bond in prestressed concrete applications following heat exposure.

Sagar et al. (1982) performed pull-out tests with concrete to evaluate bond changes with various reinforcing steels due to elevated temperatures. In this study, it was found that the strength and stiffness of the bond was highly dependent on the quality of the hardened cement paste matrix. For specimens tested at specified maximum temperatures, aggregate type and strength grade of concrete were compared (Sagar et al. 1982).

The two aggregates chosen in this study were quartz and limestone. Negligible differences existed between both aggregate types up to 400°C (750°F) exposures. However, above 400°C (750°F) a larger drop occurred in the quartz aggregate samples compared to the limestone aggregate samples. At 600°C (1110°F), the bond failure stress was only 25 percent of a control, room-temperature specimen for quartz aggregate concrete. This was comparatively low in reference to the 75-percent retention in bond failure stress for limestone aggregate concrete (Sagar et al. 1982).

The concrete compressive strength also played a role in bond strength changes for the unstressed specimens tested at a desired maximum temperature. In the experiment by Sagar et al. (1982), 55-MPa (8-ksi) and 25-MPa (4-ksi) normal-weight concretes experienced very different failure bond stresses at room temperature; however, their relative failure bond stresses were nearly identical. The room temperature failure bond stress of the 55-MPa (8-ksi) concrete was nearly twice that of the 25-MPa (4-ksi) concrete. The bond stiffness of the 55-MPa (8-ksi) concrete was also greater than the 25-MPa (4-ksi) concrete. In this comparison, the ultimate displacements of the 55-MPa (8-ksi) concrete samples were smaller than 25-MPa (4-ksi) concrete samples. Negligible losses were noticed at exposures of 400°C (750°F) and below. However, the 55-MPa (8-ksi) samples began to lose bond stress at 400°C (750°F). The 25-MPa (4-ksi) concretes did not experience any losses at 400°C (750°F), but the 55-MPa (8-ksi) concrete bond stresses were still superior to the 25-MPa (4-ksi) concrete despite the losses. Above 600°C (1110°F), both the 25- and 55-MPa concretes had lost nearly all bond stress (Sagar et al. 1982).

A study by Royles et al. (1982) evaluated residual bond stresses using deformed or ribbed bars of two sizes, 8 and 16 mm (0.3 and 0.6 inches). This study showed that bond stresses in heat-affected specimens were weaker than control specimens between 20 and 100°C (70 and 210°F). An increase in bond stresses was noticed primarily between 100 and 300°C (212 and 572°F). Above 300°C (570°F), failure bond stresses decreased. Royles et al. also noticed that the variation in maximum residual bond stresses was

similar to that of the maximum compressive strength and that smaller bars performed relatively better than larger bars (Royles et al. 1982).

A study by Diederichs et al. (1982) evaluated bond behavior of ribbed steel bars, plain round bars, and deformed prestressing bars with different types of concrete, using cylindrical concrete specimens. Diederichs et al. discovered that bond stresses and adhesion reduced as temperatures increased for plain round bars in siliceous aggregate. However, plain round bars in basalt aggregate showed no decrease in adhesion until reaching an exposure of 800°C (1470°F). The prestressing bars also retained adhesion up to 800°C (1470°F) in addition to having higher bond stresses with siliceous aggregate concrete. For the ribbed steel bars, siliceous aggregate displayed lower initial bond stresses and adhesion for 0.31-inch (8-mm) bars in comparison to 16-mm (0.6-inch) bars. However, as temperatures rose above 800°C (1470°F), the 8-mm (0.3-inch) bars experienced higher bond stresses and adhesions compared to the 16-mm (0.6-inch) bars. When embedded in basalt aggregate concrete, the 16-mm bars experienced higher bond strengths and adhesions regardless of temperature. The differences resulting from the two aggregates were attributed to the different thermal strains associated with each aggregate. For instance, siliceous aggregate is known to expand at temperatures above 350° C (660°F) compared to steel bars, whereas basalt aggregate shrinks in comparison to steel bars (Diederichs et al. 1982).

Additionally, microstructural changes at the concrete-steel interface were evaluated to determine reasons for bond stress changes. The interfacial zone of the concrete and reinforcing steel was evaluated using differential thermal analysis (DTA)

investigations and scanning electron microscope (SEM) micrographs. Results showed that differing thermal strains between steel and concrete caused numerous cracks primarily throughout the interfacial zone, leading to the primary cause of microstructural damage and a decrease in bond stresses (Diederichs et al. 1982).

2.7 Thermogravimetric Analysis Techniques for Concrete

Thermogravimetric analysis (TGA) is a thermal analysis technique used to monitor the mass losses in a specimen as it is heated. Since there are several irreversible dehydration reactions which occur in cement as it is heated resulting in mass losses, TGA techniques have been proven by several researchers as a helpful tool in determining the maximum temperature cement has experienced (Harmathy 1968, Alarcon-Ruiz et al. 2005).

Harmathy (1968) experimented with TGA as a way to determine the temperature history of concrete constructions following fire exposure. Harmathy suggested that samples be collected within one or two days following a fire because some dehydration reactions are reversible. These reversible reactions may occur slowly; however, to avoid adverse affects from these reactions, the maximum temperature of a heated specimen is thought to be more accurately predicted from specimens collected immediately following a fire. Harmathy also suggested the use of TGA as a means of determining a pattern of heat penetration within a concrete sample, although all research was performed on cement paste samples and not mortar or concrete (Harmathy 1968).

Further research on the use of TGA in evaluating heated cement samples was carried out by Alarcon-Ruiz et al. (2005). This work provided an in-depth look at the change in the mineralogical composition of the cement as it was heated in increments of 100°C (210°F) up to 800°C (1470°F). When heated between 30 and 105°C (90 and 220°F), evaporable water and some bound water was shown to evaporate, and at 120°C (250°F) all evaporable water was considered to be eliminated. Between 110 and 170°C (230 and 340°F), water was lost from the carboaluminate hydrates. Water continued to evaporate during the decomposition of the C-S-H and carboaluminate hydrates when heated between 180°C (360°F) and 300°C (570°F). Between 450 and 550°C (840 and 1020°F), dehydroxylation of the calcium hydroxide occurs, and decarbonation of calcium carbonate occurs when heated between 700 and 900°C (1290 and 1650°F) (Alarcon-Ruiz et al. 2005).

In the research of Alarcon-Ruiz et al. (2005), three rapid weight losses were present through TGA studies. The first occurred between 100 and 200°C (210 and 390°F) and was attributed to the dehydration reactions of hydrates. The second occurred between 450 and 500°C (840 and 930°F) and was attributed to the dehydroxylation of portlandite, or calcium hydroxide. Finally, the third major loss occurred at approximately 750°C (1380°F) and was attributed to the decarbonation of calcium carbonate. By comparing heated samples, the peak of decarbonation of calcium carbonate was shown to be the most influential area to compare in determining temperature history because it completely disappeared at 800°C (1470°F). Since calcium hydroxide was still present in heated samples at 800°C (1470°F) as shown in Figure 2.5, a recrystallization of calcium

hydroxide was proven to occur during the cooling process. This reversible reaction further presented the need for collecting samples within the first two days following a fire in order to obtain more accurate results (Alarcon-Ruiz et al. 2005).

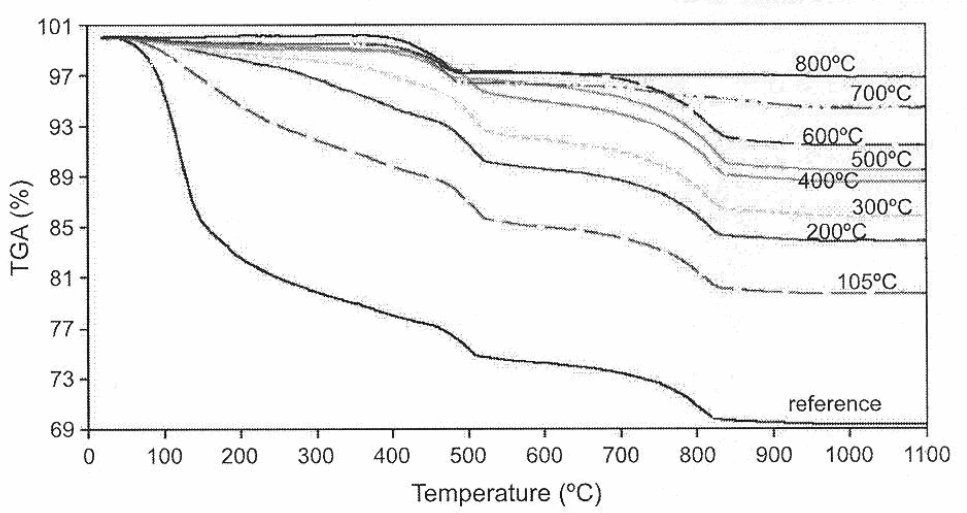

Figure 2.5: TGA curves of cement paste samples heated to various maximum temperatures by Alarcon Ruiz et al. (2005).

CHAPTER THREE

EXPERIMENTAL TESTING METHODS

Experimental testing was performed to evaluate the material property changes associated with the exposure of concrete and prestressing steel to elevated temperatures. Concrete cylinders were tested in compression to determine changes in compressive strength and modulus of elasticity of concrete. Steel prestressing strands were tested in tension to evaluate changes in yield strength and modulus of elasticity. To evaluate the bond stress changes between prestressing steel and concrete, pull-out tests were performed on concrete cylinders with embedded prestressing steel strands to evaluate relative pull-out strengths as a function of temperature. Additionally, thermogravimetric analysis was investigated as a tool for predicting maximum temperature exposure of heat-affected concrete by testing cement paste, mortar, and concrete samples subjected to elevated temperatures. Specimen preparation, heating methods, and all experimental testing procedures are described within this Chapter.

3.1 Specimen Designation

Specimens were identified in such a way as to distinguish the particular heating regime as well as the type and number of each sample. The first part of all specimen designations begins with the heating regime. For example, a "1h600C" heating regime indicated that the kiln temperature was held constant for 1 hour at 600°C (1112°F). All control samples, or those tested unheated, were labeled "Control." The second portion of

any sample name identified the type of specimen. For plain concrete cylinders used for compression testing, a number was assigned, indicating its position within the kiln as shown in Figure 3.1. For example, a compression cylinder was named 1h600C-1, indicating it is the first compression cylinder specimen of the 1h600C heating regime. Cylinders containing embedded steel prestressing strands used for bond stress tests were labeled with an "S" in front of the specimen number, indicating the concrete cylinder and steel combination. The numbering scheme was related to the placement of the bond stress specimen within the kiln, as shown in Figure 3.1. A typical example of a bond stress specimen is 1h600C-S1, indicating that it is the first bond strength test specimen in the 1h600C heating regime. Steel prestressing strand specimens used for tension testing were labeled with a "T" designation followed by a number indicating the order at which it was tested in the series. This number did not correspond to any specific placement within the kiln during the heating process, because the steel prestressing specimens were all located within a close proximity of one another. A steel specimen heated to 600°C (1112°F) for one hour would be labeled 1h600C-T1. Figure 3.1 serves as a reference, indicating the placement of each specimen within the kiln during the heating process.

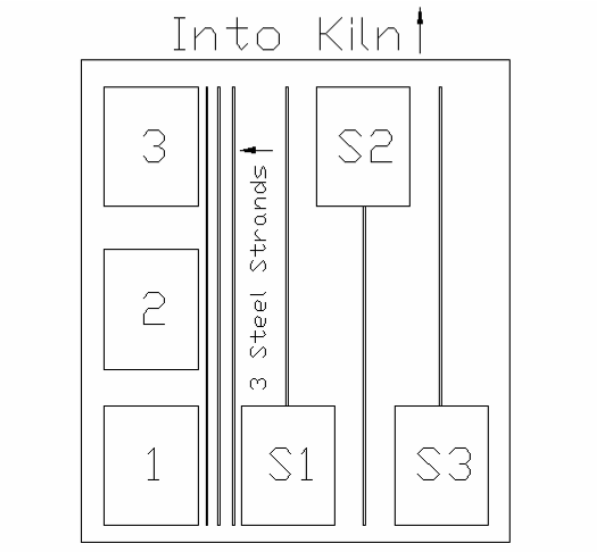

Figure 3.1: Overhead view of concrete cylinders, bond stress specimens, and steel prestressing strands in kiln.

3.2 Specimen Description

Compressive Test Specimens

In order to determine the compressive strength and modulus of elasticity of the concrete when exposed to elevated temperatures, concrete cylinders were cast and tested. All concrete specimens evaluated in this project were standard 6-inch diameter by 12-inch high cylinders. The 6-inch diameter by 12-inch high cylinders were used in order to remain consistent with the bond test specimens, which required appropriate cover for embedded steel prestressing strands.

Bond Test Specimens

In order to evaluate the interaction between prestressing steel and concrete, 6-inch diameter by 12-inch high concrete cylinders were cast, each with an embedded steel

prestressing strand. The specimens provided a concrete cover of approximately 3 inches for the steel. In addition to testing the changes in pull-out strength using these specimens, a thermocouple was affixed to the end of the prestressing steel to measure the internal temperature at the steel-concrete interface for each concrete cylinder.

The steel prestressing strands used for the pull-out tests were classified as 7-wire, ½-inch special strands with a tensile strength of 270 ksi. The "special" designation meant that it had a diameter slightly larger than half an inch (PCI 2004). Prior to the placement of concrete, the strands were each wiped with a clean, dry cloth to remove residual dirt, grease, or oils that may have accumulated on the surface of the steel strand.

Embedment lengths of 3, 6, and 9 inches were tested in a preliminary experiment to determine the embedment length of the steel prestressing strands for the test specimens. The 3-inch embedment depth was inappropriate because it did not allow a sufficient amount of bond. Both the 6- and 9-inch embedment depths provided a reasonable embedment for measuring pull-out strengths. The shorter embedment depth of 6 inches was advantageous for preventing splitting of the concrete cylinder during pull-out. Although neither of the 6- or 9-inch embedment length test specimens displayed any signs of splitting during preliminary testing, the concern for splitting cylinders was still present. This concern was based on the concrete strength used in the preliminary specimens. The concrete specimens created for the preliminary experiment were of a lower strength than those to be used in the actual experiment, which is known to have some effect on the bond stress.

The embedment length of 6 inches was also advantageous for the placement of embedded thermocouples used to monitor the internal temperature of the concrete throughout the heating and cooling processes. The thermocouple was placed on the end of the strand in order to measure the temperature of the center of the cylinder, as shown in Figure 3.2.

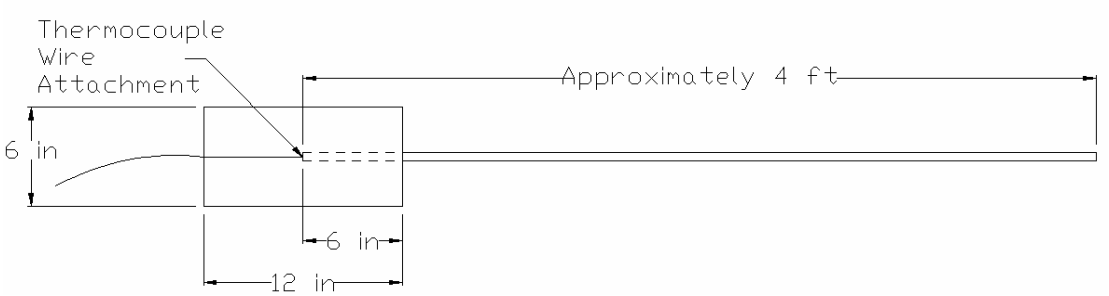

Figure 3.2: Bond test specimens.

The thermocouples were 24-gage, type-K thermocouples. These were used throughout the experiment to collect temperatures within the specified ranges of the heating regimes. These thermocouples were also compatible with the data acquisition system used to monitor the kiln temperature at the National Brick Research Center.

The thermocouples were attached to the steel prestressing strand with glue. The glue was only needed to hold the thermocouple wires in place during cylinder casting. Thermocouple wires were insulated using Nextel high temperature ceramic insulation with a standard braid. Nextel fiber insulation was chosen because of its resistance to high temperatures. The fiber insulation can resist up to 2000°F (1093°C) (Omega), which is well above the maximum temperature for the established heating regimes. The Nextel

insulation was threaded onto the thermocouple wires after they were removed from the plastic cylinder molds. The Nextel fiber insulation was attached to the concrete cylinder using a fireproofing caulk, 3M Fire Barrier Sealant CP 25WB+, which was capable of resisting temperatures up to 1000°F (537°C). Another caulk, DAP High Heat, was used for all heating regimes reaching 600°C (1112°F) because it was capable of resisting temperatures up to 2000°F (1090°C).

Steel Tension Test Specimens

Specimens for the steel tension tests were used to determine the material property changes, including the tensile stress and modulus of elasticity, of prestressing steel following heat exposure. The specimens were approximately 4 feet in length for ease of handling during testing and to allow for a gage length of at least 24 inches when measuring elongations during tension testing. The 24-inch minimum gage length is required by ASTM A370-05 for mechanical testing of steel products (ASTM A370-05).

3.3 Concrete Preparation

All concrete cylinders were cast at Metromont Corporation located in Greenville, SC using Metromont's standard concrete mix design for prestressed concrete products. One batch of concrete was mixed and used for all cylinders to ensure consistent material properties in all specimens. This mix was considered to be a self-consolidating concrete, incorporating both a type A water reducer and a high-range water reducer. The concrete mix was very workable, and had a specified compressive strength of 7000 psi. A

summary of the concrete mix is provided in Table 3.1, and a copy of the detailed ticket of the mix on the day of casting is shown in Figure A.1.

Table 3.1: Mix design of concrete used for specimens.

Material	Amount per cubic yard
Coarse aggregate (67 Stone)	1300 lb
Sand (ASTM 33)	1264 lb
MB-AE 90 (air entrainer)	8 oz
Poz 80 (Type A water reducer)	33 oz
Glenium 3400 (HRWR, super)	34 oz
Hot water at 75%	133 lb
Type 3 cement	712 lb
Flyash	112 lb
Moisture from sand	2.95 %

In order to transport the cylinders safely after casting, racks were constructed to hold the cylinders. These racks, as shown in Figure 3.3, were manufactured to hold both the compressive and bond specimens during casting, transportation, and curing. The racks also held the steel prestressing strands in place at the desired embedment length for the bond specimens, as shown in Figure 3.4. A small guide was also constructed to centrally locate the prestressing strand in the concrete cylinders used for bond strength evaluations. This guide was placed over the top of the cylinder molds during casting.

Figure 3.3: Racks used to hold concrete cylinder specimens during casting and curing.

Figure 3.4: Steel prestressing strands anchored to racks for bond specimens.

Concrete Cylinder Consolidation

Since there is no ASTM standard for the preparation of test specimens for self-consolidating concrete, Metromont Corporation employees were consulted prior to preparing the cylindrical specimens. Self-consolidating concrete should theoretically require no vibration or tamping for proper consolidation. However, it was suggested that the side of the cylinder be tapped to ensure proper consolidation within the cylinder mold. Tapping the sides has been their standard protocol for preparing 4-inch diameter by 8-inch high cylindrical specimens, and previous experience has proven this method to be appropriate.

The racks constructed to hold the cylinders during transport did not provide enough space between the cylinders to tap the sides as suggested. Because of this, a modified procedure was used. Concrete was placed into the cylinder molds in one layer and tamped 25 times with a tamping rod. Since segregation could possibly occur while tamping self-consolidating concrete, the tamping was minimized to a single layer.

Concrete Curing

After casting the concrete cylinders, they were covered with plastic and steam cured overnight using a kerosene heater. A thermocouple was placed in the center of one cylinder to monitor the internal temperature of the concrete throughout the steam curing process. The steam curing process was utilized because it is typically used by prestressing manufacturers to speed the curing process as a means to increase production.

A copy of the thermocouple data taken from the steam curing process is shown in Figure A.2.

Half of the concrete cylinders were taken to the Wind Engineering and Structures Laboratory (WESL) one day after the casting process. The remaining cylinders were transported to WESL two days after the casting process. The concrete cylinders were stored at room temperature, where they remained in the plastic cylinder molds until shortly before testing.

3.4 Heating Methods

Procedures were developed for the heating process. These procedures include the specific heating regimes using a kiln, preparation of specimens for heating, and post-heating storage.

Heating Regimes and Cooling Method

Heating regimes were established for analyzing the effects of elevated temperatures on concrete, prestressing steel, and bond properties. The peak temperatures for all heating regimes ranged between 200 and 600°C (392 and 1112°F). The durations for holding peak temperatures in the kiln ranged between 0.5 and 4 hours. These durations were established based on current fire ratings, with a maximum required rating of four hours. Samples were initially heated at 5°C (40°F) per minute until explosive spalling occurred during the 4h500C heating regime, the second test using this method. As action to prevent similar incidents from occurring, the heating rate was slowed to

2.5°C (37°F) per minute, and a low temperature drying method was implemented to reduce the moisture content of the concrete cylinders. A matrix of all heating regimes, including the kiln time and the regime identification pattern, is shown in Table 3.2.

All specimens were cooled by blowing room-temperature air through the kiln following each heating regime. Data on the internal temperature of the concrete cylinders and the kiln temperature was continually measured during the cooling process for twelve hours following each heating regime. A typical set of data included the temperature of the kiln and the internal temperature of the three bond strength specimens, as shown in Figure 3.5 for the 4h600C heating regime.

Table 3.2: Heating regimes and total heating phase time.

Heating Regime	Duration at Maximum Temperature, hours	Maximum Temperature, °C (°F)	Total Heating Phase Time, hours
1h200C	1	200 (392)	2.22
2h200C	2	200 (392)	3.22
4h200C	4	200 (392)	4.61
0.5h400C	0.5	400 (752)	3.05
1h400C	1	400 (752)	3.55
2h400C	2	400 (752)	4.55
4h400C	4	400 (752)	6.55
0.5h500C	0.5	500 (932)	3.72
1h500C	1	500 (932)	4.22
2h500C	2	500 (932)	5.22
4h500C	4	500 (932)	7.22
0.5h600C	0.5	600 (1112)	4.39
1h600C	1	600 (1112)	4.89
2h600C	2	600 (1112)	5.89
4h600C	4	600 (1112)	7.89

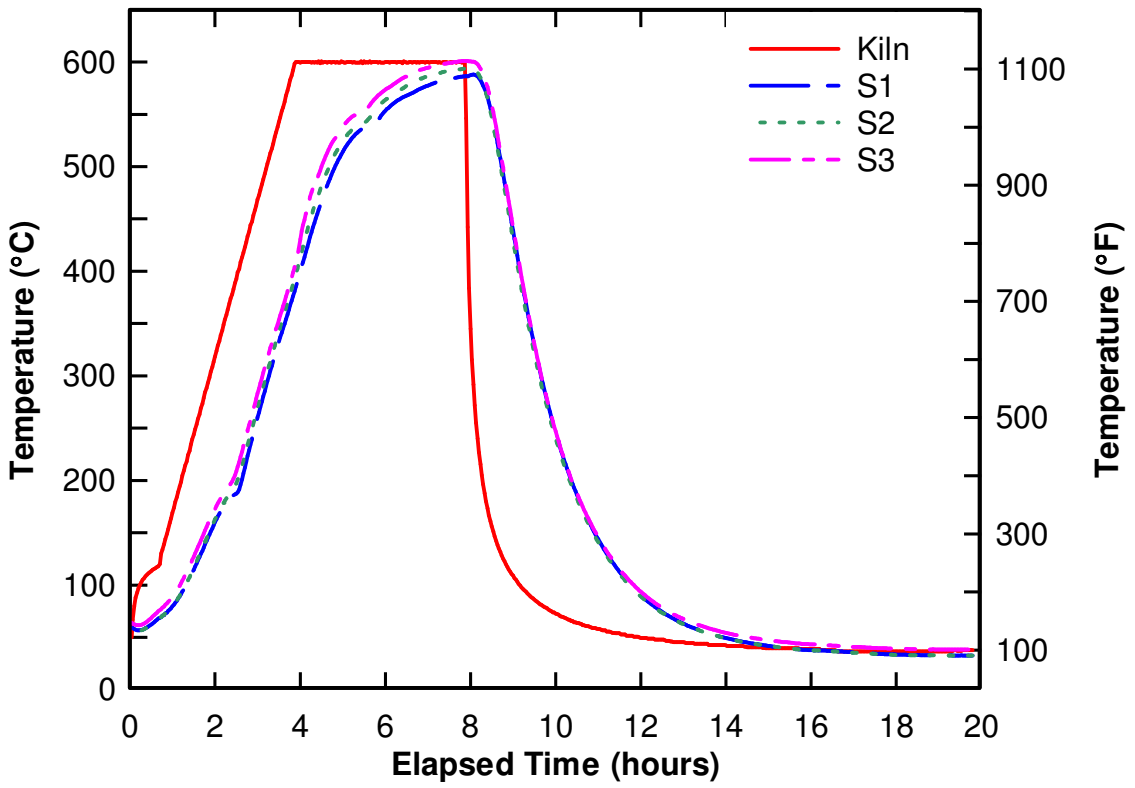

Figure 3.5: Typical data collected during a heating regime (shown: 4h600C).

Preparing Specimens for Heating in Kiln

As mentioned previously, the 4h500C heating regime resulted in spalling of the concrete cylinders. The spalling was thought to have occurred during the heat increase prior to reaching the maximum temperature. This conclusion is based on evaluation of the data retrieved from the thermocouple readings of the bond specimens. These readings had several sudden spikes in temperature, followed by continuous readings above those registered in the kiln. The inconsistencies in the thermocouple readings during the temperature increase to 500°C (932°F) led to this conclusion. This explosive spalling

ultimately destroyed all specimens in the kiln during this test. Figure 3.6 shows the remains of the cylinders after this particular test.

Figure 3.6: Explosive spalling resulted from 4h500C heating regime.

The specimens used for the 4h500C test resulting in explosive spalling were 29 days old. Due to their early age, it is concluded that the specimens contained a sufficient amount of moisture to cause pore pressures to develop, resulting in explosive spalling. Following this incident, all specimens were subsequently exposed to a low temperature drying process prior to heating in the kiln to reduce the moisture content of the concrete. In this low temperature drying process, all remaining concrete specimens were dried in a LINGI oven at 110°C (230°F) for at least 48 hours prior to each heating regime. During

the drying stages, the free ends of the thermocouples were wrapped in Kaowool, a fireproofing insulation, to protect them from the 110°C (220°F) heat in the drying oven, as shown in Figure 3.7.

Figure 3.7: Cylinders in LINGI oven prepared for low temperature drying process.

The thermocouple insulation attachment procedure was also changed as a result of subsequent tests. Since the insulation did not completely eliminate the heat from penetrating to the thermocouple wires, data was lost on several of the latter heating regimes as a result of the plastic coatings of the thermocouple wires melting. As the plastic coatings melted, the wires were in contact at several points, resulting in very

inconsistent temperature readings. Following these incidents, the two thermocouple wires were insulated individually.

After drying the concrete cylinders in the LINGI oven, they were transferred to the Swindell Dressler kiln at the National Brick Research Center. Three bare steel prestressing strands to be used in tensile testing were also placed in the kiln. The kiln heated the specimens using four gas burners, located at the bottom four corners of the rectangular kiln. Although specimens were labeled with a permanent marker, they were arranged in the same configuration in the kiln for each heating regime, as previously shown in Figure 3.1. This was done to recognize specimens if the labeling faded during a test or if spalling occurred such that the label was lost during heating.

All test specimens were placed on the same rack of the kiln above the burners to be at the same height as the control thermocouple used to measure the internal temperature of the kiln. In order to assume the exterior surface of the cylinders was approximately the same temperature as the air temperature of the kiln, they were placed at a similar height above the burners as the thermocouple registering this internal kiln temperature. Because the kiln had some variability in temperature as it was heated from the base burners, the bottom of each cylinder was labeled as a reference. It was assumed that the temperature gradient through the concrete cylinders resulted in slightly off-center concentric circles, as shown in Figure 3.8.

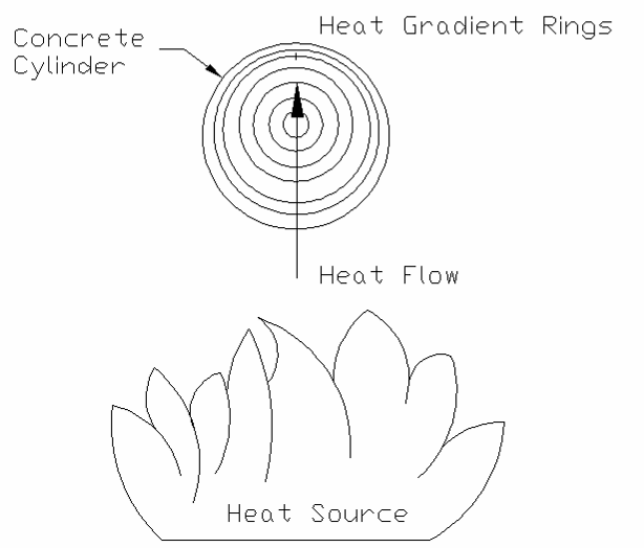

Figure 3.8: Simplified heat contours through concrete cylinder as heated from below.

The embedded steel prestressing strands within bond strength test specimens were insulated during the heating process using Kaowool to reduce the amount of heat penetrated into the concrete through the steel strands. First, a Kaowool square was threaded onto the strand and placed on the face of the cylinder with the embedded steel prestressing strand. Next, the strands were wrapped in Kaowool. The Kaowool was held in place using steel wire, creating a Kaowool "sock" for the strand. These Kaowool socks are shown in Figure 3.9.

Figure 3.9: Kaowool "socks" for placing over steel on bond strength test specimens.

The insulated thermocouple wires were connected to the same computer system that controlled the Swindell Dressler kiln. For all 200°C (390°F) tests, the thermocouple wires were connected inside the kiln using plastic connectors that were blanketed with Kaowool. A thermocouple wire extension was used to connect the wires to the data collection system because the embedded thermocouple wires were too short to extend outside the kiln. However, after extreme discoloration occurred on the plastic connectors, high-temperature ceramic connectors with a Nextel fiber insulated thermocouple wire attachment were used to connect the wires to the computer system. All tests above 200°C (390°F) utilized this new method using ceramic connectors.

Specimen Storage Post-Heating

Because all specimens were heated in the kiln prior to any material testing, the storage of the specimens was crucial in order to preserve the concrete. Since concrete is

known to form calcium carbonate with exposure to carbon dioxide in air (Villain et al. 2006), the samples were stored in vacuum sealed plastic bags. First, the concrete specimens were thoroughly wrapped in plastic wrap and placed in a plastic garbage bag. The bag was tied and sealed using tape. A small hole was created by puncturing the plastic garbage bag to remove air from the bag using an air compressor. After all or most of the air was removed from the bag, the small hole was sealed using tape, as shown in Figure 3.10. This method was used on all concrete specimens following the heating-cooling process.

Figure 3.10: Cylinder wrapped in plastic wrap and vacuum sealed in plastic post heating.

3.5 Concrete Material Properties Testing

Testing methodologies for determining basic concrete material properties were established based on the American Society for Testing and Materials Standards (ASTM).

The cylinders were tested to measure concrete compressive strength and modulus of elasticity. All tests were performed using a 250-kip Universal Testing Machine (UTM) in the Quality Control Laboratory at Tindall Corporation in Spartanburg, SC.

For each heating regime, three plain cylinders were available for compressive tests. Two cylinders from each set were used for determining the modulus of elasticity. In order to establish an initial compressive strength value, one cylinder from each heating regime was chosen at random to be tested for maximum compressive load. After the first cylinder was used to determine an approximate maximum capacity for a particular heating regime, this value determined how many deformation readings would be taken for the other two cylinders in a particular heating regime. This process was done to ensure that the concrete cylinders did not crush while the deformation readings were taken.

Compressive Strength

The compressive strengths of the 6-inch diameter by 12-inch high cylinders were measured using the Standard Test Method for Compressive Strength of Cylindrical Concrete Specimens (ASTM C39). The cylinders were capped on both top and bottom using steel caps containing neoprene pads and loaded to failure, as shown in Figure 3.11. The specimens were loaded between 20 and 50 psi per second in accordance with the standard.

Figure 3.11: Failure of concrete specimen after compressive testing.

Modulus of Elasticity

The Standard Test Method for Static Modulus of Elasticity and Poisson's Ratio of Concrete in Compression (ASTM C469-02e1) was used to determine the modulus of elasticity of the concrete cylinders. As shown in Figure 3.12, a standard compressometer was used to measure strain as the cylinders were loaded.

Figure 3.12: Test set-up for modulus of elasticity determination.

An initial load reading was taken at a known deformation with a calculated strain of 50 microstrains, according to ASTM C469-02e1 (ASTM C469-02e1). Following this initial reading, deformations were measured at 5000-pound intervals up to approximately 60 percent of the previously measured maximum compressive strength of a concrete cylinder chosen at random for each heating regime. These measurements were taken to ensure that 40 percent of the compressive strength was recorded. This value of 40 percent of the maximum compressive strength was used in determining the chord modulus of elasticity according to ASTM C469-02e1 (ASTM C469-02e1). Each cylinder was loaded three times according to ASTM C469-02e1 (ASTM C469-02e1), and strain

measurements were recorded on the last two loadings. The maximum compressive strength of each cylinder was determined following the three successive loadings.

3.6 Measurement of Steel Prestressing Strand Material Properties

The steel prestressing strand material properties, tensile stress and modulus of elasticity, were determined in accordance with a modified version of the ASTM A370-05 standard (ASTM A370-05). A ±2-inch LVDT measured elongation of the strand as it was loaded to approximately 50 percent of the tensile strength to determine the modulus of elasticity. One steel prestressing strand was initially tested for tensile strength prior to measuring elongation values to estimate this 50 percent load. A gage length of 28 inches was used to measure the elongation, which is larger than the minimum value of 24 inches required by the standard. The strand was loaded continuously between 10,000 and 100,000 psi per minute (ASTM A370-05). Data was collected for these tests using a program created in DT Measure Foundry, as shown in Figure 3.13. Load and extension of the prestressing strand were monitored throughout the testing process.

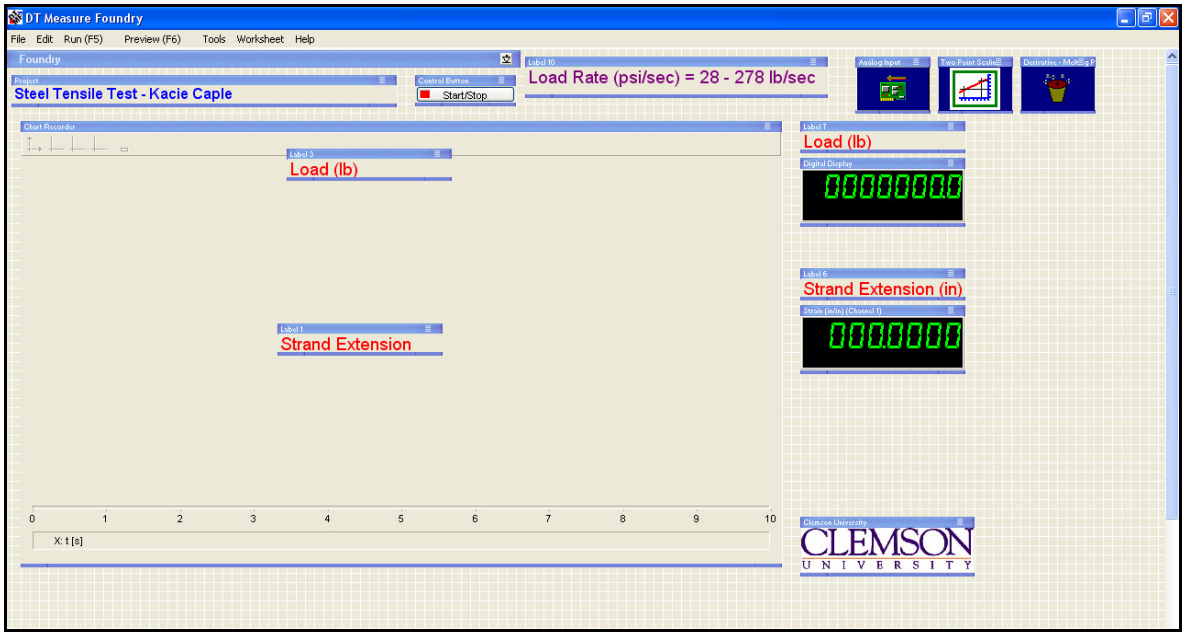

Figure 3.13: DT Measure Foundry program used for data acquisition.

Gripping Devices

The ASTM A370-05 procedure recommends several attachment methods for the strand while conducting the tension test (ASTM A370-05). Since the ASTM standard recommends several attachment mechanisms for the steel prestressing strand, several gripping methods were evaluated to determine an appropriate method.

Table 3.3 provides a list of the gripping methods investigated. For each method, a chuck was used as the bottom anchorage to attach an external load cell to the testing system. Although not recommended for testing purposes, a chuck was the only device available to anchor one end of the steel strand in order to monitor loads with the external load cell. Several cushioning methods were also tested, as indicated by Table 3.3.

Table 3.3: Methods of anchorage investigated for prestressing steel tensile testing.

Method No.	Top Anchorage	Top Cushioning	Bottom Anchorage	Bottom Cushioning
1	Chuck	None	Chuck	None
2	Chuck	Aluminum foil	Chuck	Aluminum foil
3	V-grips*	None	Chuck	None
4	V-grips*	Aluminum foil	Chuck	Aluminum foil
5	V-grips*	Steel pipe attached with J.B. Weld compound	Chuck	Aluminum foil
6	V-grips*	Aluminum, flexible conduit attached with fast-set epoxy	Chuck	Aluminum foil
7	V-grips*	Duct tape	Chuck	Duct tape and aluminum foil

* V-grips had 15 serrated teeth per inch.

After evaluating and reviewing all methods, Method 7 as listed in Table 3.3 was chosen. This method incorporated the use of duct tape to cushion the strand within standard V-grips, having 15 serrated teeth per inch. The duct tape was wrapped tightly in two layers for at least eight inches along one end of the steel strand to be placed in the V-grips. The chuck was cushioned using one layer of duct tape and 2 to 3 layers of aluminum foil. This method was chosen for safety reasons and because it resulted in some fractures between the gripping devices, as shown in Figure 3.14. According to ASTM A370-05, the fracture strength of a steel specimen is only valid if a fracture occurs between the free span of the gripping devices (ASTM A370-05).

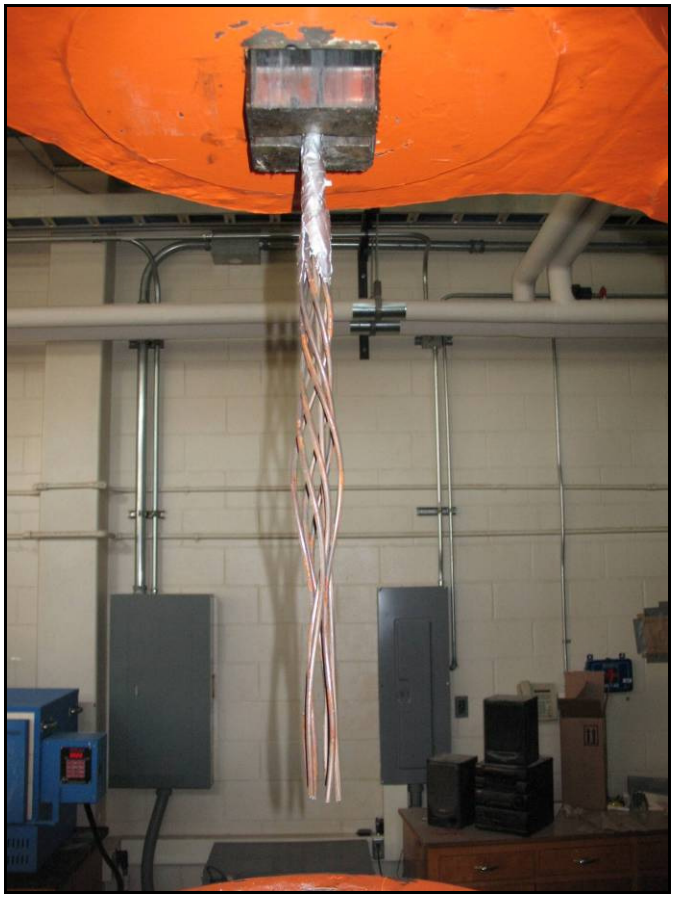

Figure 3.14: Fracture of steel prestressing strand within free span of gripping devices.

Steel Modulus of Elasticity

The modulus of elasticity test was performed prior to determining the tensile stress of the steel prestressing strand. Strain was measured during the entire loading process using a ±2-inch LVDT with a gage length of 28 inches, as shown in Figure 3.15. The LVDT was attached firmly at the top point to establish the upper end of the gage length. The LVDT was also loosely attached at the lower end for stabilization during testing. The lower end of the gage length was hidden within the cross-head of the UTM.

Strain measurements were collected using a DT Measure Foundry program, and the modulus of elasticity of the strand was calculated based on these readings.

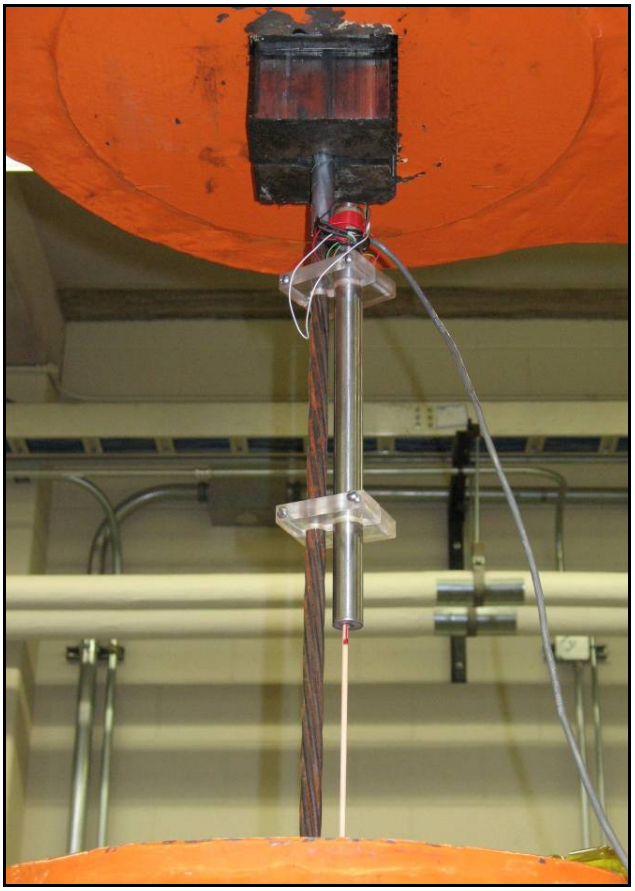

Figure 3.15: LVDT anchored to steel prestressing strand to measure deformations over 26-inch gage length.

Ultimate Strength

The ultimate strength of the steel prestressing strand was determined by testing the strands to their ultimate capacity. After the steel strand was loaded to determine elongations, it was loaded to fracture. The ultimate strength was considered the load at

which one or more strands fractured. In accordance with ASTM A370-05, the ultimate strength was not considered valid unless the fracture occurred in all strands simultaneously between the free span of the two gripping ends (ASTM A370-05).

3.7 Bond Stress Testing

A bond stress test was performed on the concrete cylinders with embedded steel prestressing strands. The purpose of the test was to evaluate relative changes in the magnitude of bond stress developed at the steel strand and concrete interface as a function of temperature. In order to evaluate this parameter, these specimens were tested using a UTM to pull the steel strand out of the concrete cylinder. Because this was not a standard test procedure, results were evaluated on a comparative basis with unheated, control samples.

The strand was gripped at the top of the UTM using the same V-grips as used in the steel prestressing strand tensile strength test. A neoprene pad with a centrally located 0.5-inch hole was placed over the strand and on top of the concrete cylinder to transfer load evenly throughout the test. A 6-inch by 6-inch by 0.75-inch thick steel plate with a 0.5-inch hole at the center was placed on top of the neoprene pad. A load cell was placed on top of the steel plate, and another steel plate of similar dimensions was placed on top of the load cell to bear against the bottom plate of the UTM. A ±1-inch LVDT was attached to the prestressing strand to measure elongation of the strand, and a ±2-inch LVDT was mounted near the plate above the cylinder within the bottom cross-head to

measure slippage of the prestressing strand as it was pulled from the concrete cylinder. The test configuration for the bond stress test is shown in Figure 3.16.

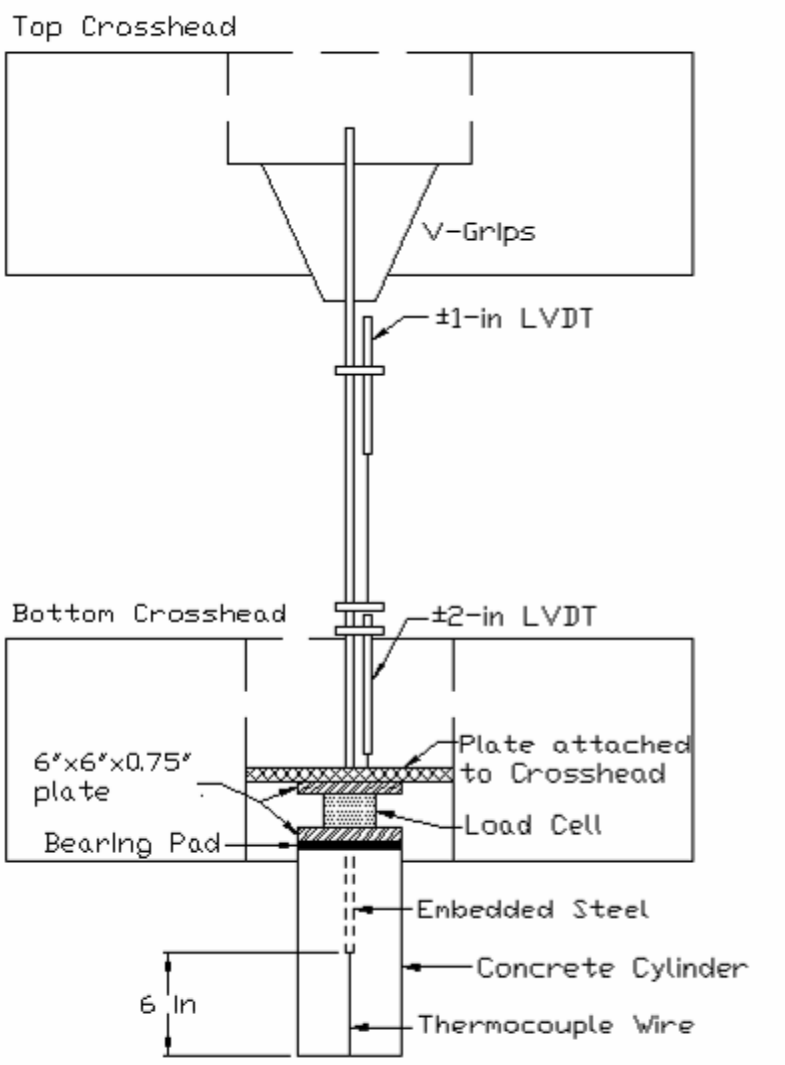

Figure 3.16: Bond stress test configuration in UTM.

A program using DT Measure Foundry was utilized to collect data during the bond stress tests. Data collection included load, loading rate, slippage of the strand, and

elongation of the strand. The samples were loaded at a rate between 50 and 250 pounds per second. This rate was used because it was within the rate of loading used for the tensile testing of the steel prestressing strands. Bond tests were terminated if, while loading, the load dropped and was never regained or the strand was pulled completely from the cylinder. Although measures were taken to reduce the splitting of bond specimens by using a 6-inch embedment, several specimens did split during testing. In these cases, the test was terminated upon fracture of the specimens.

3.8 Thermogravimetric Analysis

A study was conducted to evaluate the potential of thermogravimetric analysis (TGA) as a practical tool for estimating the maximum temperature to which concrete has been exposed. A series of tests were performed on small cement paste and mortar samples to evaluate the accuracy of the TGA procedure. Thermogravimetric analysis was then performed to estimate a temperature profile within a concrete sample. For all TGA testing, sample sizes between 15 and 20 mg were ground using a mortar and pestle. All samples were flushed with nitrogen gas, to prevent carbonation of the samples by exposure to carbon-dioxide present in air (Villain et al. 2006). A TGA/SDTA851[e] machine was used for performing all thermogravimetric analysis.

Cement and Mortar Comparison

The thermogravimetric analysis technique for estimating the maximum temperature attained by a concrete sample was first evaluated by testing cement paste and

mortar samples in a controlled environment. Small cement paste and mortar cylinder samples were cast using a similar mix design to that of the concrete used in the concrete cylinders. The paste and mortar samples were approximately 0.5 inches in diameter and 2 inches in height. A water-to-cement ratio of 0.42 was used in the cement paste and mortar samples to ensure complete hydration (KOSMATKA 2002). The samples were cured in a water bath for 28 days prior to performing the TGA. The mix proportions used for the laboratory samples are shown in Table 3.4.

Table 3.4: Mixture proportions of cement paste and mortar samples.

Material	Cement Paste	Mortar
Sand (ASTM 33)	0 g	221.2 g
Poz 80 (Type A water reducer)	0.4 g	0.4 g
Glenium 3400 (HRWR)	0.4 g	0.4 g
MB-AE 90 (air entrainer)	0.1 g	0.1 g
Flyash	19.6 g	19.6 g
Cement	124.6 g	124.6 g
Water	52.3 g	52.3 g

TGA was performed on the samples to validate the use of TGA as a means to detect high temperature exposure in cementitious materials, not as a comparison to the concrete samples. Therefore, it was not required that the mix proportions or the curing conditions be the same for both the cement paste, mortar, and concrete samples. For each set of samples, several heat treatments were performed. To prepare the samples for the heat treatments, they were ground to a fine powder using a mortar and pestle. The TGA

machine was used to heat a sample at 10°C (50°F) per minute from 60°C (140°F) to a desired intermediate temperature, first. This intermediate temperature, or heat treatment temperature, was held for 15 minutes to ensure the sample was thoroughly heated. The temperature was then decreased to 60°C (140°F) at a rate of 10°C (50°F) per minute. Following the cooling process, the sample was reheated from 60 to 800°C (140 to 1472 °F) at 10°C (50°F) per minute. This heat treatment process was performed on both mortar and cement paste samples using intermediate temperatures of 200, 400, 500, and 600°C (392, 752, 932, and 1112°F). A control sample was also analyzed by heating from 60 to 800ºC (140 to 1470°F) directly with no intermediate temperature. This was done to create a control TGA curve for evaluation purposes. A typical heat treatment is shown below in Figure 3.17, marking important areas of the curve.

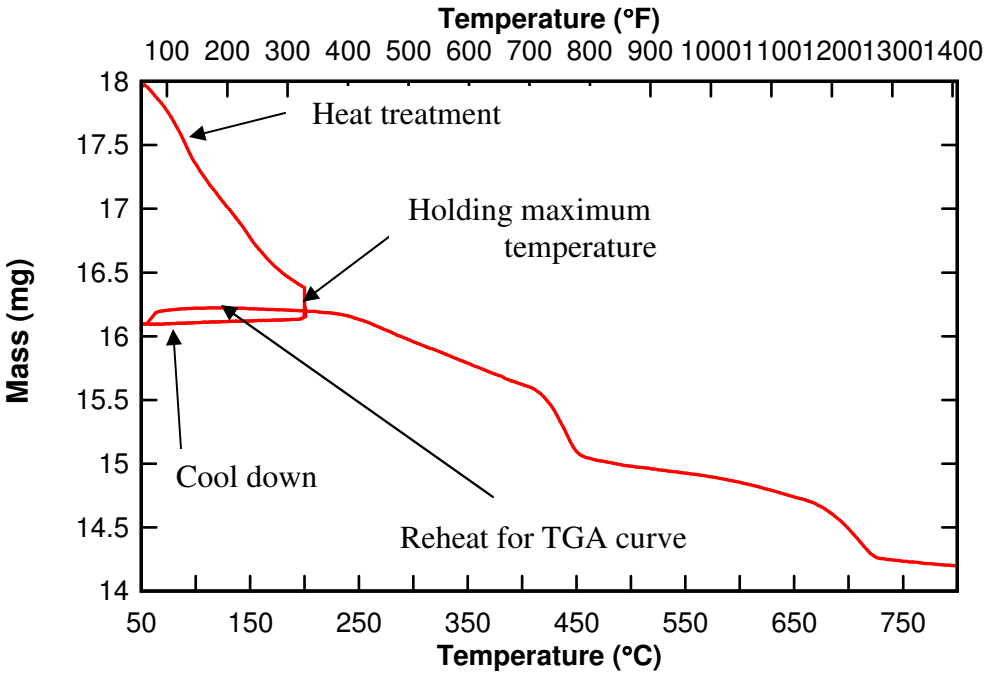

Figure 3.17: TGA curve for 200ºC (392°F) heat treatment.

Concrete Heat Profile

TGA was performed on the 1h500C-S2 cylinder to predict a heat profile. Samples were extracted from the center of the cylinder at 1-inch intervals along the cross-section between the bottom and top of the cylinder as shown in Figure 3.18. The heat profile was mapped by comparing data from samples that were heated from 60 to 800°C (140 to 1470°F) at 10°C (50°F) per minute. A sample was also extracted from the center of an unheated concrete specimen as a control comparison. Once extracted, samples were ground to a fine powder using a mortar and pestle, similar to the cement and mortar paste samples.

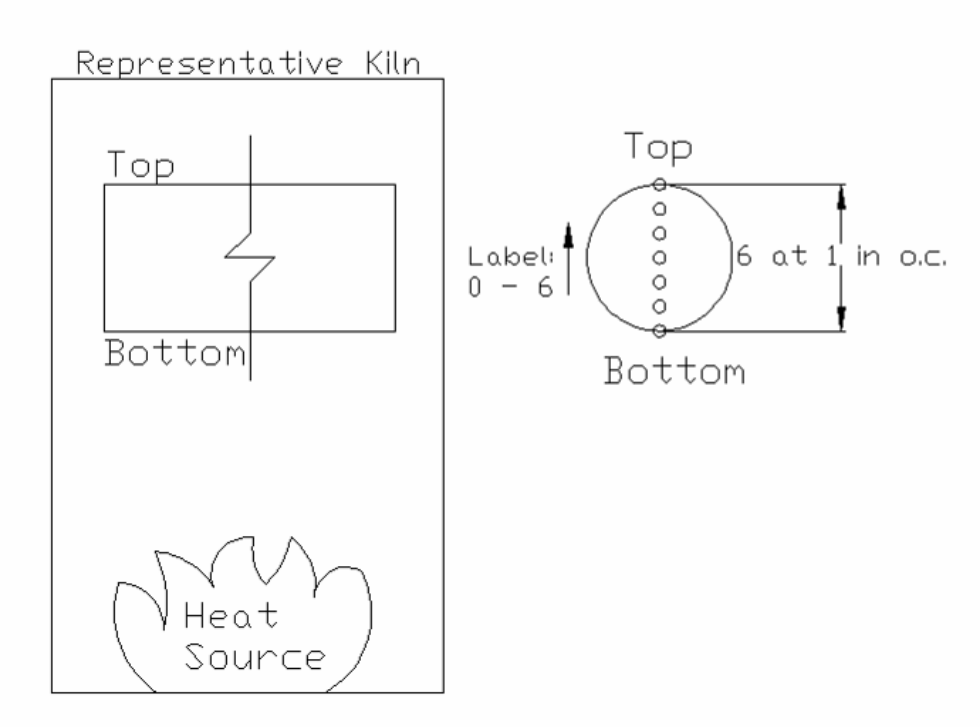

Figure 3.18: Locations of samples taken from cylinder to generate heat profile.

CHAPTER FOUR

EXPERIMENTAL TEST RESULTS

This Chapter presents all data that was collected throughout experimental testing to determine the material property changes in prestressed concrete when subjected to elevated temperatures. This data includes the moisture content losses due to low-temperature drying, heat exposure curves, concrete compressive strengths, concrete modulus of elasticity values, steel ultimate stresses, steel modulus of elasticity values, maximum bond stresses, and the maximum pull-out forces reached during bond testing. The TGA results of the cement paste, mortar, and concrete samples are also presented in this Chapter.

4.1 Low Temperature Drying Weight Changes

In order to prevent explosive spalling from occurring due to high moisture contents of the relatively "green" concrete, all concrete cylinders were subjected to a low temperature drying process in an oven at the National Brick Research Center prior to their scheduled heating exposures. Weights before and after heating were recorded to establish the amount of water weight lost by the drying process. Additionally, the moisture content losses of the concrete were calculated.

Tables 4.1, 4.2, and 4.3 summarize the weights before and after the drying process, weight losses, and moisture content losses of each cylinder recorded. The loss in moisture content was calculated using Equation 4.1, where M_{loss} is moisture content loss

in percentage. An average of weights before the drying process, weights after drying, weight losses, and moisture content losses were also calculated.

$$M_{loss}(\%) = \left(\frac{L}{W_0} \right) * 100 \tag{4.1}$$

Table 4.1: Summary of weight change data due to low temperature drying of concrete cylinders for 400ºC (752°F) heating regimes.

Heating Regime	Cylinder Recognition	Weight Before Pre-heating (lb)	Weight After Pre-heating (lb)	Weight Loss (lb)	Moisture Content (%)
0.5h400C	1	27.6	27.0	0.6	2.17
	2	27.6	27.0	0.6	2.17
	3	27.8	27.2	0.6	2.16
1h400C	1	27.8	27.0	0.8	2.88
	2	27.4	26.6	0.8	2.92
	3	27.4	26.4	1.0	3.65
4h400C	1	27.6	27.0	0.6	2.17
	2	27.6	27.0	0.6	2.17
	3	27.8	27.2	0.6	2.16

Table 4.2: Weight change data due to low temperature drying of concrete cylinders for 500ºC (932°F) heating regimes.

Heating Regime	Cylinder Recognition	Weight Before Pre-heating (lb)	Weight After Pre-heating (lb)	Weight Loss (lb)	Moisture Content (%)
0.5h500C	1	27.2	27.0	0.2	0.74
	2	27.2	27.0	0.2	0.74
	3	27.0	26.8	0.2	0.74
1h500C	1	27.8	27.2	0.6	2.16
	2	27.6	26.8	0.8	2.90
	3	27.8	27.0	0.8	2.88
2h500C	1	27.6	27.2	0.4	1.45
	2	27.8	27.2	0.6	2.16
	3	27.2	26.6	0.6	2.21
4h500C	1	27.6	26.8	0.8	2.90
	2	27.6	27.0	0.6	2.17
	3	27.4	26.8	0.6	2.19

Table 4.3: Weight changes due to low temperature drying of concrete cylinders for 600ºC (1112°F) heating regimes and averages of all concrete cylinder low-temperature drying results.

Heating Regime	Cylinder Recognition	Weight Before Pre-heating (lb)	Weight After Pre-heating (lb)	Weight Loss (lb)	Moisture Content (%)
0.5h600C	1	28.2	27.6	0.6	2.13
	2	28.2	27.6	0.6	2.13
	3	28.0	27.6	0.4	1.43
1h600C	1	28.4	27.8	0.6	2.11
	2	28.2	27.6	0.6	2.13
	3	28.4	27.8	0.6	2.11
2h600C	1	27.8	27.2	0.6	2.16
	2	27.8	27.2	0.6	2.16
	3	28.0	27.4	0.6	2.14
4h600C	1	27.6	27.0	0.6	2.17
	2	27.6	27.2	0.4	1.45
	3	27.8	27.4	0.4	1.44
Average:		27.7	27.1	0.6	2.1

As shown in Table 4.1, the average weight of the plain concrete cylinders was 27.7 lbs. The average weight loss due to drying was approximately 0.6 lbs, which gave the concrete cylinders an approximate moisture content loss of 2.1 percent after drying. The maximum and minimum weight losses were 1.0 and 0.2 pounds, respectively. Although one cylinder, 0.5h600C-3, was broken during the heating process, it is not thought to have occurred due to explosive spalling due to the condition of the cylinder when it was found. The cylinder fell from the rack supporting the specimens, causing it to split. The cylinder was partially in-tact, split through the middle longitudinally along the 12-inch length. Another split occurred perpendicular to this longitudinal split, causing one of the longitudinal sections to be split into two nearly equal sections, as shown in Figure 4.1. The cause of the fall is unknown.

Figure 4.1: Splitting of cylinder 0.5h600C-3.

Tables 4.4, 4.5, and 4.6 provide information regarding the weights before and after the low temperature drying process, weight losses, and moisture content losses of all bond specimens. The weight losses and averages were calculated in the same way as those used in Table 4.1 for the plain cylinders. However, the loss of moisture content was calculated differently due to the additional weight of the steel. The loss of moisture content for the concrete cylinders containing embedded steel prestressing strands was calculated using Equation 4.2, where M_s is the moisture content of the cylinders with embedded steel and W_{st} is an approximate weight of the steel prestressing strand.

$$M_s(\%) = \left(\frac{L}{W_i - W_{st}} \right) * 100 \tag{4.2}$$

The length of each embedded strand was approximately 4 feet. According to the PCI Design Manual, the weight of the ½-inch Special strand is 0.53 plf (PCI 2004). Based on this, the approximate weight of the prestressing strand was determined to be 2.1 pounds.

The average weight of each cylinder was 30.0 pounds, and the average weight loss per cylinder was 0.7 pounds, similar to the weight loss of cylinders containing no steel. The maximum and minimum weight losses for cylinders containing steel were 1.2 and 0.4 pounds, respectively. However, the moisture content losses, calculated using the alternate formula to account for steel weight, were higher on average as compared to the cylinders without steel. The average moisture content of the cylinders containing steel was estimated to be 2.9 percent, which is 0.8 percent higher than the cylinders without steel. One possible reason for the difference is that the moisture was able to easily escape

through air spaces between the individual tendons of the steel prestressing strand. Because the prestressing steel strand is composed of seven individual wire tendons, moisture could have evaporated through the areas between the tendons. Also, the prestressing steel strands were not insulated during the drying process, allowing heat to be transferred directly to the center of the cylinder by the prestressing steel.

Table 4.4: Weight change data due to low temperature drying of bond stress specimens for 400ºC (752°F) heating regimes.

Heating Regime	Specimen Recognition	Weight Before Drying, Wi (lb)	Weight After Drying, W (lb)	Weight Loss, L (lb)	Moisture Content, Ms (%)
0.5h400C	S1	30.0	29.4	0.6	2.87
	S2	30.0	29.4	0.6	2.87
	S3	30.0	29.6	0.4	2.87
1h400C	S1	29.8	28.8	1.0	2.89
	S2	30.0	29.0	1.0	2.87
	S3	29.8	28.8	1.0	2.89
4h400C	S1	30.2	29.6	0.6	2.85
	S2	29.8	29.2	0.6	2.89
	S3	29.8	29.2	0.6	2.89

Table 4.5: Weight change data due to low temperature drying of bond stress specimens for 500ºC (932°F) heating regimes.

Heating Regime	Specimen Recognition	Weight Before Drying, Wi (lb)	Weight After Drying, W (lb)	Weight Loss, L (lb)	Moisture Content, Ms (%)
0.5h500C	S1	30.2	29.6	0.6	2.85
	S2	29.8	29.0	0.8	2.89
	S3	30.0	29.4	0.6	2.87
1h500C	S1	30.0	29.2	0.8	2.87
	S2	30.2	29.4	0.8	2.85
	S3	30.0	29.2	0.8	2.87
2h500C	S1	30.0	29.0	1.0	2.87
	S2	29.8	29.4	0.4	2.89
	S3	29.2	28.8	0.4	2.95
4h500C	S1	30.0	29.2	0.8	2.87
	S2	30.2	29.4	0.8	2.85
	S3	30.0	29.2	0.8	2.87

Table 4.6: Weight change data due to low temperature drying of bond stress specimens for 600ºC (1112°F) heating regimes and average weight change data for all heating regimes.

Heating Regime	Specimen Recognition	Weight Before Drying, Wi (lb)	Weight After Drying, W (lb)	Weight Loss, L (lb)	Moisture Content, Ms (%)
0.5h600C	S1	30.2	29.6	0.6	2.85
	S2	30.2	29.6	0.6	2.85
	S3	30.2	29.6	0.6	2.85
1h600C	S1	30.4	29.8	0.6	2.83
	S2	30.0	29.2	0.8	2.87
	S3	30.0	29.6	0.4	2.87
2h600C	S1	30.0	29.4	0.6	2.87
	S2	30.2	29.4	0.8	2.85
	S3	29.8	29.0	0.8	2.89
4h600C	S1	30.0	28.8	1.2	2.87
	S2	30.0	29.2	0.8	2.87
	S3	30.2	29.2	1.0	2.85
Average:		30.0	29.3	0.7	2.90

4.2 Heat Exposure Curves

Heat exposure curves provided information on the heat penetration within the concrete cylinders over time as they were heated and cooled. The *Heating Phase* is the portion of the curve in which heat was increased at 2.5°C (4.5ºF) per minute. The sustained portion at the specified maximum temperature is known as the *Duration Phase,* which always resulted in a plateau for the kiln temperature readings. After the duration was completed, the burners inside the kiln were turned off, and blowers injected room-temperature air into the kiln to cool the specimens. This portion of the curve is known as the *Cooling Phase*. Each of these phases was distinct on the heat exposure curves using the kiln temperature curve as a guide. Figure 4.2 shows a representative heat load curve of the kiln temperature, illustrating the three distinct phases within the entire kiln heating and cooling processes. This Figure can be used as a reference throughout the text as these phases are referenced.

It is expected that the internal temperatures of the cylinders would develop heat exposure curves in a lazy "S" shape. As the kiln is initially heated, it is expected to take some time for the center of the cylinder to register this temperature. Therefore, the beginning of the curve is expected to have a relatively low slope that gradually increases, representing the bottom of the lazy "S" shape. As the heating process continues, the temperature of the cylinder is expected to steadily climb in a linear trend, lagging behind the kiln temperature. As the heat is held constant within the kiln, the center of the concrete cylinder should slowly increase in temperature, creating the top of the lazy "S" shape. As the temperature is held constant, the heat differences between the exterior and

the center of the concrete cylinder decrease, causing a reduction in the rate at which the heat is transferred.

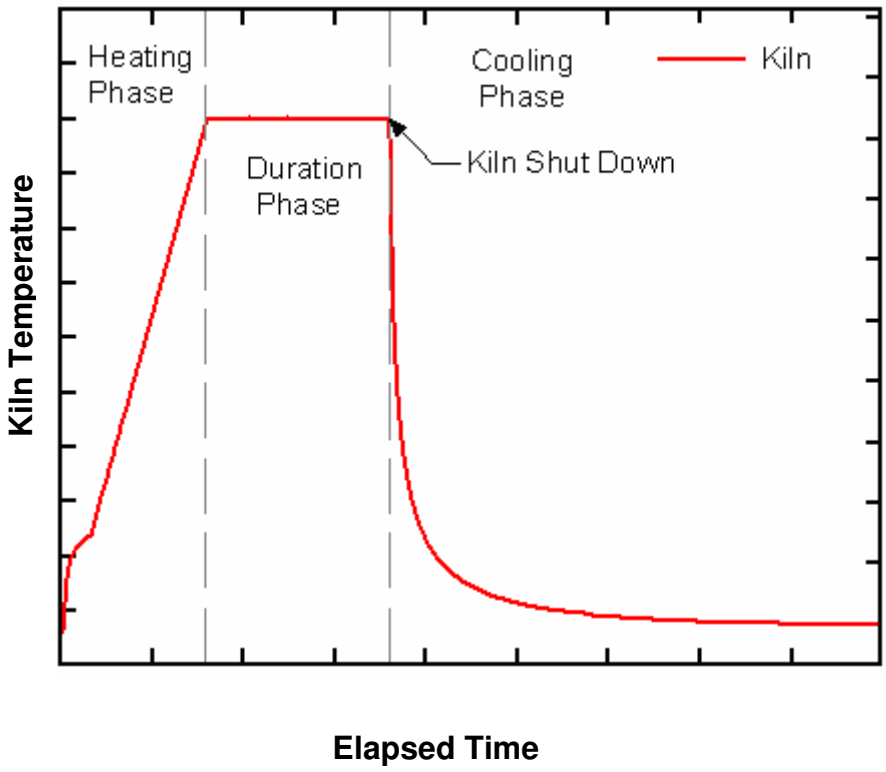

Figure 4.2: Representative heat load curve, illustrating the heating, duration, and cooling phases.

200°C Heat Exposure Curves

The first curves presented are those in which 200°C (392°F) is the maximum temperature. Figures 4.3, 4.4, and 4.5 are the heat exposure curves for the 1-, 2-, and 4-hour duration tests, respectively, at 200°C (392°F). As shown in Figure 4.3, the only reasonable curve is that of cylinder 1h200C-S1. The other two curves reveal some

inconsistencies in the cooling phase. The reason for these inconsistencies is unknown. As shown in Figure 4.4, all cylinders produced reasonable heat exposure curves for the two hour exposure at 200°C (392°F). These cylinders were the first to experience the low temperature drying process, which is the reason for the high internal temperature of the cylinders at the beginning of the test. These cylinders were transferred quickly from the oven used for low temperature drying to the kiln, causing their initial temperatures to be above ambient. Figure 4.5 reveals that something occurred at 200°C (392°F), as the thermocouples of two of the cylinders displayed a sudden heat increase as they approached 200°C (392°F). Since cylinder 4h200C-S1 shows no sudden heat increase as the other two cylinders, this irregularity is likely to have been a result of the placement of the 4h200C cylinders. These cylinders were placed on a lower rack within the kiln below the main heating thermocouple, causing them to be closer to the heat source. Therefore, it is possible that 4h200C-S2 and S3 actually did reach temperatures above 200°C (392°F) throughout the heating process due to their low height within the kiln. Another noticeable feature evident in all heat exposure curves is that the maximum temperature occurs after the kiln was shut down. This was expected based on the lazy "S" curves. After the kiln was shut down, the heat continued to transfer to the core of the cylinder for some short duration, resulting in a maximum temperature past the designated duration of heat exposure.

400°C Heat Exposure Curves

Figures 4.6, 4.7, 4.8, and 4.9 show the heat exposures curves for the 0.5, 1, 2, and 4-hour sustained exposures, respectively, at 400°C (752ºF). The 0.5h400C heat exposure

curves are shown in Figure 4.6. As shown in this Figure, faulty wiring resulted in a loss of data with cylinders S2 and S3. However, the S1 cylinder contained reasonable data for a heat exposure curve. Figure 4.7 reveals that all data was lost for the 1h400C test, resulting in no heat exposure data for this heating regime. Figure 4.8 shows the heat exposure curves for the 2h400C test. In this test, only two cylinders contained thermocouples because some thermocouple wires were destroyed as the cylinders were removed from the plastic molds. The two cylinders containing thermocouples provided reasonable heat exposure curves, although cylinder S2 displayed some errors in readings, likely associated to having loose connections to the data collection system. Data was completely lost again on the 4h400c test. As temperatures increased, the plastic coatings surrounding the thermocouple wires melted, allowing the wires to be in contact in multiple locations within the insulation. This prevented precise readings at the center point within the cylinder.

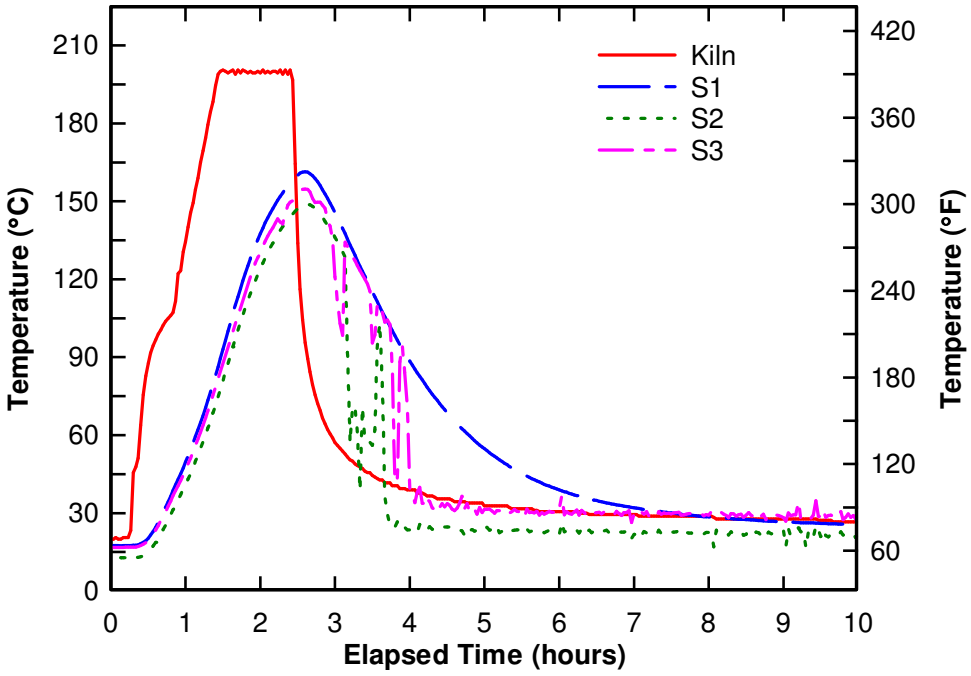

Figure 4.3: 200°C (392ºF) sustained for one hour (1h200C) heat exposure curves.

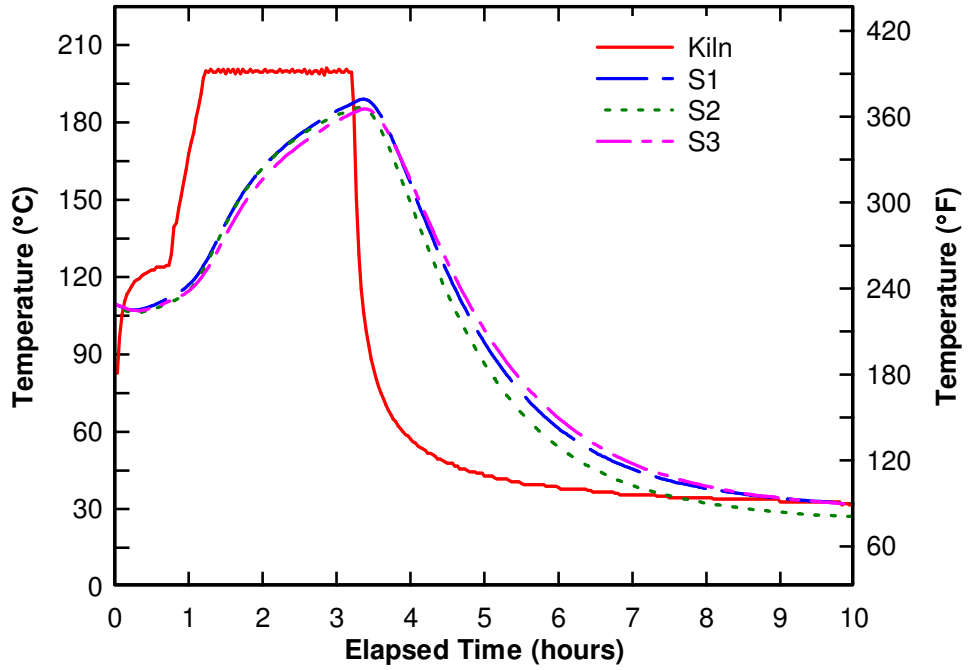

Figure 4.4: 200°C (392ºF) sustained for two hours (2h200C) heat exposure curves.

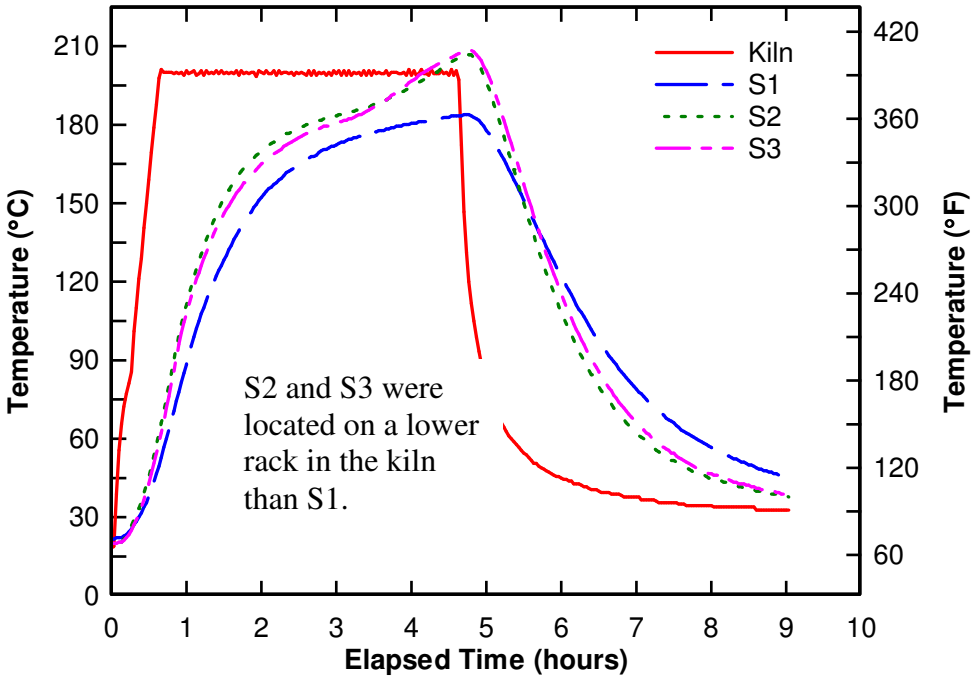

Figure 4.5: 200°C (392ºF) sustained for four hours (4h200C) heat exposure curves.

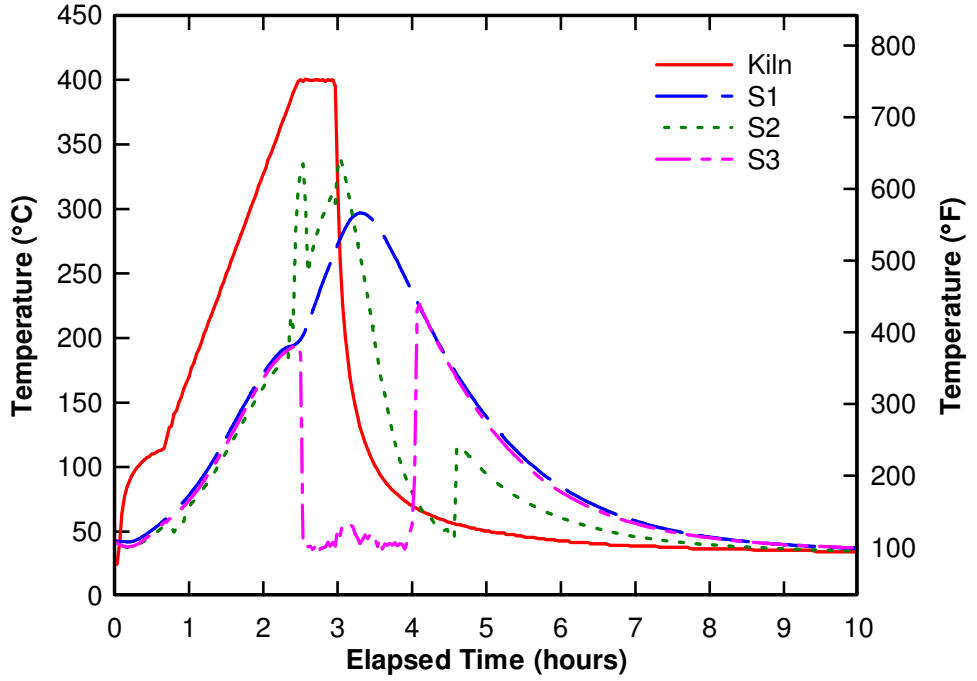

Figure 4.6: 400°C (752ºF) sustained for 0.5 hours (0.5h400C) heat exposure curves.

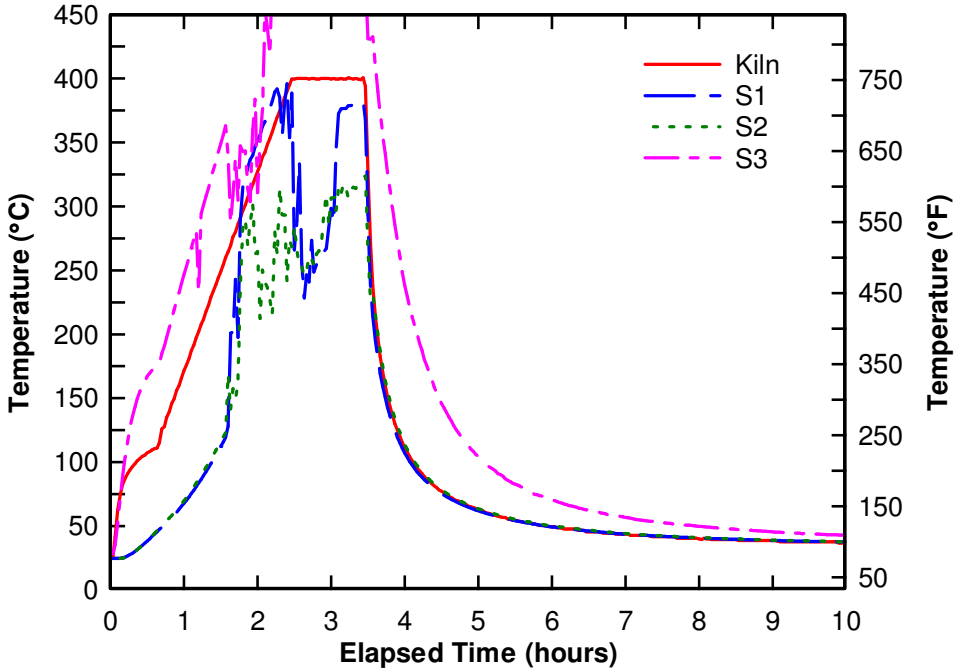

Figure 4.7: 400°C (752ºF) sustained for 1 hour (1h400C) heat exposure curves.

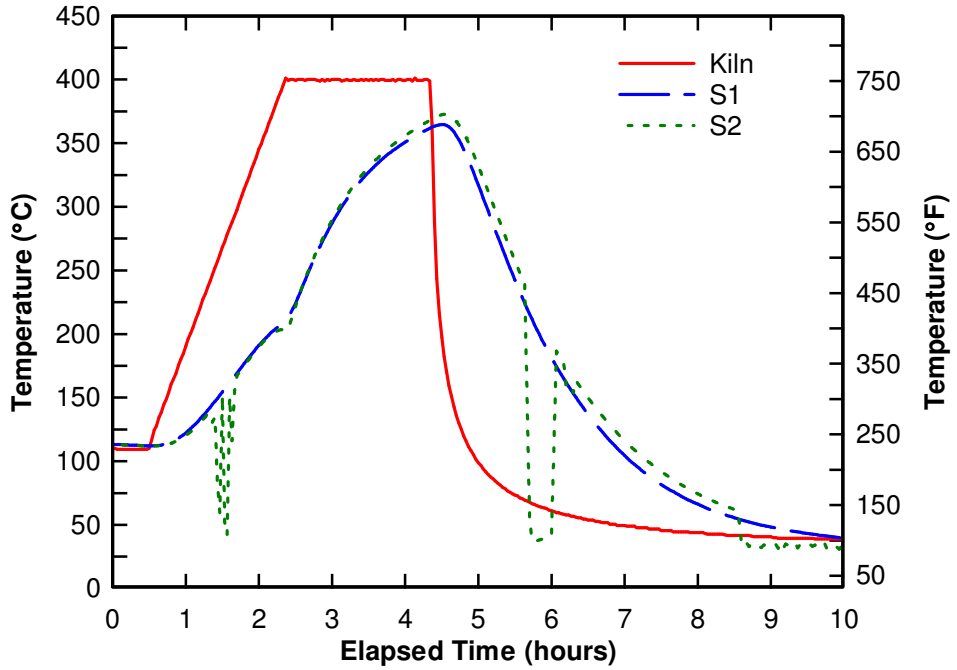

Figure 4.8: 400°C (752ºF) sustained for 2 hours (2h400C) heat exposure curves.

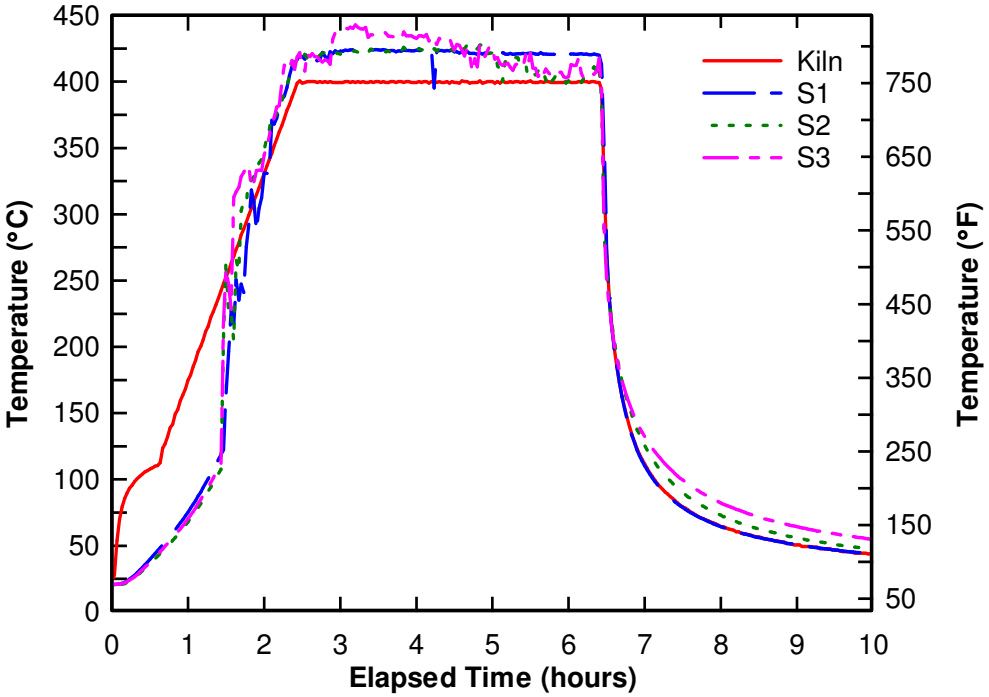

Figure 4.9: 400°C (752ºF) sustained for 4 hours (4h400C) heat exposure curves.

500°C Heat Exposure Curves

The 500°C (932ºF) heat exposure curves are shown in Figures 4.10, 4.11, 4.12, and 4.13 with 0.5-, 1-, 2-, and 4-hour durations, respectively. Figure 4.10 displays two similar heat curves for the 0.5h500C tests with the S2 and S3 cylinders; however, the S1 cylinder displayed a sudden increase in heat transfer at approximately three hours into the *Heating Phase*. This sudden spike is possibly a result of melted plastic coatings of the thermocouples wires, as mentioned previously. As shown in Figure 4.11 and 4.13, reasonable heat exposure curves were attained for the 500°C (932ºF) 1- and 4-hour durations, respectively. Only two cylinders were equipped with thermocouple wires in

the 2-hour exposure at 500°C (932ºF), as shown in Figure 4.12. Cylinder S3 displayed some irregularities in early stages of the *Heating Phase* and late stages of the *Cooling Phase*.

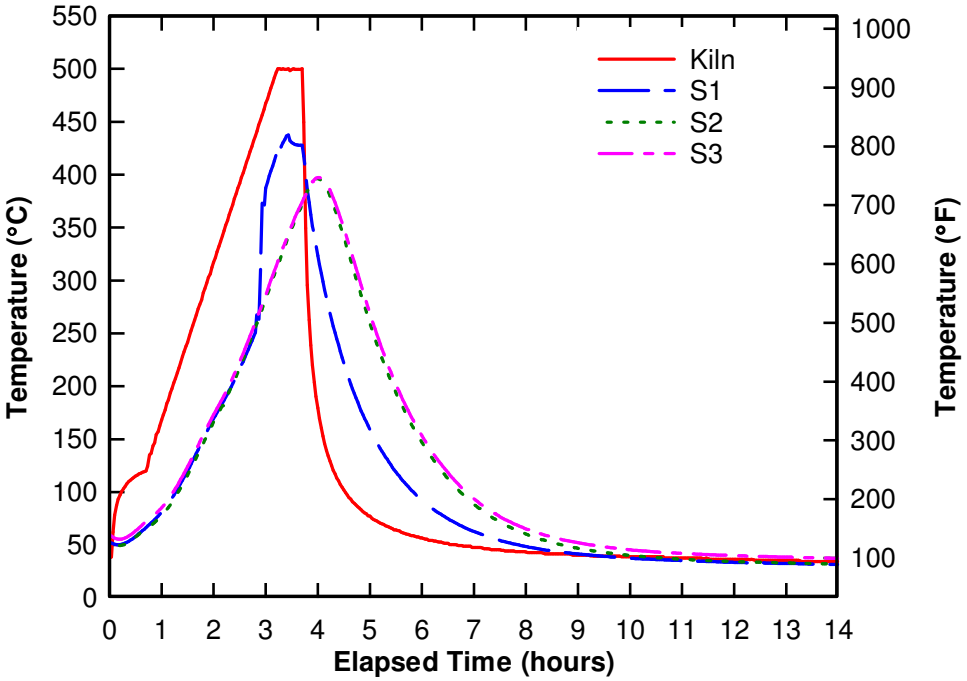

Figure 4.10: 500°C (932ºF) sustained for 0.5 hours (0.5h500C) heat exposure curves.

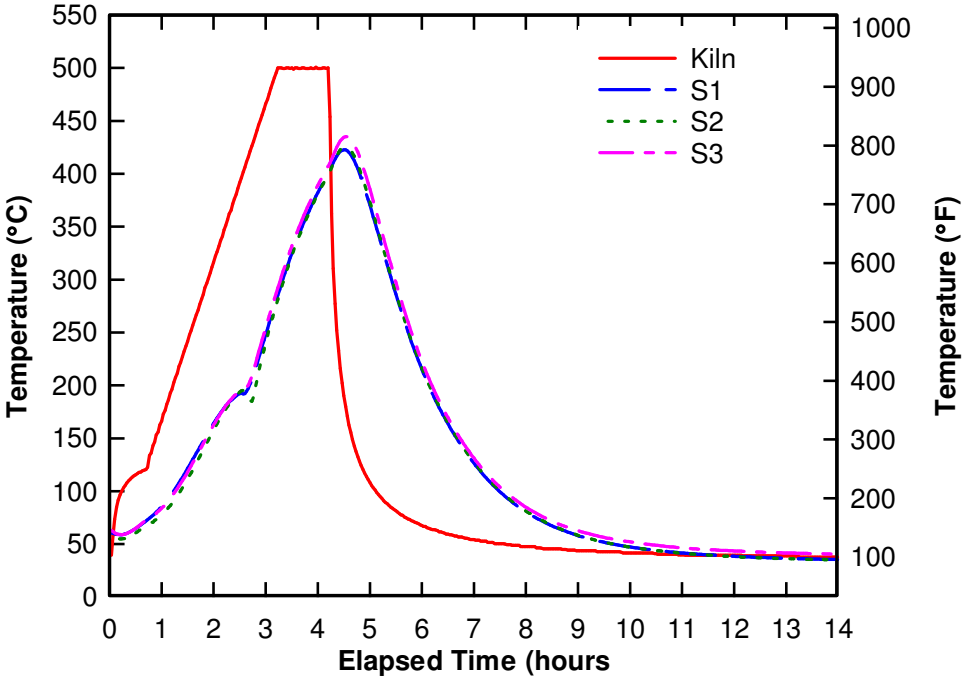

Figure 4.11: 500°C (932ºF) sustained for 1 hour (1h500C) heat exposure curves.

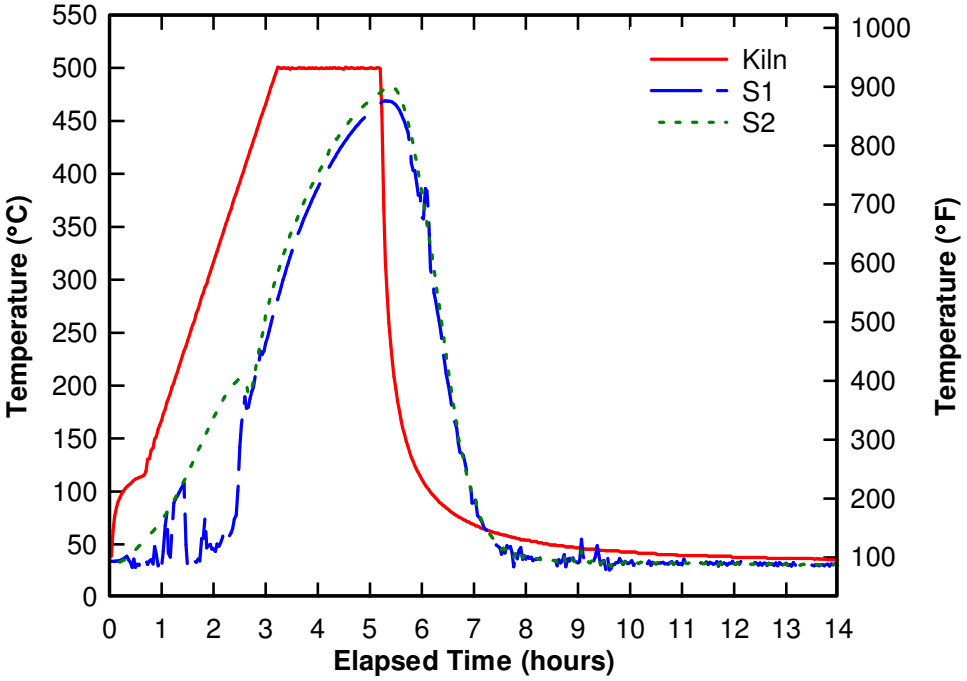

Figure 4.12: 500°C (932ºF) sustained for 2 hours (2h500C) heat exposure curves.

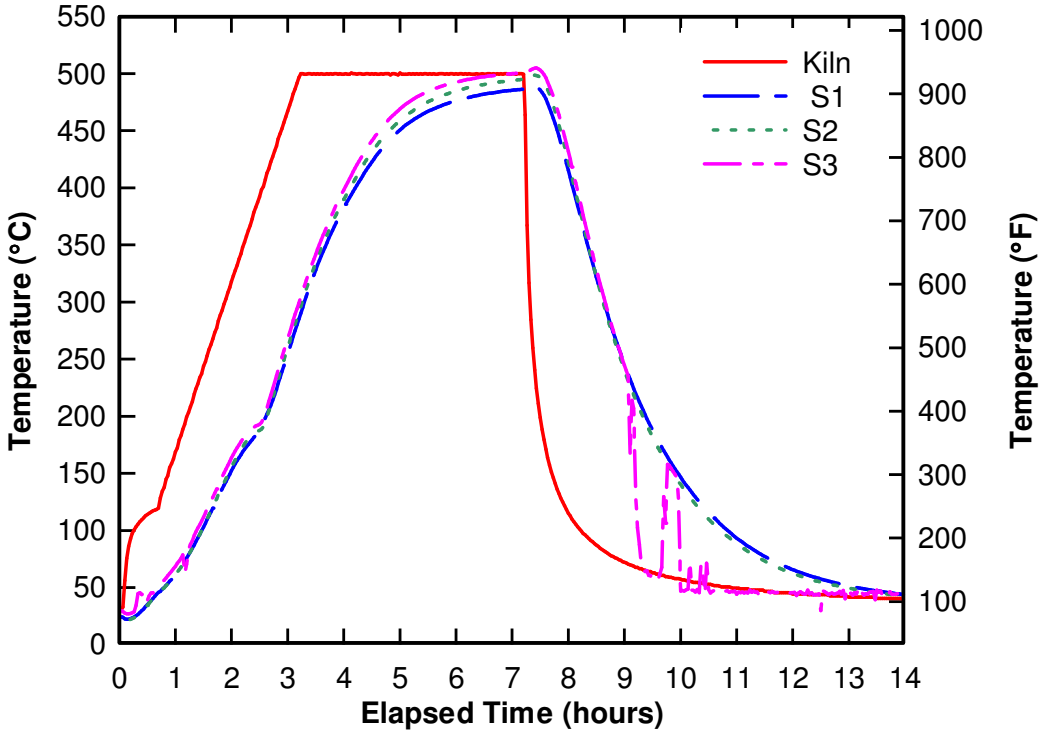

Figure 4.13: 500°C (932ºF) sustained for 4 hours (4h500C) heat exposure curves.

600°C Heat Exposure Curves

Because the 600°C (1112ºF) heat exposure curves were the last to be performed, they were executed with the most updated methods, reducing the possibility of melting wires and poor connections to the system. Figures 4.14, 4.15, 4.16, and 4.17 display the 600°C (1112ºF) heat exposure curves for the 0.5-, 1-, 2-, and 4-hour durations. Only two cylinders were equipped with thermocouples in the 0.5- and 1-hour tests. Also, during the 1-hour test, cylinder S1 did not begin heating immediately and displayed a delay as it was heated. This was not typical and was not easily explained by a loose connection or melting wires. A feature that was very evident through the 4h600C test was that each

cylinder experienced a slightly different heat curve due to their placement within the kiln. Cylinder S3 was placed closest to the edge of the kiln, nearest the burners, and cylinder S1 was placed closer toward the middle of the kiln. Cylinder S2 was placed between S1 and S3. The heat exposure curves display the slight inconsistency within the kiln, as the temperatures are slightly higher for those cylinders closer to the burners at a specific time.

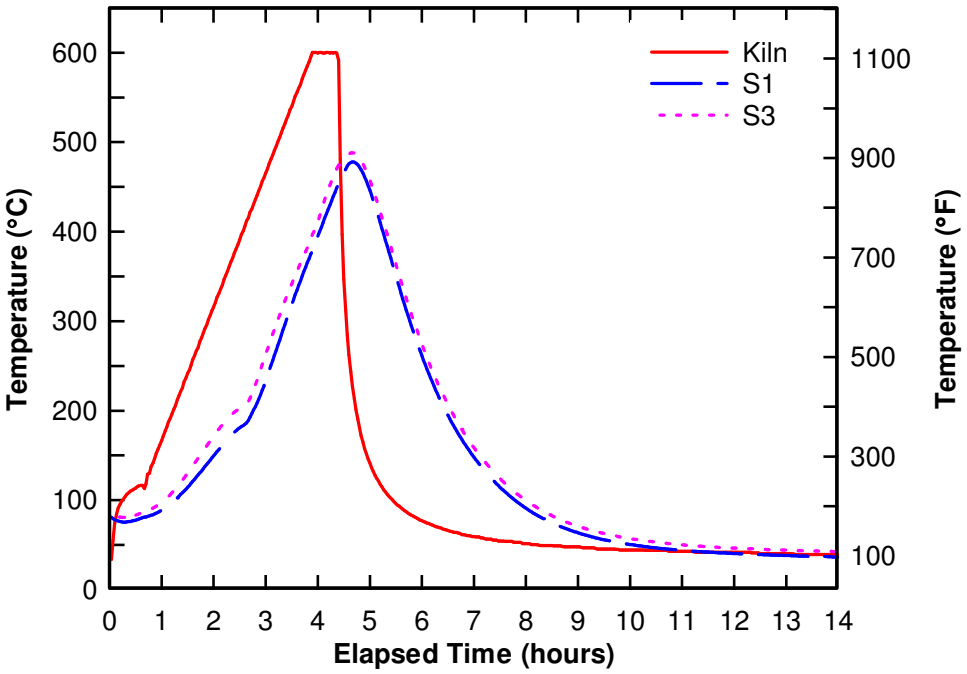

Figure 4.14: 600°C (1112ºF) sustained for 0.5 hours (0.5h600C) heat exposure curves.

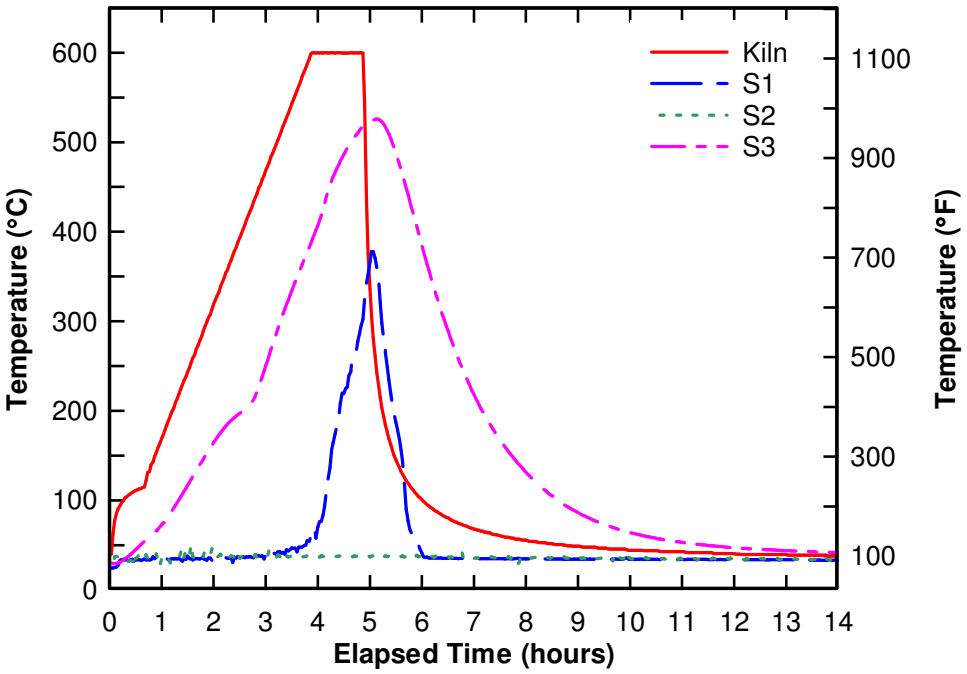

Figure 4.15: 600°C (1112ºF) sustained for 1 hour (1h600C) heat exposure curves.

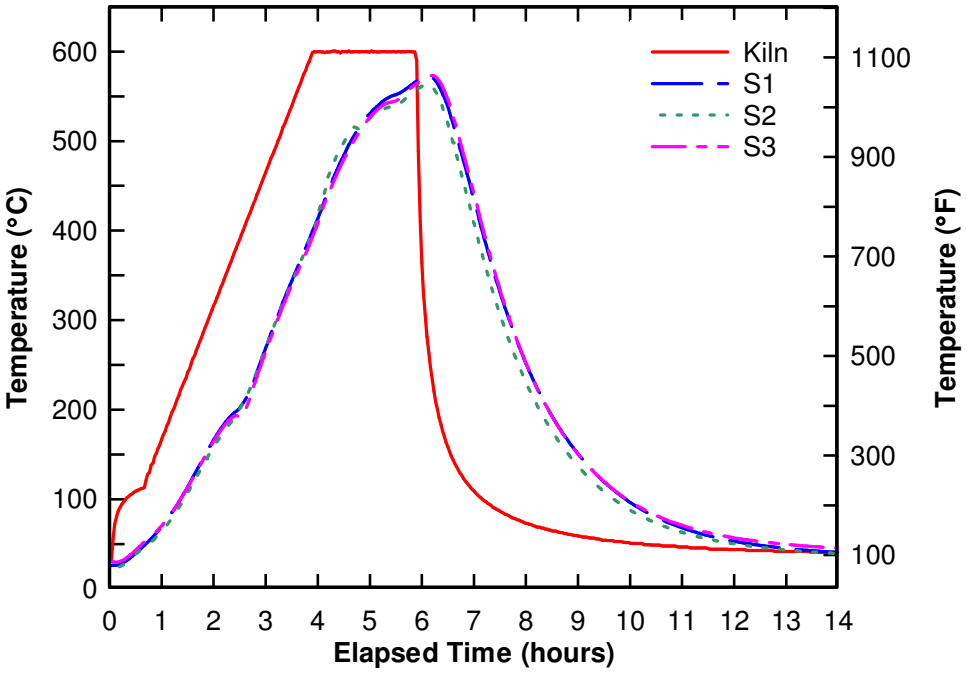

Figure 4.16: 600°C (1112ºF) sustained for 2 hours (2h600C) heat exposure curves.

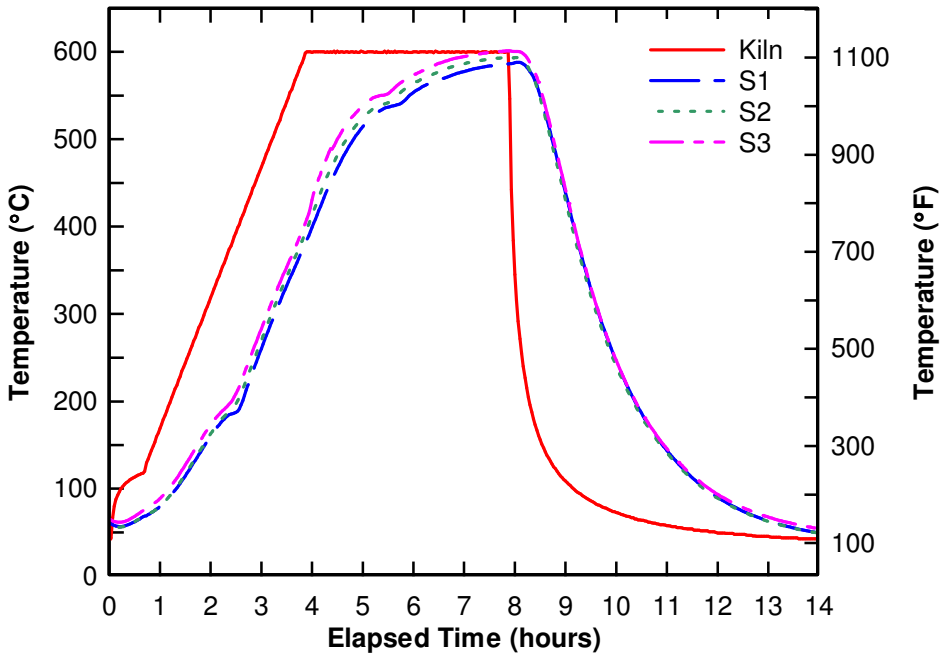

Figure 4.17: 600°C (1112ºF) sustained for 4 hours (4h600C) heat exposure curves.

4.3 Concrete Appearance Post-heating

After being heated, physical changes were observed in color and cracking on the exterior of the concrete cylinders. These physical changes indicated that a change had taken place in the concrete, possibly influencing the material properties.

Color Changes

As concrete was heated to 200°C (392°F), no apparent color changes occurred. The concrete remained the original dark gray color, as if it had not been fired. After the concrete was heated to a maximum temperature of 400°C (752°F), the concrete had a slight pinkish tint. Similarly, concrete heated to a maximum temperature of 500°C

(932°F) also experienced this same color alteration. When heated to 600°C (1112°F), the concrete cylinders experienced a different color change. These cylinders changed color from a dark gray to a light tan, as shown in Figure 4.18. The duration at which the concrete was held at the maximum temperature did not appear to play a role in the extent of the color change.

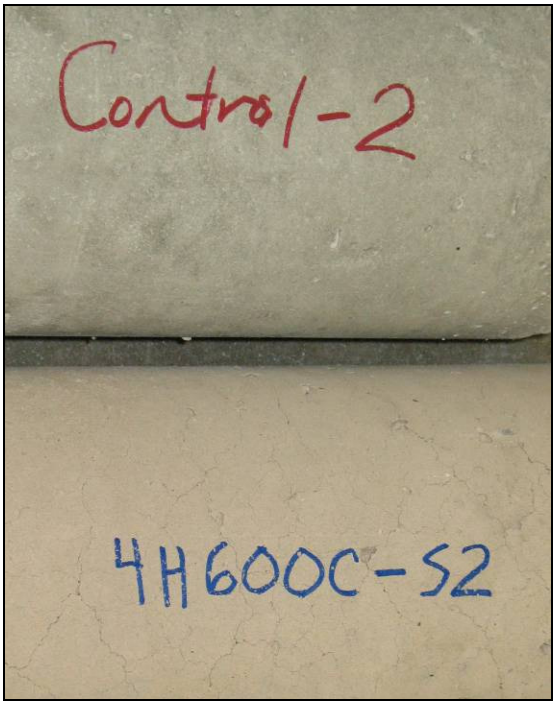

Figure 4.18: Color changes in concrete after a 600ºC (1112ºF) heat exposure compared to unheated control sample.

Cracking Patterns and Extents

As concrete was heated to increasing temperatures, the extent of surface cracking increased. At exposures of 200°C (392°F), no visible surface cracks were recognized on the cylinders. As temperatures were increased to 400°C (752°F), small visible cracks

were noticeable. The cracking appeared to stem from the visible pores and imperfections on the exterior surface, linking these areas with small cracks. As temperatures increased to 500 and 600°C (932 and 1112°F), cracks widened and crack networks expanded. It was assumed that the durations would affect the cracking patterns. However, durations did not affect the crack networks or widths to any noticeable extent, but rather the maximum temperature served as the primary constituent in cracking of the concrete. An example of the cracks formed in concrete exposed to 600ºC (1112ºF) is shown in Figure 4.19.

Figure 4.19: Typical cracking patterns of concrete exposed to 600ºC (1112ºF).

4.4 Concrete Materials Properties

Compressive Strength of Concrete

The compressive strength values for each individual concrete cylinder are shown in Tables 4.7, 4.8, 4.9, and 4.10. Unheated, control concrete cylinders were also tested for comparisons in order to determine average compressive strength losses for each heating regime. The average compressive strengths for each heating regime and average compressive strength losses are shown in Table 4.11. The average compressive strength losses were determined in accordance with Equation 4.3, where $f_{c,avg,c}$ is the average control compressive strength, and $f_{c,avg,n}$ is the average compressive strength of heating regime, n.

$$Loss(\%) = \left(1 - \frac{f_{c,avg,n}}{f_{c,avg,c}}\right) * 100 \tag{4.3}$$

Table 4.7: Compressive strength values for control concrete and concrete exposed to 200ºC (392°F) heating regimes.

Heating Regime	Cylinder Recognition	Actual Compressive Strength, f_c (ksi)	Internal Temperature ºC (°F)
Control	1	7.3	20 (68)
	e	7.2	20 (68)
	3	7.6	20 (68)
1h200C	1	6.0	155 (311)
	2	6.3	155 (311)
	3	6.2	155 (311)
2h200C	1	6.8	187 (369)
	2	6.4	187 (369)
	3	6.4	187 (369)
4h200C	1	6.8	200 (392)
	2	7.5	200 (392)
	3	7.1	200 (392)

Table 4.8: Compressive strengths of concrete exposed to 400ºC (752ºF) heating regimes.

Heating Regime	Cylinder Recognition	Actual Compressive Strength, f_c (ksi)	Internal Temperature ºC (°F)
0.5h400C	1	5.1	297 (567)
	2	4.6	297 (567)
	3	5.1	297 (567)
1h400C	1	3.8	~
	2	3.6	~
	3	3.7	~
2h400C	1	4.0	369 (696)
	2	3.5	369 (696)
	3	3.2	369 (696)
4h400C	1	3.5	~
	2	3.3	~
	3	3.4	~

~ Temperature unknown.

Table 4.9: Compressive strengths of concrete exposed to 500ºC (932ºF) heating regimes.

Heating Regime	Cylinder Recognition	Actual Compressive Strength, f_c (ksi)	Internal Temperature ºC (°F)
0.5h500C	1	3.0	397 (747)
	2	3.0	397 (747)
	3	2.8	397 (747)
1h500C	1	3.5	428 (802)
	2	3.0	428 (802)
	3	3.0	428 (802)
2h500C	1	3.4	476 (889)
	2	2.8	476 (889)
	3	3.3	476 (889)
4h500C	1	2.2	497 (927)
	2	2.4	497 (927)
	3	2.2	497 (927)

Table 4.10: Compressive strengths of concrete exposed to 600ºC (1112ºF) heating regimes.

Heating Regime	Cylinder Recognition	Actual Compressive Strength, f_c (ksi)	Internal Temperature ºC (°F)
0.5h600C	1	2.6	483 (901)
	2	Broken During Heating	483 (901)
	3	2.9	483 (901)
1h600C	1	2.8	526 (979)
	2	2.3	526 (979)
	3	2.1	526 (979)
2h600C	1	2.3	570 (1058)
	2	2.1	570 (1058)
	3	2.1	570 (1058)
4h600C	1	2.2	594 (1101)
	2	2.0	594 (1101)
	3	2.1	594 (1101)

Table 4.11: Average compressive strength values and percentage losses.

Heating Regime	Average Compressive Strength, $f_{c,avg}$ (ksi)	Percentage Loss	COV (%)
Control	7.4	0	2.69
1h200C	6.2	17	2.60
2h200C	6.5	12	3.48
4h200C	7.1	4	5.00
0.5h400C	4.9	34	5.41
1h400C	3.7	50	1.90
2h400C	3.6	52	11.76
4h400C	3.4	54	2.76
0.5h500C	2.9	60	5.13
1h500C	3.2	57	9.34
2h500C	3.2	57	9.74
4h500C	2.3	69	5.41
0.5h600C	2.8	62	7.21
1h600C	2.4	67	13.85
2h600C	2.2	71	4.19
4h600C	2.1	72	4.87

Modulus of Elasticity of Concrete

The modulus of elasticity was determined in accordance with the ASTM C469-02e1 standard. The chord modulus of elasticity, E, was determined in accordance with the standard. The equation for E is shown in Equation 4.4, where S_2 is the stress corresponding to 40 percent of the maximum stress resisted by the cylinder, S_1 is the stress corresponding to a strain of 0.00005, and e_2 is the longitudinal strain of S_2.

$$E = \frac{(S_2 - S_1)}{(e_2 - 0.00005)} \tag{4.4}$$

Tables 4.12, 4.13, 4.14, and 4.15 display the modulus of elasticity values for the concrete cylinders arranged by heating regime, and Table 4.16 displays the average modulus of elasticity values and losses for each heating regime. The average percent losses of the modulus of elasticity values were determined using a similar equation as that used to calculate the percent losses in average compressive strength. Concrete cylinders that were not measured for modulus of elasticity are marked with an asterisk. These cylinders were chosen at random from each heating regime to determine the expected compressive strength for a particular heating regime. Three cylinders were tested for the control concrete because the expected compressive strength was known, based on the specified compressive strength by the manufacturer. According to ACI 318, the modulus of elasticity of concrete is defined by Equation 4.5 (assuming the weight of concrete, w_c, is 145 pcf), where f'_c is the specified strength of the concrete in psi. The percent of the measured modulus of elasticity values compared to the ACI 318 value is provided in Table 4.16, also.

$$E_c(psi) = 57,000\sqrt{f_c'} \tag{4.5}$$

Table 4.12: Modulus of elasticity of control concrete and concrete exposed to 200ºC (392ºF) heating regimes.

Heating Regime	Cylinder Recognition	Modulus of Elasticity, E (ksi)	Internal Temperature ºC (°F)
Control	1	4600	20 (68)
	2	3900	20 (68)
	3	3700	20 (68)
1h200C	1	3300	155 (311)
	2	3500	155 (311)
	3	*	155 (311)
2h200C	1	*	187 (369)
	2	3000	187 (369)
	3	2900	187 (369)
4h200C	1	*	200 (392)
	2	3300	200 (392)
	3	3200	200 (392)

* Cylinders not tested for modulus of elasticity.

Table 4.13: Modulus of elasticity of concrete exposed to 400ºC (752ºF) heating regimes.

Heating Regime	Cylinder Recognition	Modulus of Elasticity, E (ksi)	Internal Temperature ºC (°F)
0.5h400C	1	1900	297 (567)
	2	*	297 (567)
	3	1900	297 (567)
1h400C	1	1400	~
	2	*	~
	3	1300	~
2h400C	1	1500	369 (696)
	2	*	369 (696)
	3	1100	369 (696)
4h400C	1	1200	~
	2	*	~
	3	1200	~

* Cylinders not tested for modulus of elasticity

~ Temperature unknown.

Table 4.14: Modulus of elasticity of concrete exposed to 500ºC (932ºF) heating regimes.

Heating Regime	Cylinder Recognition	Modulus of Elasticity, E (ksi)	Internal Temperature ºC (°F)
0.5h500C	1	1000	397 (747)
	2	900	397 (747)
	3	*	397 (747)
1h500C	1	1000	428 (802)
	2	900	428 (802)
	3	*	428 (802)
2h500C	1	900	476 (889)
	2	*	476 (889)
	3	800	476 (889)
4h500C	1	*	497 (927)
	2	700	497 (927)
	3	600	497 (927)

* Cylinders not tested for modulus of elasticity.

Table 4.15: Modulus of elasticity of concrete exposed to 600ºC (1112ºF) heating regimes.

Heating Regime	Cylinder Recognition	Modulus of Elasticity, E (ksi)	Internal Temperature ºC (°F)
0.5h600C	1	600	483 (901)
	2	*	483 (901)
	3	800	483 (901)
1h600C	1	600	526 (979)
	2	*	526 (979)
	3	500	526 (979)
2h600C	1	400	570 (1058)
	2	*	570 (1058)
	3	400	570 (1058)
4h600C	1	400	594 (1101)
	2	300	594 (1101)
	3	*	594 (1101)

* Cylinders not tested for modulus of elasticity.

Table 4.16: Average modulus of elasticity values, percentage losses, percent of ACI 318 value, and COV.

Heating Regime	Average Modulus of Elasticity, Eavg (ksi)	Percentage Loss (%)	Percent of ACI 318 E (%)	COV (%)
Control	4070	NA	82.4	10.74
1h200C	3390	17	68.7	3.10
2h200C	2930	28	59.4	0.94
4h200C	3260	20	66.0	2.25
0.5h400C	1870	54	37.8	0.66
1h400C	1380	66	27.9	5.94
2h400C	1340	67	27.2	21.60
4h400C	1230	70	24.9	0.20
0.5h500C	960	76	19.5	3.54
1h500C	970	76	19.6	7.94
2h500C	890	78	18.0	8.66
4h500C	680	83	13.9	11.27
0.5h600C	710	83	14.3	11.53
1h600C	540	87	11.0	20.03
2h600C	400	90	8.02	14.51
4h600C	370	91	7.41	8.88

4.5 Steel Material Properties

Tensile Stress of Prestressing Steel

The tensile strength of the steel prestressing strands was considered to be the maximum load resisted by the prestressing steel that results in the rupture of one or more of the strands. From the tensile strength value, the tensile stress was calculated. The approximate tensile strength and tensile stress values for all steel prestressing strand specimens are listed in Tables 4.17, 4.18, 4.19, and 4.20, and the average values of the valid tensile stresses for each heating regime are tabulated in Table 4.21. Those values marked with an asterisk (*) indicate that a fracture between the free span of the gripping jaws occurred, resulting in a valid test result (per ASTM A370-05). Only those marked

with asterisks were used in the average value calculations in Table 4.21. Although the tensile strength of 4h500C-S1 was considered valid, it was not used in the calculation of the average because it had a much lower tensile strength value compared to the other strands within the 4h500C heating regime. It should be noted that although some test results were deemed invalid because of their failure method, those values were often similar to valid results exposed to similar conditions. Also, some heating regimes did not contain any valid failure results. These are marked with a tilde (~), as indicated in Table 4.21, because the results are not applicable in these cases. Those heating regimes containing only one valid test result did not have an applicable coefficient of variation. These values were also marked with a tilde (~).

Table 4.17: Tensile strengths and stresses of control steel prestressing strands and those exposed to 200ºC (392ºF) heating regimes.

Heating Regime	Specimen	Tensile Strength (k)	Tensile Stress (ksi)
Control	T1*	40.0	239.5
	T2*	40.3	241.3
	T3*	42.0	251.5
1h200C	T1	42.7	255.7
	T2	44.6	267.1
	T3	45.4	271.9
2h200C	T1	40.2	240.7
	T2*	41.4	247.9
	T3	46.1	276.0
4h200C	T1	45.8	274.3
	T2	44.8	268.3
	T3*	41.6	249.1

*Indicates valid results.

Table 4.18: Tensile strengths and stresses of control steel prestressing strands and those exposed to 400ºC (752ºF) heating regimes.

Heating Regime	Specimen	Tensile Strength (k)	Tensile Stress (ksi)
0.5h400C	T1	41.1	246.1
	T2	35.4	212.0
	T3	39.2	234.7
1h400C	T1*	43.8	262.3
	T2*	39.0	233.5
	T3*	39.5	236.5
2h400C	T1	39.0	233.5
	T2	42.7	255.7
	T3	41.6	249.1
4h400C	T1*	19.7	118.0
	T2*	30.8	184.4
	T3*	31.2	186.8

*Indicates valid results.

Table 4.19: Tensile strengths and stresses of control steel prestressing strands and those exposed to 500ºC (932ºF) heating regimes.

Heating Regime	Specimen	Tensile Strength (k)	Tensile Stress (ksi)
0.5h500C	T1	34.4	206.0
	T2	31.9	191.0
	T3*	31.3	187.4
1h500C	T1*	31.6	189.2
	T2	35.1	210.2
	T3	31.2	186.8
2h500C	T1*	27.4	164.1
	T2*	26.9	161.1
	T3*	27.4	164.1
4h500C	T1*	25.1	150.3
	T2*	29.5	176.6
	T3*	29.6	177.2

*Indicates valid results.

Table 4.20: Tensile strengths and stresses of control steel prestressing strands and those exposed to 600ºC (1112ºF) heating regimes.

Heating Regime	Specimen	Tensile Strength (k)	Tensile Stress (ksi)
0.5h600C	T1	23.3	139.5
	T2	25.9	155.1
	T3*	24.0	143.7
1h600C	T1*	22.0	131.7
	T2	22.2	132.9
	T3	21.7	129.9
2h600C	T1*	20.1	120.4
	T2	20.7	124.0
	T3	20.0	119.8
4h600C	T1	20.8	124.6
	T2	20.9	125.1
	T3	20.2	121.0

*Indicates valid results.

Table 4.21: Average valid tensile stress values of steel prestressing strand specimens.

Heating Regime	Average Tensile Stress (ksi)	COV (%)
Control	244	3
1h200C	~ 275	~3
2h200C	248	~7
4h200C	249	~6
0.5h400C	~ 231	~5
1h400C	244	6
2h400C	~ 246	~5
4h400C	186	21
0.5h500C	187	~5
1h500C	189	~7
2h500C	163	1
4h500C	168	9
0.5h600C	144	~6
1h600C	132	~1
2h600C	120	~2
4h600C	~ 124	~2

~ Indicates results are not applicable.

Modulus of Elasticity of Prestressing Steel

The modulus of elasticity, E, was determined by generating a trend line using Microsoft Excel to calculate the slope of a selected portion of the elastic region of the stress-strain curve. The selected portion was typically located within the middle of the elastic region measured. An example of this procedure is shown in Figure 4.20. For each heating regime, two specimens were tested to determine the modulus of elasticity since the first specimen for each heating regime was tested to rupture in order to determine a safe range of loading over which to measure deflections of subsequent specimens. Tables 4.22, 4.23, 4.24, and 4.25 contain the modulus of elasticity values for all steel specimens, and the steel specimens not used to determine modulus of elasticity values are marked by an asterisk. Table 4.26 contains the average modulus of elasticity values for each heating regime and indicates the variability of the specimens by the coefficient of variation.

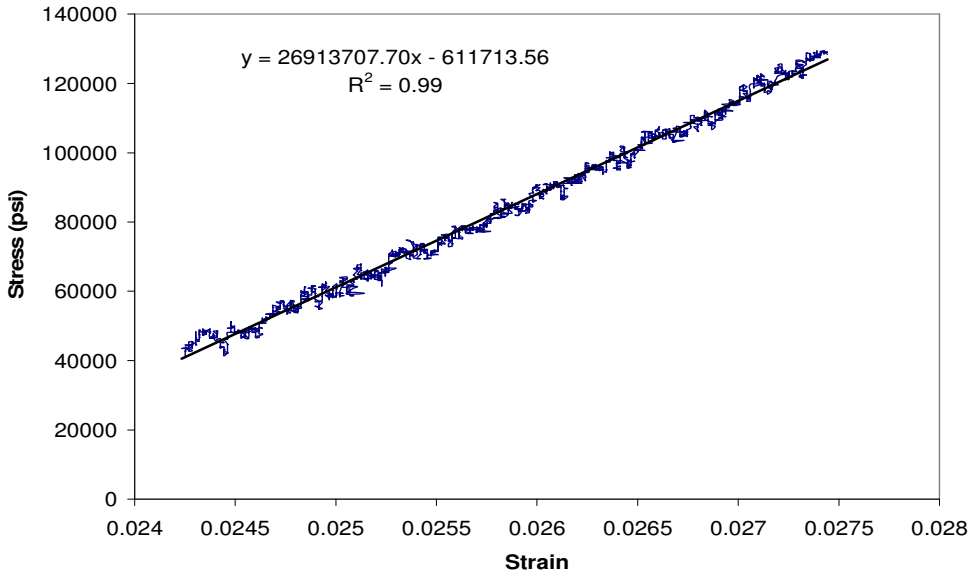

Figure 4.20: Graphical determination of the modulus of elasticity of prestressing steel (4h200C-S3).

Table 4.22: Modulus of elasticity values for control steel prestressing strands and those exposed to 200ºC (392ºF) heating regimes.

Heating Regime	Specimen	Modulus of Elasticity, E (ksi)
Control	T1	*
	T2	30,700
	T3	28,100
1h200C	T1	*
	T2	30,100
	T3	30,500
2h200C	T1	*
	T2	26,500
	T3	29,800
4h200C	T1	*
	T2	27,300
	T3	26,900

*Specimen not tested for modulus of elasticity.

Table 4.23: Modulus of elasticity values for steel prestressing strands exposed to 400ºC (752ºF) heating regimes.

Heating Regime	Specimen	Modulus of Elasticity, E (ksi)
0.5h400C	T1	*
	T2	26,400
	T3	24,300
1h400C	T1	*
	T2	23,900
	T3	23,900
2h400C	T1	*
	T2	29,900
	T3	47,300
4h400C	T1	*
	T2	24,700
	T3	30,200

*Specimen not tested for modulus of elasticity.

Table 4.24: Modulus of elasticity values for steel prestressing strands exposed to 500ºC (932ºF) heating regimes.

Heating Regime	Specimen	Modulus of Elasticity, E (ksi)
0.5h500C	T1	*
	T2	26,700
	T3	26,800
1h500C	T1	*
	T2	31,000
	T3	27,400
2h500C	T1	*
	T2	22,100
	T3	24,000
4h500C	T1	*
	T2	27,700
	T3	28,700

*Specimen not tested for modulus of elasticity.

Table 4.25: Modulus of elasticity values for steel prestressing strands exposed to 600ºC (1112ºF) heating regimes.

Heating Regime	Specimen	Modulus of Elasticity, E (ksi)
0.5h600C	T1	*
	T2	18,700
	T3	29,200
1h600C	T1	*
	T2	23,800
	T3	20,900
2h600C	T1	*
	T2	22,000
	T3	23,700
4h600C	T1	*
	T2	21,700
	T3	21,200

*Specimen not tested for modulus of elasticity.

Table 4.26: Average modulus of elasticity values for each heating regime.

Heating Regime	Average Modulus of Elasticity (ksi)	COV (%)
Control	29,400	6
1h200C	30,300	1
2h200C	28,150	8
4h200C	27,100	1
0.5h400C	25,350	6
1h400C	23,900	0
2h400C	29,900	NA
4h400C	27,450	14
0.5h500C	26,750	0
1h500C	29,200	9
2h500C	23,050	6
4h500C	28,200	3
0.5h600C	29,200	NA
1h600C	22,350	9
2h600C	22,850	5
4h600C	21,450	2

4.6 Bond Properties

The bond changes for each cylinder were compared based on two parameters. The first parameter was the maximum load reached during testing as the steel strand was pulled from the cylinder. The second parameter was the computed maximum bond stress developed assuming a linear distribution of stress along the embedded length. In each sample, the maximum internal temperature of the concrete cylinder measured by the thermocouple was assumed to be the maximum temperature experienced by the bond area.

Maximum Average Load

As shown in Tables 4.27, 4.28, 4.29, and 4.30, the maximum load reached in each heating regime decreased with increasing temperature and duration. Table 4.31 contains the average maximum load values for each heating regime, revealing the highest variation among specimens in maximum load values occurs with the control specimens, having a coefficient of variation of 25 percent.

Table 4.27: Maximum loads for Control and 200°C (392°F) heating regime bond specimens.

Heating Regime	Specimen	Maximum Load (lb)
Control	S1	7500
	S2	7700
	S3	11,500
1h200C	S1	6900
	S2	7600
	S3	7600
2h200C	S1	6100
	S2	5000
	S3	6100
4h200C	S1	6100
	S2	5300
	S3	4800

Table 4.28: Maximum loads for 400°C (752°F) heating regime bond specimens.

Heating Regime	Specimen	Maximum Load (lb)
0.5h400C	S1	5000
	S2	4600
	S3	4900
1h400C	S1	4900
	S2	4900
	S3	3400
2h400C	S1	3900
	S2	4700
	S3	4000
4h400C	S1	4000
	S2	3600
	S3	3900

Table 4.29: Maximum loads for 500°C (932°F) heating regime bond specimens.

Heating Regime	Specimen	Maximum Load (lb)
0.5h500C	S1	3200
	S2	3600
	S3	3200
1h500C	S1	2800
	S2	3200
	S3	3900
2h500C	S1	3300
	S2	4000
	S3	3300
4h500C	S1	2700
	S2	4000
	S3	3700

Table 4.30: Maximum loads for Control and 600°C (1112°F) heating regime bond specimens.

Heating Regime	Specimen	Maximum Load (lb)
0.5h600C	S1	4100
	S2	3400
	S3	3400
1h600C	S1	3500
	S2	3300
	S3	3500
2h600C	S1	2600
	S2	2400
	S3	2500
4h600C	S1	2600
	S2	2300
	S3	2900

Table 4.31: Average maximum loads and coefficient of variation for each heating regime.

Heating Regime	Average Maximum Load (lb)	COV (%)
Control	8900	25
1h200C	7400	5
2h200C	5700	10
4h200C	5400	12
0.5h400C	4800	5
1h400C	4400	20
2h400C	4200	11
4h400C	3800	6
0.5h500C	3300	8
1h500C	3300	16
2h500C	3500	10
4h500C	3500	18
0.5h600C	3700	11
1h600C	3400	3
2h600C	2500	3
4h600C	2600	11

Maximum Bond Stress

The maximum bond stress was also used as a relative comparison of the bond changes after exposure to high temperatures. The bond stresses, μ, were calculated by dividing the pull-out load, F_{PO}, by an estimated surface area of the steel prestressing strand in the cylinder at that time as shown in Equation 4.6. A value of $C_b = 1.45$ was used as the estimated circumference in inches of the steel prestressing strand, based on a cross-sectional area of 0.167 square inches of the steel prestressing strand determined from the PCI Design Handbook (PCI 2004). The length of steel strand in the concrete cylinder was determined by subtracting the amount of slippage, l_s, measured by an LVDT from the original embedment length, l_e, of 6 inches.

$$\mu = \frac{F_{PO}}{C_b(l_e - l_s)} \tag{4.6}$$

The maximum bond stress values for each individual cylinder are listed in Tables 4.32, 4.33, 4.34, and 4.35. These values also reveal a decrease in bond with exposure to high temperatures. The average maximum bond stresses for all heating regimes are shown in Table 4.36, revealing that the data has similar inconsistencies as the maximum load data. A relatively larger variation in values is present among the control samples, as well as the 4h200C and 4h600C heating regimes.

Table 4.32: Maximum bond stresses for control and 200°C (392°F) heating regime bond specimens.

Heating Regime	Specimen	Maximum Bond Stress (psi)
Control	S1	1307
	S2	1123
	S3	1805
1h200C	S1	1199
	S2	1171
	S3	1452
2h200C	S1	994
	S2	1110
	S3	960
4h200C	S1	994
	S2	1254
	S3	870

Table 4.33: Maximum bond stresses for 400°C (752°F) heating regime bond specimens.

Heating Regime	Specimen	Maximum Bond Stress (psi)
0.5h400C	S1	678
	S2	591
	S3	630
1h400C	S1	629
	S2	628
	S3	517
2h400C	S1	707
	S2	648
	S3	563
4h400C	S1	544
	S2	598
	S3	556

Table 4.34: Maximum bond stresses for 500°C (932°F) heating regime bond specimens.

Heating Regime	Specimen	Maximum Bond Stress (psi)
0.5h500C	S1	412
	S2	502
	S3	474
1h500C	S1	456
	S2	384
	S3	503
2h500C	S1	543
	S2	515
	S3	455
4h500C	S1	461
	S2	515
	S3	502

Table 4.35: Maximum bond stresses for 600°C (1112°F) heating regime bond specimens.

Heating Regime	Specimen	Maximum Bond Stress (psi)
0.5h600C	S1	541
	S2	439
	S3	463
1h600C	S1	467
	S2	512
	S3	498
2h600C	S1	356
	S2	360
	S3	369
4h600C	S1	454
	S2	336
	S3	437

Table 4.36: Average maximum bond stress and coefficient of variation for all heating regimes.

Heating Regime	Average Maximum Bond Stress (psi)	COV (%)
Control	1410	25
1h200C	1270	12
2h200C	1020	8
4h200C	1040	19
0.5h400C	630	7
1h400C	590	11
2h400C	640	11
4h400C	570	5
0.5h500C	460	10
1h500C	450	13
2h500C	500	9
4h500C	490	6
0.5h600C	480	11
1h600C	490	5
2h600C	360	2
4h600C	410	16

4.7 Thermogravimetric Analysis

Thermogravimetric analysis (TGA) was analyzed as a tool for generating temperature profiles in heat-affected concrete. Initial tests incorporated cement paste and mortar samples to determine the effectiveness of TGA on estimating maximum temperature exposure of cementitious materials. Samples were then extracted from a bond strength concrete specimen to generate a heat gradient throughout the cylinder, with known temperatures at the center and exterior.

Cement Paste Samples

Samples were subjected to heat treatments in the TGA machine, as described in Chapter Three. The TGA results of the cement paste samples after heat treatments are presented in Figure 4.21. The initial weight loss of the control sample is due to water loss, and the mass losses at approximately 450 and 700°C (800 and 1290°F) indicate the amount of calcium-hydroxide and calcium-carbonate present in the sample, respectively. These are known temperatures of microstructural changes, as noted by other researchers (Alarcon-Ruiz et al. 2004). These TGA values were normalized such that 100 percent was the sample mass immediately following the cooling process of the heat treatment. This is shown in Figure 4.22, indicating a percentage of mass-loss with increasing temperature for each heat treatment. It is shown here that immediately following the heat treatment, there is a relatively small mass gain. The reason for this increase in mass is unknown.

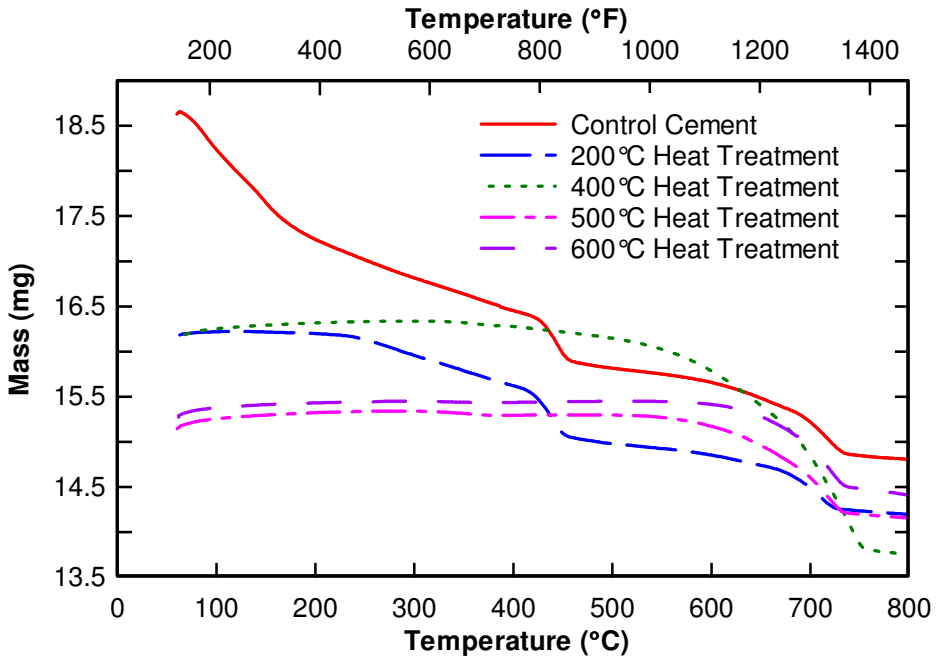

Figure 4.21: TGA results of cement paste heat treatments.

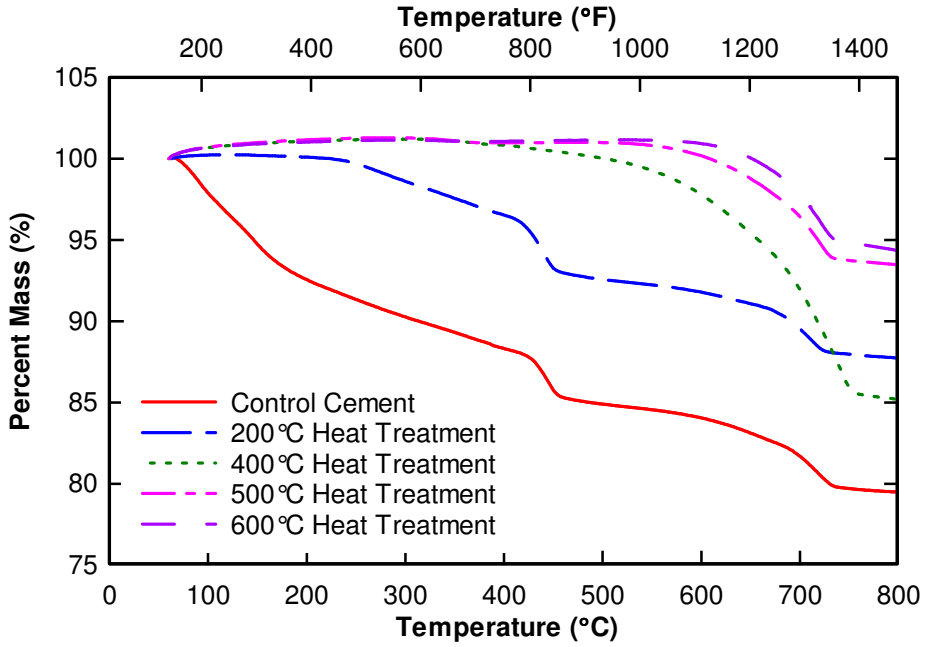

Figure 4.22: Normalized cement paste heat treatment data.

Mortar Samples

The use of TGA as a means of analyzing heat-affected mortar samples was also evaluated in a similar controlled experiment. Results from the heat treatments of mortar samples displayed that the additional sand component resulted in generally lower weight losses at the expected temperature locations, as shown in Figure 4.23. The sand within the mortar mixture caused the reduction in weight loss, because it does not undergo the same microstructural changes as cement during the heating process. These values are normalized in Figure 4.24. Again, the mass increased a small amount following the pre-heating, or heat treatment, of the samples.

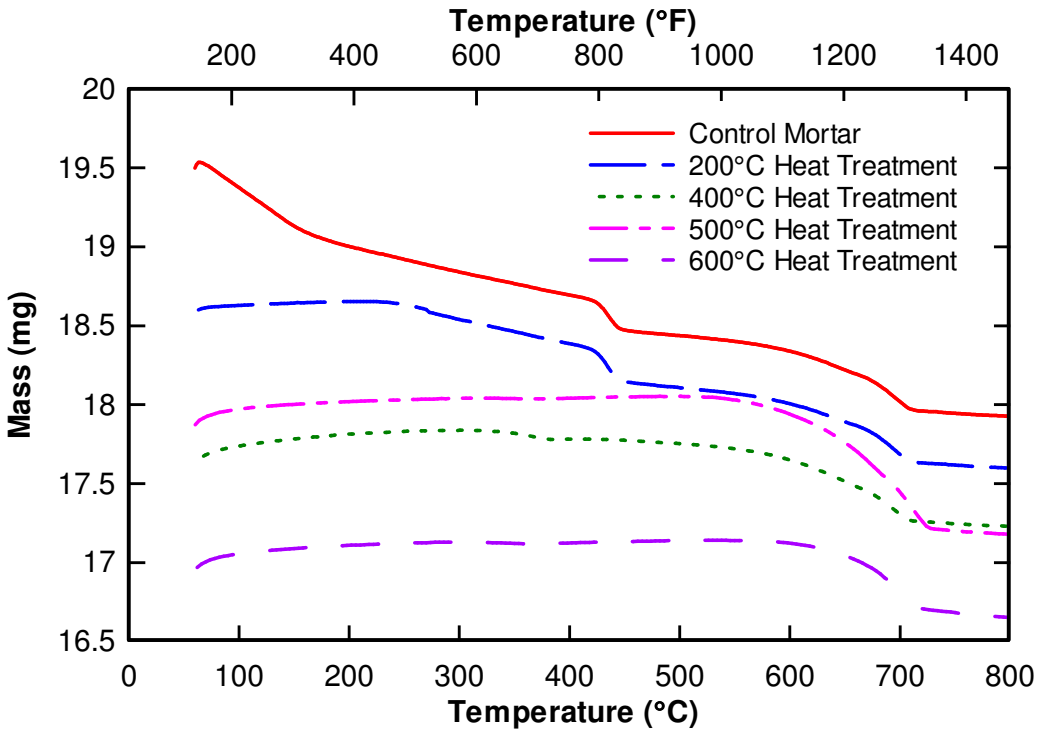

Figure 4.23: TGA results of mortar sample heat treatments.

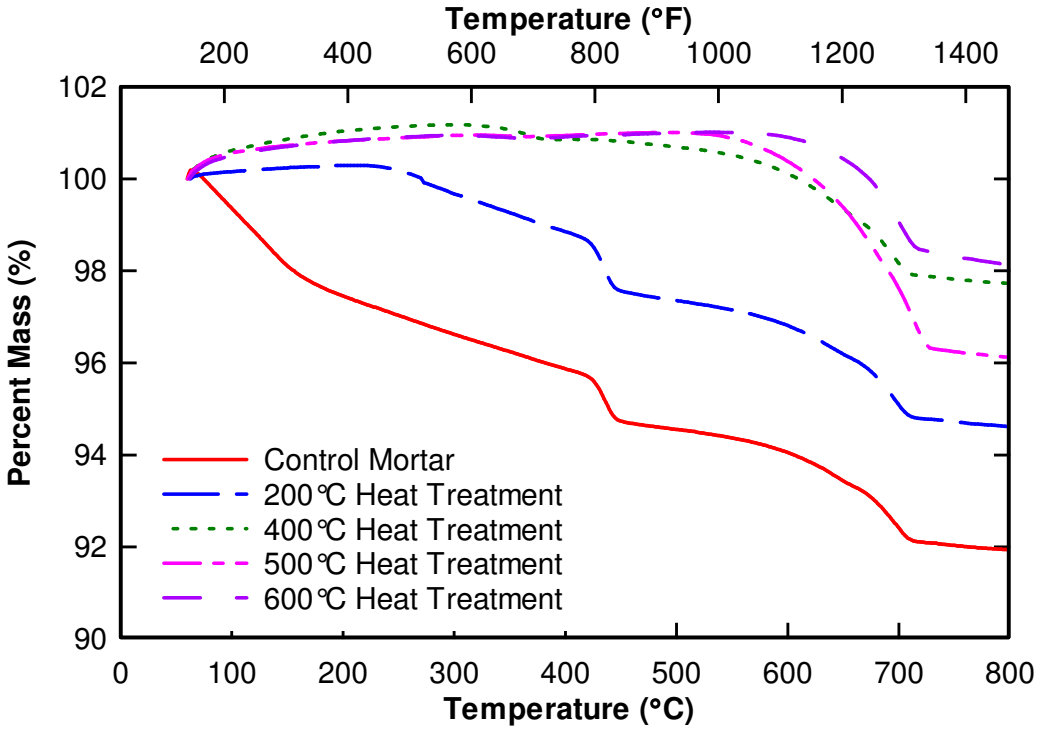

Figure 4.24: Normalized mortar TGA heat treatment data.

Concrete Heat Contours

The 1h500C-S2 specimen was evaluated using TGA as a means to predict temperature contours within the concrete cylinder. Samples were taken at 1-inch increments through the cross-section of the center of the cylinder, as shown previously in Chapter 3. Each point was labeled between 0 and 6, indicating the number of inches from the bottom exterior of the concrete cylinder. The internal temperature of the concrete cylinder reached 426°C (800°F), according to the heat profile for this specific cylinder. Other known points include the top and bottom exteriors, which were assumed to have reached the maximum air temperature of the kiln. Normalized TGA results

represented as a percent of the original mass of each point evaluated within the concrete cylinder are shown in Figures 4.25, 4.26, 4.27, and 4.28. An unheated, control sample is also included as a comparison. Figure 4.25 represents the two exterior samples, and Figure 4.26 represents the two samples taken at 1 in. from the exterior surface. Figure 4.27 represents the samples taken from 2 in. inside the exterior surface, and Figure 4.28 represents the sample taken from the center of the concrete cylinder, near the thermocouple.

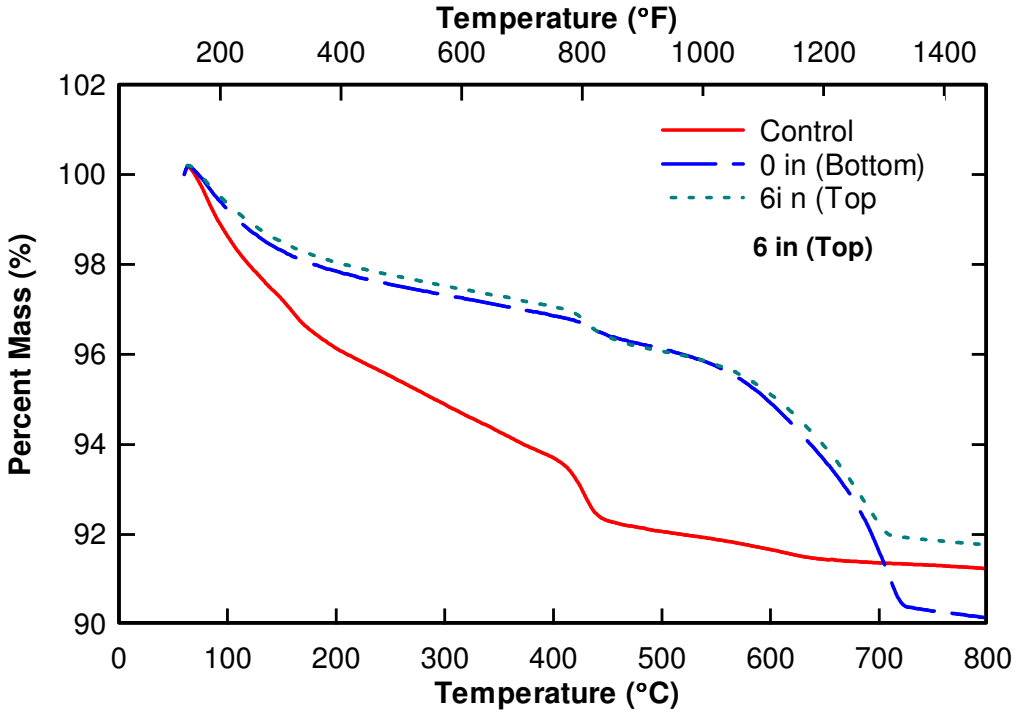

Figure 4.25: Normalized TGA data of Control, 0 in. (Bottom), and 6 in. (Top) concrete samples.

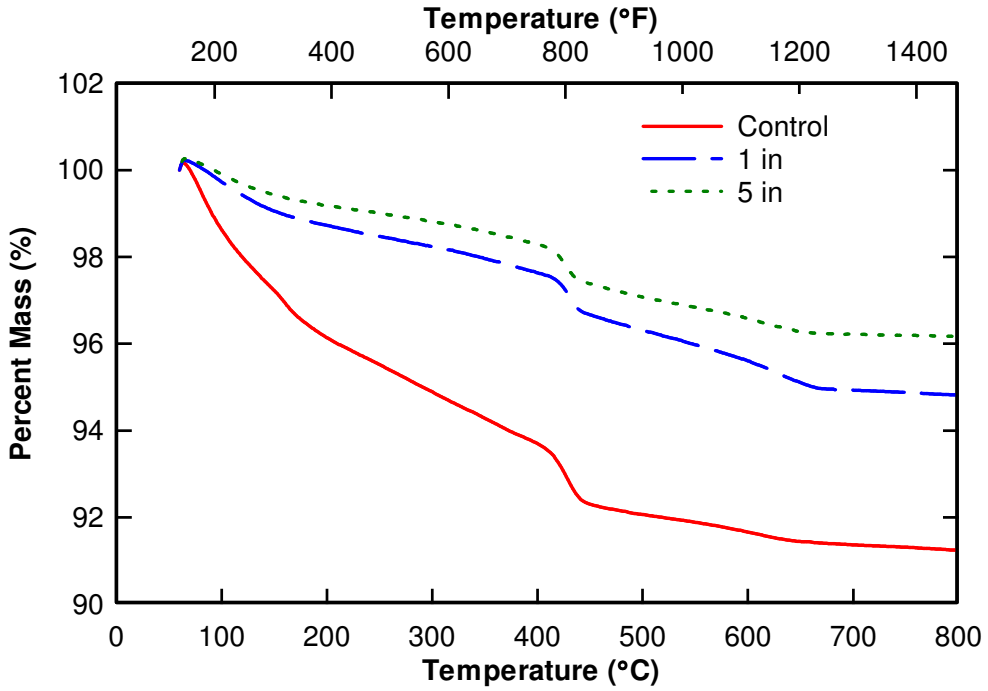

Figure 4.26: Normalized TGA data for Control, 1 in., and 5 in. concrete samples.

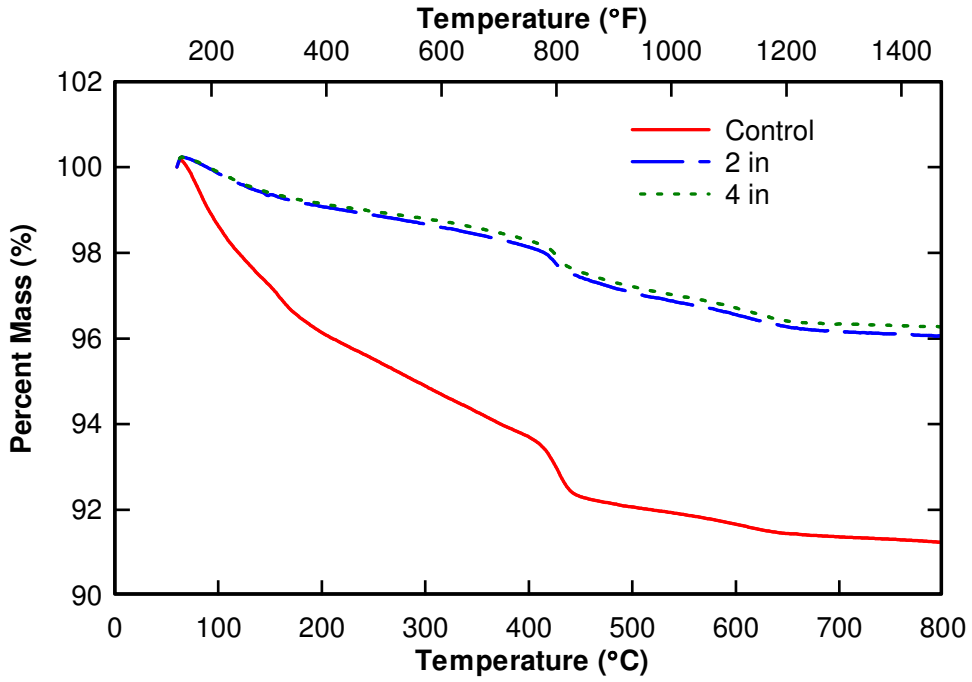

Figure 4.27: Normalized TGA data for Control, 2 in., and 4 in. concrete samples.

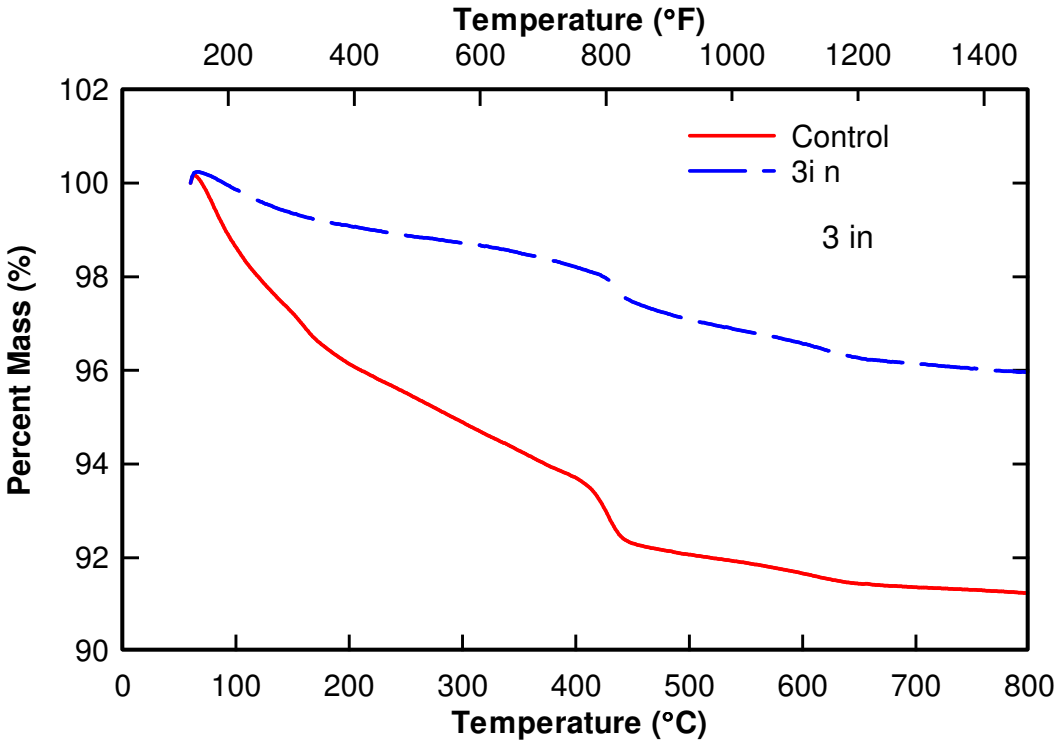

Figure 4.28: Normalized TGA results of Control and 3 in. concrete samples.

CHAPTER FIVE

EXPERIMENTAL RESULTS DISCUSSION

The experimental results reveal that apparent trends exist as concrete, prestressing steel, and bond specimens are exposed to elevated temperatures. A detailed discussion of all results is presented in this Chapter to better understand the information presented previously in Chapter Four.

5.1 Low Temperature Drying Weight Changes

As concrete was pre-heated, the evaporable water was reduced. For the purposes of this study, the evaporable water was reduced to be sure that all cylinders remained in tact so that data was obtainable for all heating exposures. By incorporating the low temperature drying process, explosive spalling was prevented, proving that this method was a successful process for preserving the concrete specimens. This method could possibly have been avoided by waiting for the concrete to age prior to testing, although it served as a proper alternative for testing "green" concrete. It was assumed that the concrete would be affected primarily by the maximum temperature of each heating regime rather than the low temperature drying process. This method also showed that when moisture was minimized in concrete, explosive spalling did not occur at temperatures at or below 600ºC (1112ºF).

5.2 Heat Exposure Curves

The heat exposure curves provided information on the heat transfer through concrete. By taking the averages of the heat exposure curves for each heating regime, this transfer was easily evaluated. The averages were based on reasonable heat exposure results, excluding any curves that were inconsistent with the general trend. In some instances, the average curve for a specific heating regime was based on a single heat exposure curve from one bond specimen.

0.5-hour Heat Exposure Curves

The 0.5-hour duration curves are shown in Figure 5.1. In these exposure curves, it can be seen that the maximum of each curve is approximately 100°C (212°F) below the air temperature held constant in the kiln. The 0.5h600C, 0.5h500C, and 0.5h400C curves reached maximum temperatures of 483°C, 397°C, and 297°C (900, 750, and 570°F), respectively. Each curve displays a similar increase in temperature throughout the *Heating* and *Duration Phases*. At approximately 200°C (392°F), the heat transfer appeared to experience a change, most distinctly shown in the 0.5h600C curve. The reason for this change in the heat-transfer is unknown.

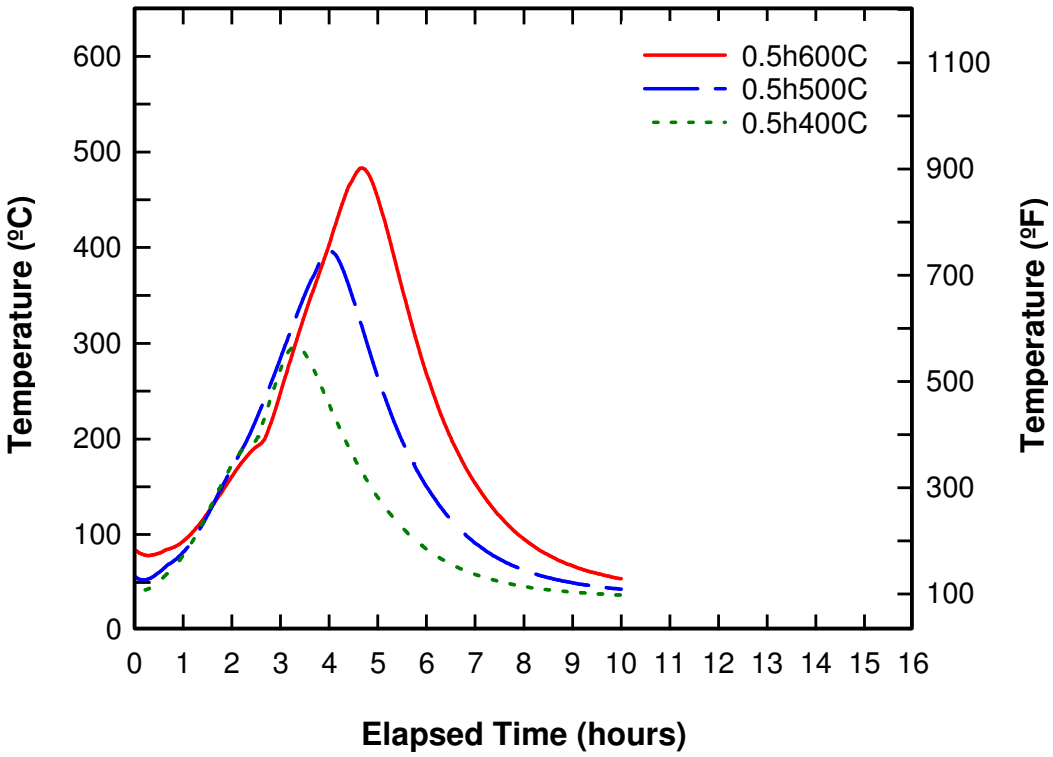

Figure 5.1: 0.5-hour duration average heat exposure curves.

1-hour Heat Exposure Curves

The 1-hour average heat exposure curves are shown in Figure 5.2. In these curves, it is more evident that there was a change in heat transfer at approximately 200°C (392°F), followed by a continuous increase in heat transfer. The maximum temperature reached for the 200, 500, and 600°C (392, 932, and 1112°F) average curves was 161, 428, and 526°C (260, 740, and 910°F), respectively. For the 500 and 600°C (932 and 1112°F) curves, this difference was approximately 70°C (90°F) lower than the maximum

air temperature. However, the 200°C (392°F) curve was approximately 40°C (40°F) lower than the maximum air temperature.

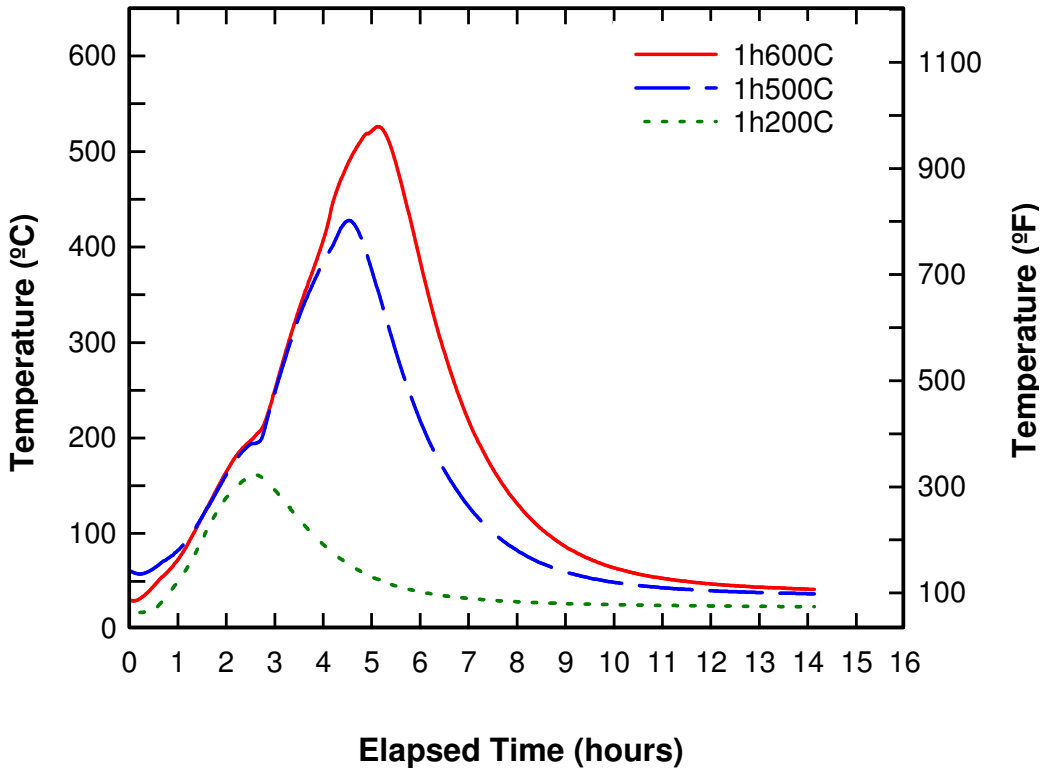

Figure 5.2: 1-hour duration average heat exposure curves.

2-hour Heat Exposure Curves

The 2-hour average heat exposure curves are shown in Figure 5.3. Heat exposure curves for all maximum temperatures were available for the 2-hour duration. With the 2-hour tests, the heat transfer changes at approximately 200°C (392°F) with the 400, 500, and 600°C (752, 932, and 1112°F) average curves. Another similar response was shown to occur at approximately 550°C (1020°F) in the 2h600C curve, similar to the change in

heat transfer at 200°C (392°F). At this point, a known significant microstructural change in the concrete occurs. Between approximately 450 and 550°C (780 and 960°F) the calcium hydroxide within the cement dehydroxylates (Alarcon-Ruiz et al. 2005). The 200, 400, 500, and 600°C (392, 752, 932, and 1112°F) average curves reached maximum temperatures of 187, 365, 483, and 570°C (370, 690, 900, and 1060°F), respectively. The differences ranged between 13 and 35°C (55 and 95°F) from the maximum air temperatures of the kiln. By moving the 2h200C and 2h400C quickly from the pre-heating stage to the scheduled heating regime, the initial temperature of the heat exposure curves are slightly higher because these cylinders were undergoing a cooling phase at the beginning of the kiln *Heating Phase.* As the kiln began heating, these cylinders were already at temperatures well above the air temperature in the kiln. This did pose a problem, because the heat exposures for these heating regimes had different initial conditions, resulting in inaccurate comparisons.

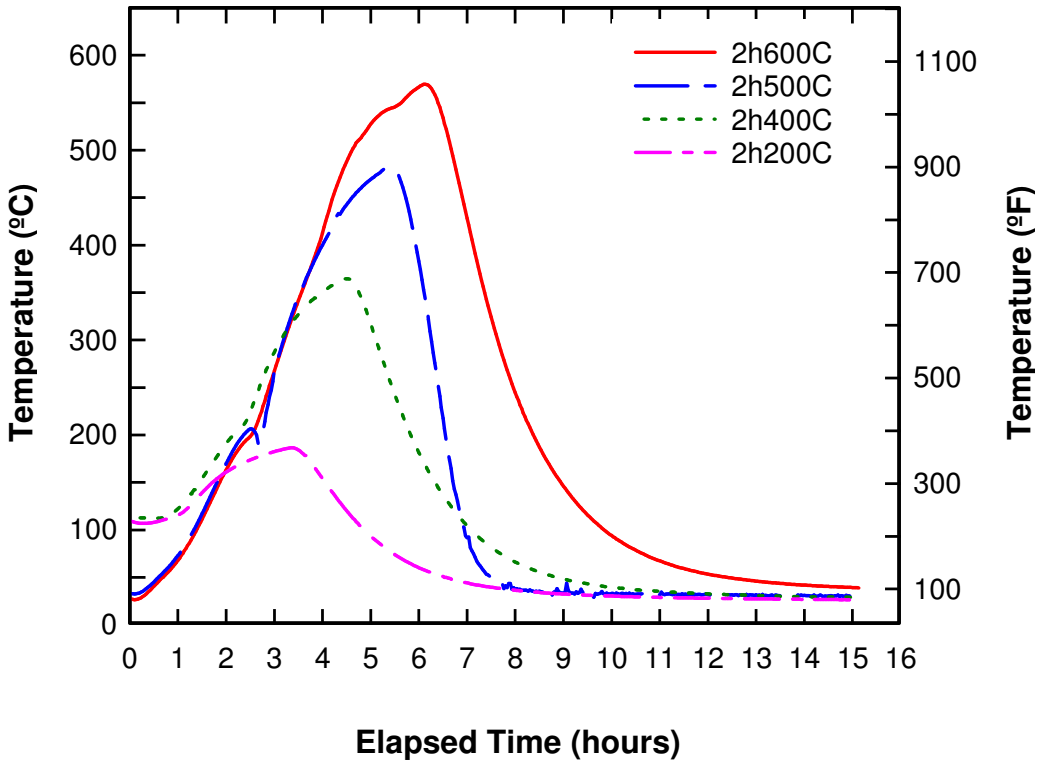

Figure 5.3: 2-hour duration average heat exposure curves.

4-hour Heat Exposure Curves

The 4-hour average heat exposure curves are shown in Figure 5.4. Similar features are noticeable in these heat exposure curves, as in previous tests. For example, the 500 and 600°C (932 and 1112°F) curves display the same change in heat transfer at approximately 200°C (392°F), and the 4h600C curve displays a similar response at approximately 550°C (1020°F). Another noticeable feature in the curves is that as time progresses through each heating regime, the heat transfer rate reduces as the maximum temperature is held. This was expected based on the lazy "S" shape discussed in Chapter

4. After 4 hours, the center of the concrete had nearly reached the maximum air temperature of the heating regime. The 200, 500, and 600°C (392, 932, and 1112°F) tests reached maximum temperatures of 200, 494, and 594°C (392, 920, and 1100°F), respectively. These curves revealed that through extended exposures of a high temperature for at least 4 hours, concrete within three inches of the surface can be affected. This suggests that clear cover required for a 4-hour fire rating should be larger than 3 inches to protect steel from high temperature exposure.

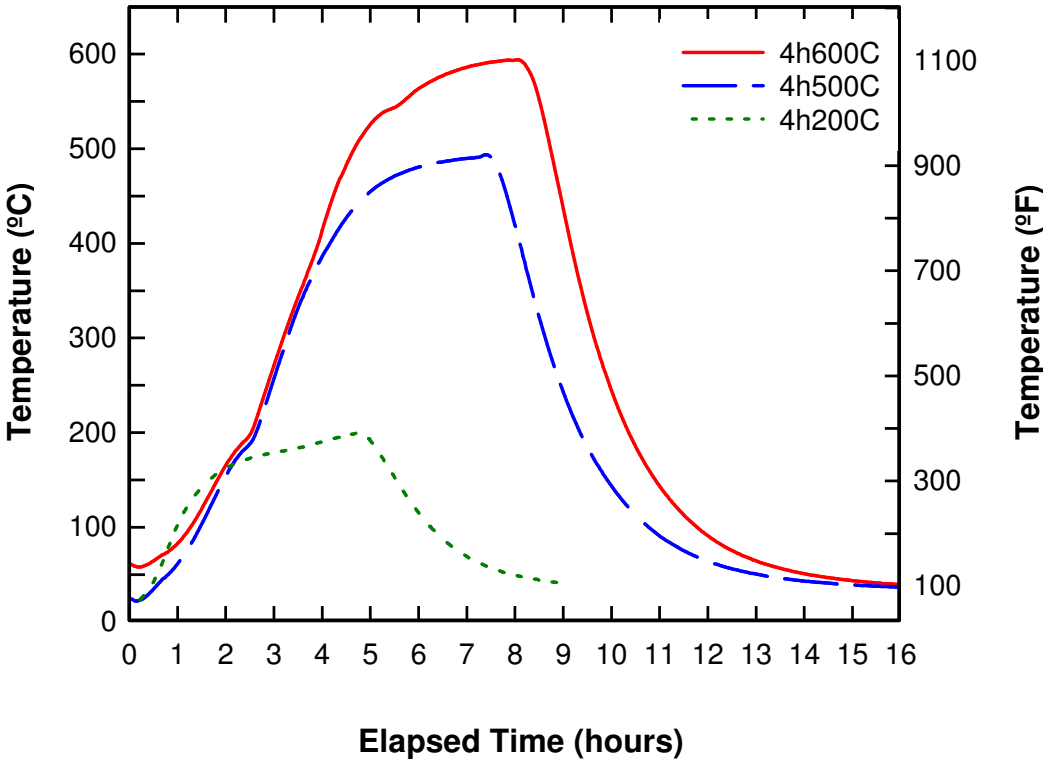

Figure 5.4: 4-hour duration average heat exposure curves.

5.3 Concrete Appearance Post-heating

Color and surface cracking changes became more distinct as the maximum temperature of exposure increased. Color changes in concrete have been attributed to chemical reactions by other researchers. These researchers claim that the majority of color changes tend to be related to aggregate (St John et al. 1998, Geogali et al. 2004). However, after breaking the concrete cylinders, the aggregates were not discolored, indicating that the color change was likely not affected by the aggregate.

The cracking patterns and network expansions were similar to those mentioned by other researchers (St John et al. 1998, Chang et al. 2006). A factor that likely affected the cracking patterns and network expansions was the cooling phase. The internal temperature of the concrete lagged behind the exterior during the Cooling Phase. The temperature differences between the exterior and interior of the concrete at this time likely attributed to a majority of the cracking.

5.4 Concrete Material Properties

Compressive Strength

As concrete cylinders were exposed to high temperatures for an increased amount of time, compressive strength losses increased slowly, as shown in Figure 5.5. From left to right, heat and duration are increased to display the effects of both increasing temperature and increasing duration on the compressive strength of cylindrical concrete specimens. Figure 5.6 shows the percentage of average compressive strength retained in

the concrete cylinders for each heating regime compared to control specimens, in which no heating was applied to the concrete.

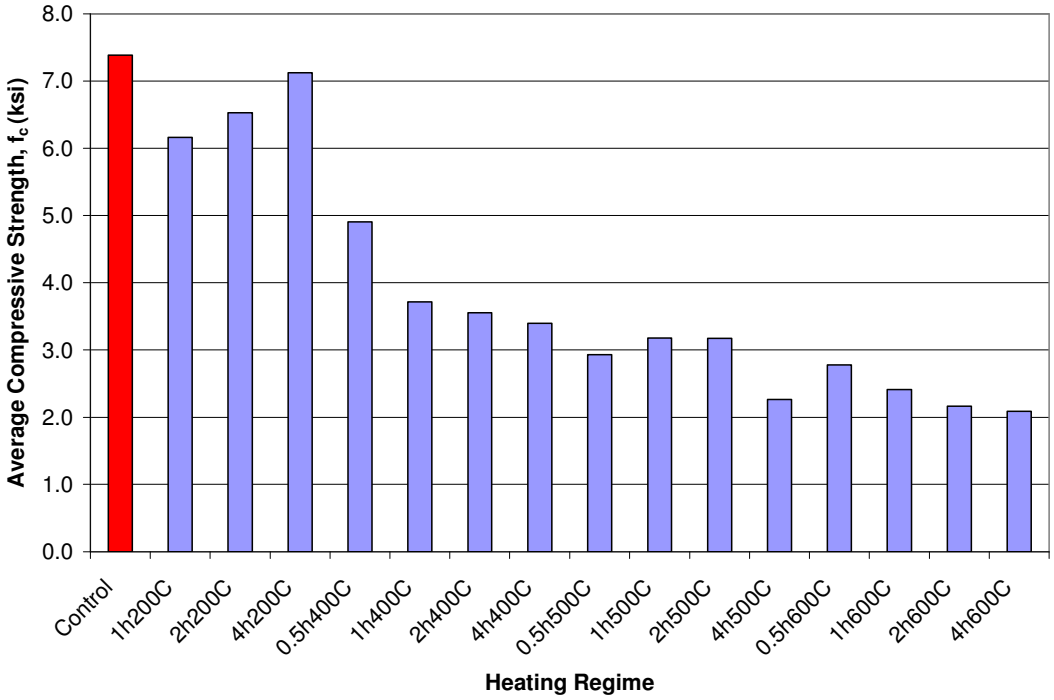

Figure 5.5: Average compressive strength of concrete for all heating regimes.

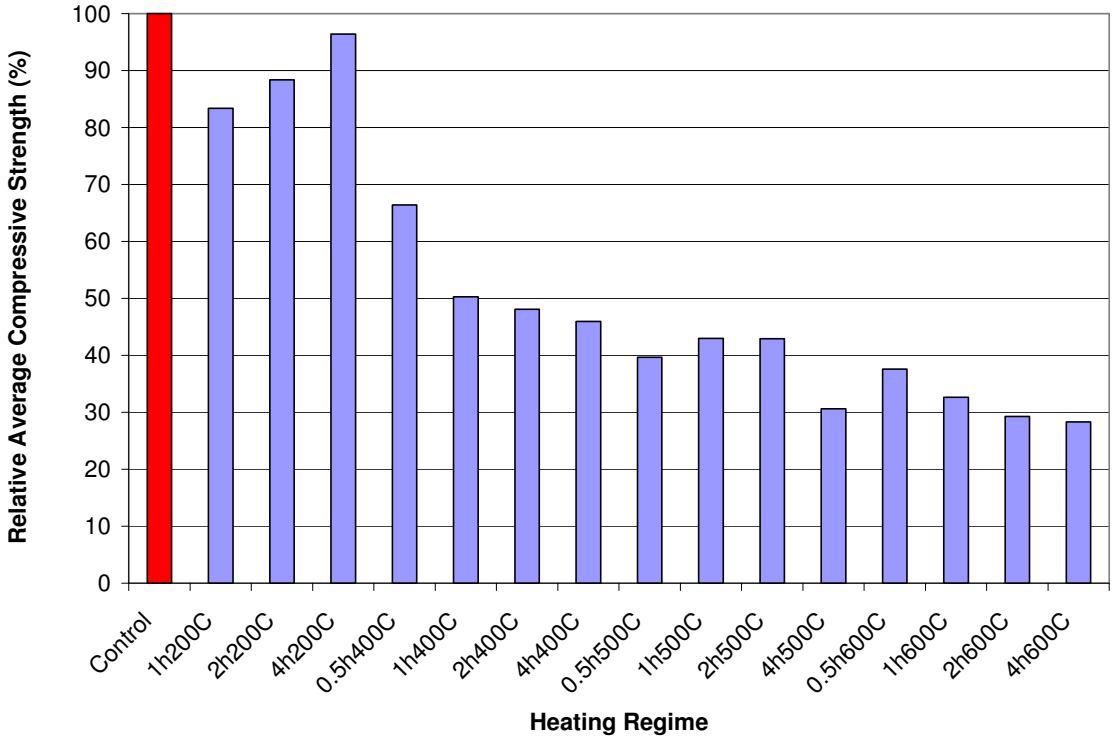

Figure 5.6: Relative average compressive strength of concrete for all heating regimes.

The concrete exposed to 200°C (392°F) experienced a drop in average compressive strength initially with a 0.5-hour exposure. However, the average compressive strength increased with increasing durations at 200°C (392°F) exposures. This was comparable to studies by other researchers, noting a strength increase with similar heat exposure (Castillo et al. 1990). The 4h200C specimens had a compressive strength that was 96 percent of the original strength, as opposed to the 1h200C samples, which retained only 83 percent of the original strength. Although it appears that an increased exposure above 4 hours at 200°C (392°F) may result in a further increase in

compressive strength that could potentially exceed the original strength, further research is required to determine whether this does or does not occur.

With exposure to maximum temperatures of 400°C (752°F), concrete reduced in compressive strength as compared to the 200°C (392°F) exposures. Only 66 percent of the original strength was retained following a short 0.5 hour exposure at 400°C (752°F). As concrete was exposed to increasing durations, the compressive strength continued to drop. After the initial loss in compressive strength, the compressive strength remained fairly constant with heat exposure at durations between 1 and 4 hours, decreasing to only 50 to 46 percent of the original strength.

With even a short exposure at 500°C (932°F) heat, the compressive strength of concrete reduced to 40 percent of the original strength. Losses in strength to this extent could drastically affect a concrete structure. With high temperature exposures of 500°C (932°F), the losses were fairly constant between 0.5 and 2 hours of exposure, and further losses resulted in 31 percent of the original compressive strength occurring as the exposure time increased to 4 hours at 500°C (932°F).

As concrete was heated to 600°C (1112°F), the compressive strength continued to decline steadily as durations increased. The differences in the compressive strength between the 500 and 600°C (932 and 1112°F) exposures were minimal, and the total percent difference in losses for all durations at the 600°C (1112ºF) exposures were within 10 percent.

Effect of Internal Temperature of Concrete on Compressive Strength

The effect of the internal temperature within the center of the concrete was analyzed to determine whether or not a trend was present based on this parameter. Because the temperature of the compressive specimens did not have an embedded thermocouple, the internal temperature of the plain concrete cylinders was assumed to be the average of the internal temperatures recorded within the bond specimens for the same heating regime. This assumption was made because both sets of specimens were heated in the same kiln at the same time.

Excel was used to approximate a trend line relating the compressive strength with respect to the internal temperature. As shown by Figure 5.7, the compressive strength decreased linearly with increasing temperature. Because the effect of all temperatures was not covered under the scope of this research project, further research should be performed in order to confirm this linear function.

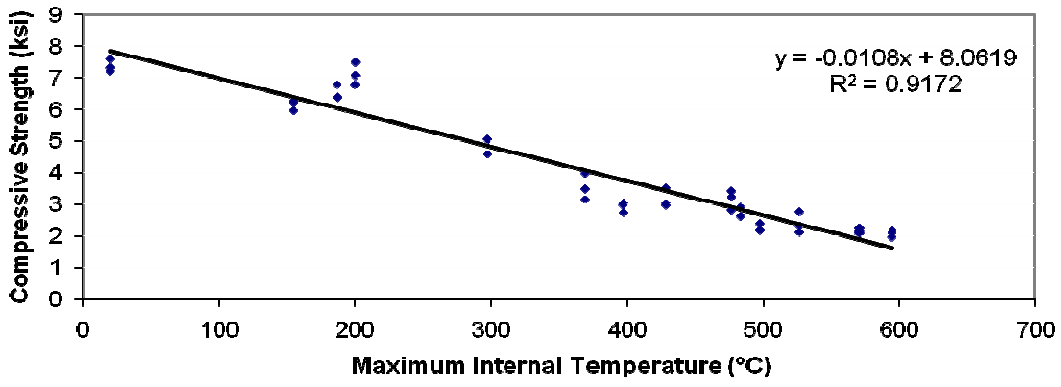

Figure 5.7: Concrete compressive strength degradation with increasing internal temperature.

Although there may be certain losses in compressive strength due to an elevated temperature exposure, a concrete member would need to be analyzed thoroughly based on the entire structural system to determine whether or not it is structurally reliable with the estimated compressive strength losses.

Modulus of Elasticity

Following high temperature exposures, the modulus of elasticity of concrete decreased, and the concrete became more susceptible to high deformations during loading. The loss in the modulus of elasticity was shown to depend on both maximum temperature and the duration at which this temperature was held, as shown in Figure 5.8. Figure 5.9 represents the relative modulus of elasticity values for each heating regime.

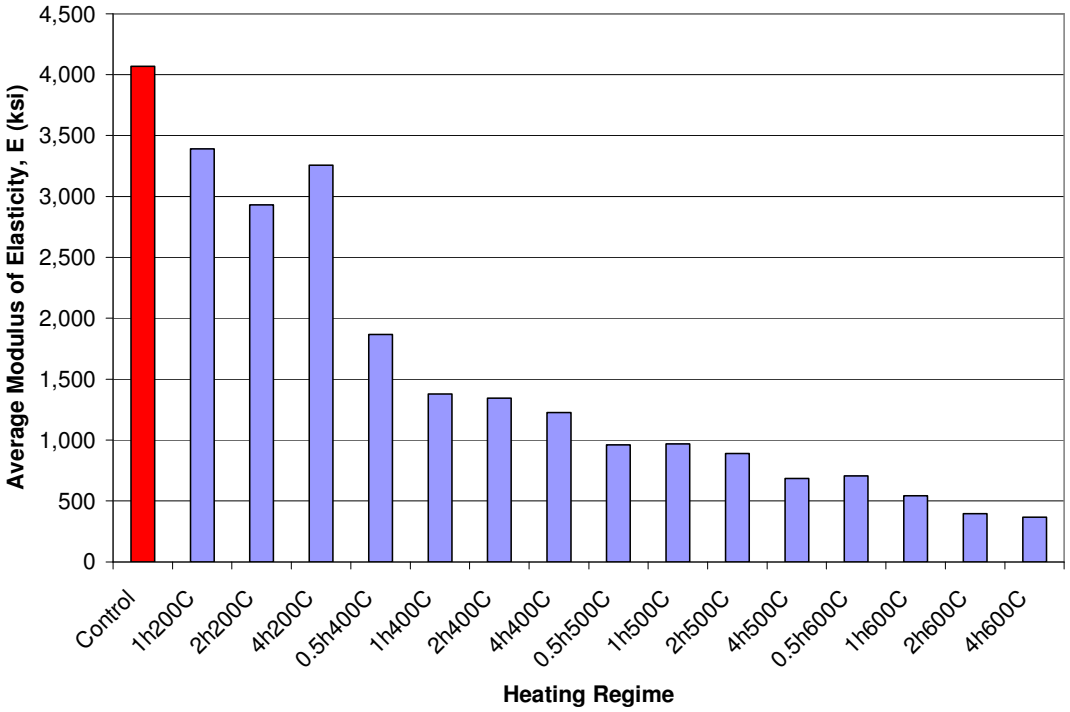

Figure 5.8: Modulus of elasticity of concrete for each heating regime.

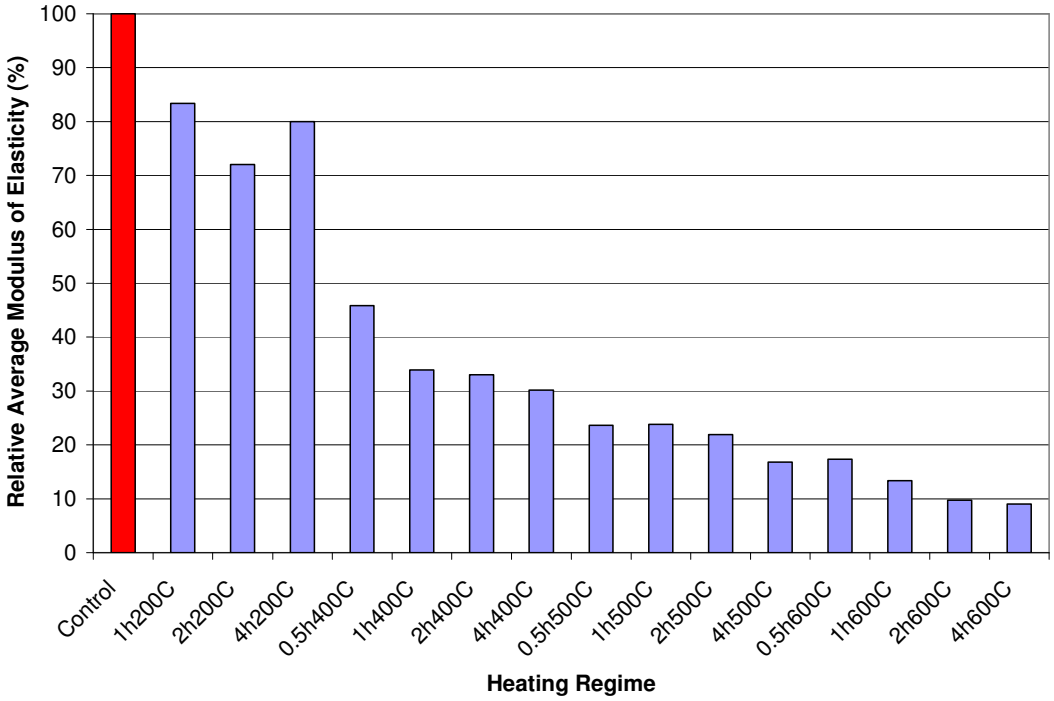

Figure 5.9: Relative average modulus of elasticity of concrete for each heating regime.

The modulus of elasticity initially decreased to 83 percent of the original value with a 1-hour exposure at 200°C (392°F). Following this initial loss, the modulus decreased as 200ºC (392ºF) was held constant. The modulus was shown to be 80-percent of the control during the 4h200C heating regime, which was inconsistent with other results.

With a 0.5-hour exposure at 400°C (752°f), the modulus decreased to 46-percent of the control value. With increased exposure time at 400°C (752°F), the elastic modulus decreased to only 30 percent of the original value at exposures up to 4 hours in length,

revealing that losses occurred dramatically with increasing temperatures and durations for the 400°C (752°F) heating regime set.

With 500°C (932°F) exposures, the average modulus of elasticity ranged between 24 and 17 percent for all durations between 0.5 and 4 hours, and only a 7-percent difference between the 0.5 and 4 hour duration exposures was observed. A gradual decline in the modulus showed that the duration at such high temperature had little effect on the modulus of elasticity.

The average modulus of elasticity continued to decrease with exposures of 600°C (1112°F), reducing to values between 17 and 9 percent for all durations between 0.5 and 4 hours. A difference of only 7 percent between the 0.5 and 4 hour durations existed, displaying a gradual decrease in the modulus at this exposure. As in the 500°C (932°F) heating regimes, the duration at which the maximum temperature of 600°C (1112°F) was held did not have a significant effect on the modulus of elasticity reductions.

Effect of Internal Temperature of Concrete on Elastic Modulus

The effect of the internal temperature of the concrete on the modulus of elasticity was also evaluated. The modulus of elasticity was shown to decrease with respect to the internal temperature of the concrete. This relationship is more easily shown in Figure 5.10. By using Excel to generate a trend line of the data, a linear curve was shown to be well suited for this trend. Similar to the compressive strength data, more temperatures should be researched in order to validate this curve.

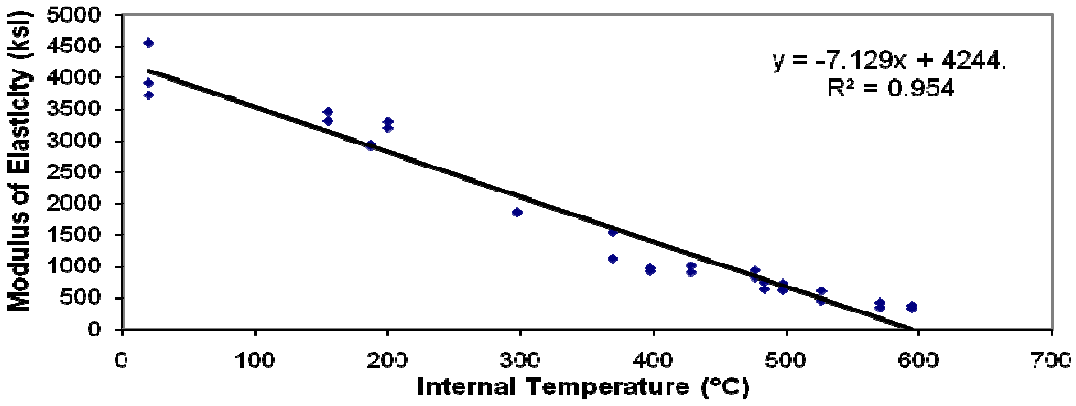

Figure 5.10: Modulus of elasticity of concrete decreases with increasing internal temperatures.

5.5 Steel Prestressing Strand Material Properties

The material properties of steel prestressing strand were shown to change after being exposed to high temperatures. Although these values were shown to reduce with exposure to high temperatures, the relative reductions in prestressing steel material properties were not as drastic as the concrete material property reductions previously discussed.

Tensile Stress

The tensile strength was shown to reduce when exposed to temperatures of at least 400°C (752ºF) and higher. However, the steel gained strength when exposed to 200°C (392°F) for durations between one and four hours. This behavior was expected based on previous research by Neves et al. (1996) who tested separate tendons of steel. Neves et al. (1996) determined that the strengths of steel tendons up to 400°C (752°f)

were fairly constant, and a decrease in strength was noticed between 400 and 700°C (752 and 1292°) (Neves et al. 1996).

According to the Precast/Prestressed Concrete Institute (2004), the tensile stress of the steel prestressing strands used throughout this project is 270 ksi (PCI 2004). However, the tensile stresses of the control specimens used in this project were shown to be lower than that defined by PCI. The average tensile stress values are shown in Figure 5.11, and the relative average tensile stress are shown in Figure 5.12.

The tensile stress of the steel prestressing strands experienced minimal reductions until reaching the 4h400C heating regime. The 500ºC (932ºF) heating regimes experienced little change between 0.5 and 4 hour durations. These heating regimes had a tensile stress of approximately 70 percent of the unheated value for all cases. Finally, in the 600ºC (1112ºF) heating regimes, the tensile stress in the steel gradually declined, resulting in a tensile stress of only 50 percent of the original.

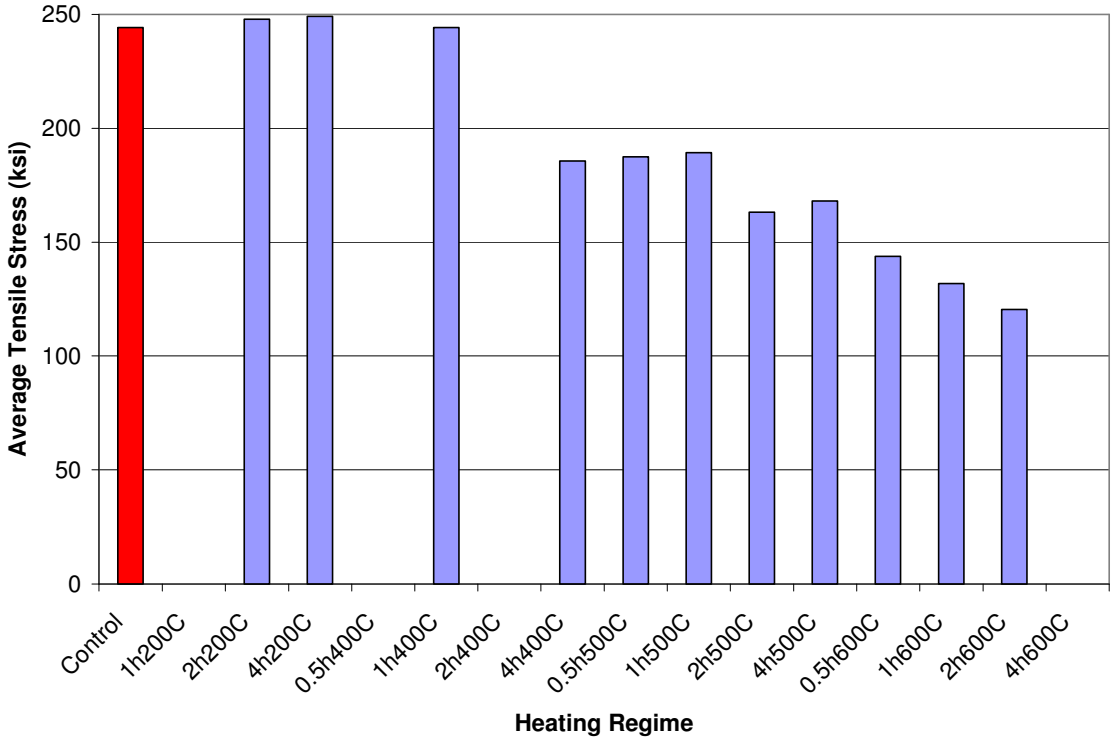

Figure 5.11: Average tensile stress of prestressing steel for all heating regimes.

As indicated by this data, the maximum temperature of exposure was the primary factor in determining tensile stress changes in prestressing steel. The duration had little effect on the tensile stress, although slight changes due to the duration of exposure were noticed in the 600ºC (1112ºF) heating regimes.

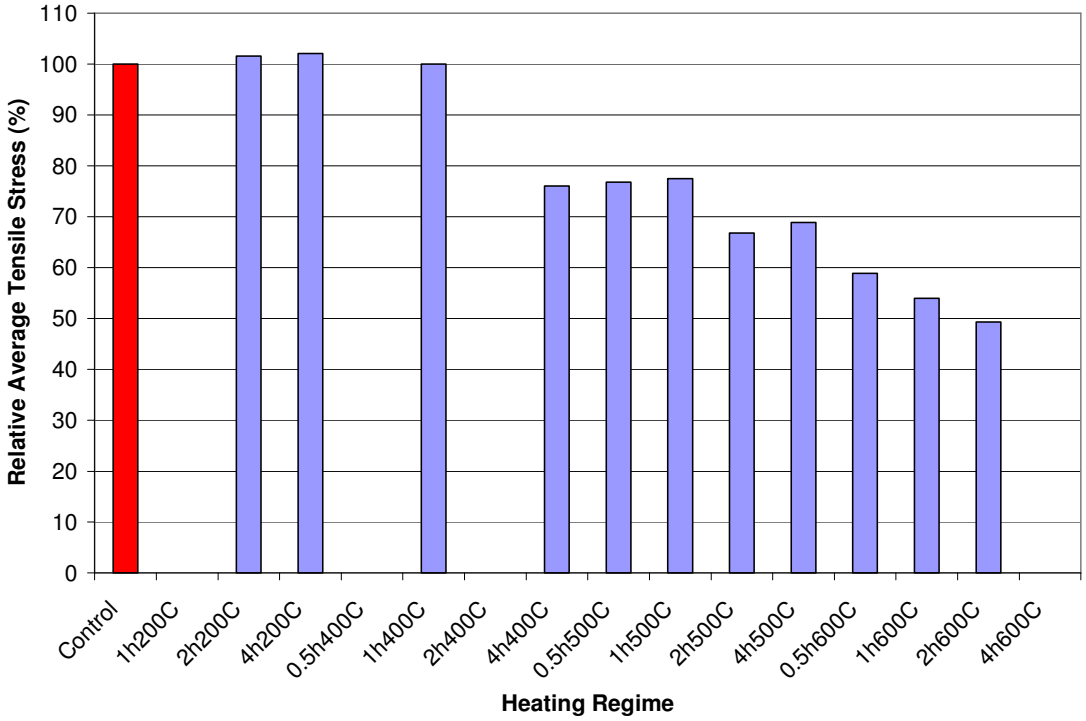

Figure 5.12: Relative average tensile stress of prestressing steel retained for all heating regimes.

Modulus of Elasticity of Prestressing Steel

Figures 5.13 and 5.14 represent the average modulus of elasticity values and the average losses in modulus of elasticity of the prestressing steel with respect to each heating regime. The modulus of elasticity of the steel was shown to decrease gradually with respect to the maximum temperature of exposure. The data shows that variations occurred in the data, with no distinct trend among the results. For instance, the 2h400C test resulted in a value that was much higher in comparison to all other results. Also, the 4h500C heating regime had an elastic modulus that was higher than the 2h500C heating

regime, which was not a common trend. Because of these inconsistencies, further testing is encouraged in order to confirm whether or not there is a trend in the modulus of elasticity of prestressing steel as it is heated. With 4 hours of exposure to 600°C (1112°F), the steel maintained approximately 70 percent of the control modulus of elasticity, indicating that the change in the steel modulus of elasticity was not as affected by the exposure of high temperatures compared to the ultimate stresses. Although values are different, the general results were fairly consistent with previous work by Holmes et al. (1982), who found that half-hour exposures up to 600°C (1112°F) result in no apparent losses in the modulus of elasticity of 7-wire steel prestressing strands (Holmes et al. 1982). Because this research did not evaluate the effects of higher durations, no comparison is available for these exposures.

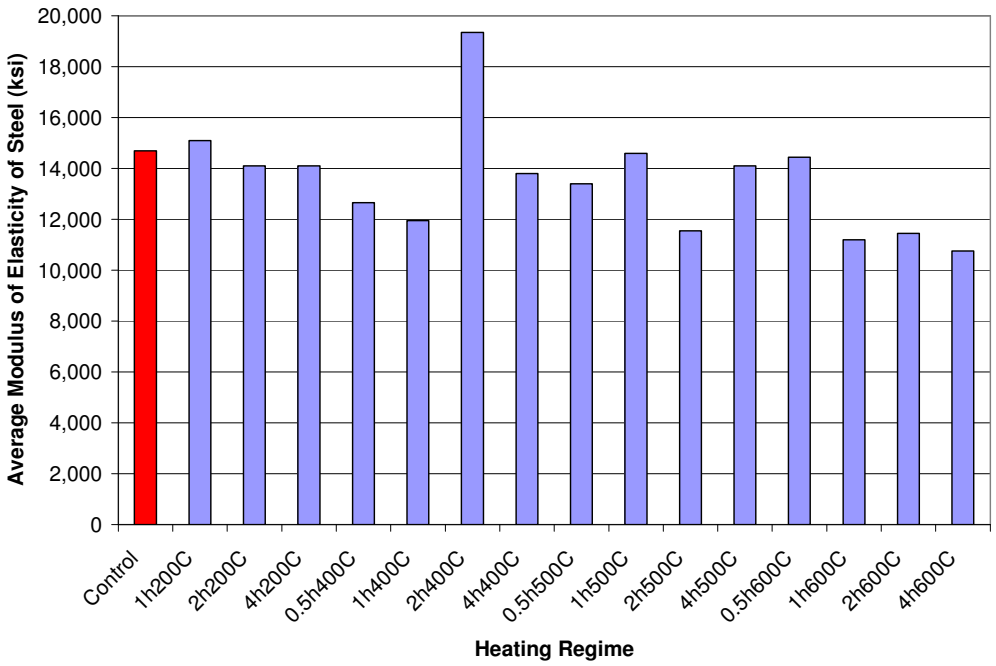

Figure 5.13: Average modulus of elasticity of prestressing steel for all heating regimes.

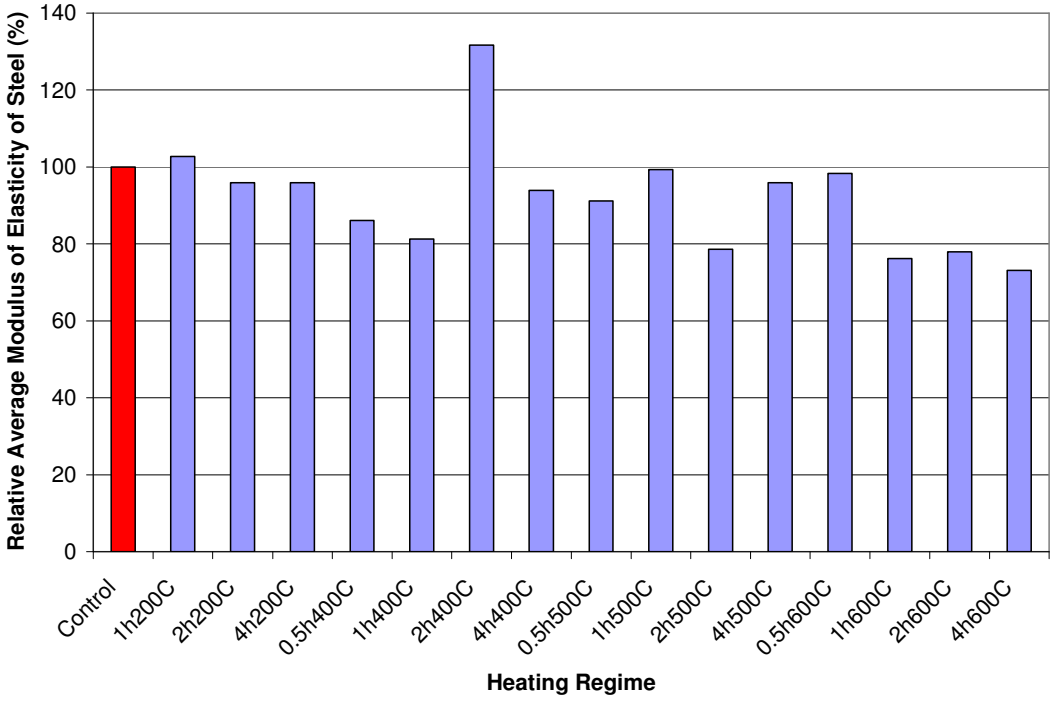

Figure 5.14: Relative average modulus of elasticity of prestressing steel for all heating regimes.

5.6 Bond Stress Tests

The bond stresses between concrete and steel prestressing strands were shown to decrease as temperatures increased from 200 to 600°C (390 to 1110°F). The temperature was shown to be the primary factor in the bond degradation. However, the duration of a heating regime appeared to play a minor role in the bond changes. Physical changes in bond strength specimens displayed that losses were occurring with increasing temperatures. The most extreme difference was noticed in the 4h600C specimens. When these specimens were lifted by the prestressing strand immediately following the heating

process, the concrete made crackling noises which were likely an effect of cracking within the bond interface.

Maximum Load

The maximum load reached during testing of the bond specimens was determined, and these values were used as a comparative analysis for evaluating changes in the bond effectiveness between concrete and steel prestressing strands after exposure to elevated temperatures. The maximum average loads decreased for each heating regime up to the 500°C (930°F) heating regimes, as shown in Figure 5.15. At this point, the maximum average loads appeared to remain fairly constant up to the 2- and 4-hour durations at the 600°C (1110°F) heating exposures.

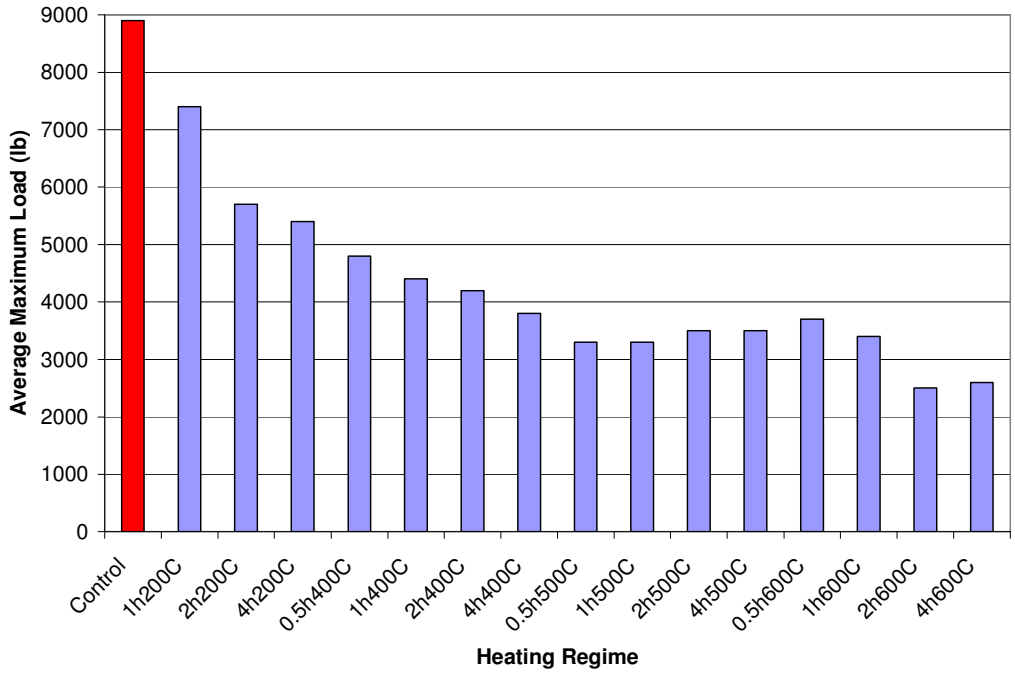

Figure 5.15: Average maximum loads resisted by bond specimens for all heating regimes.

When exposed to a maximum temperature of 400°C (752°F), the bond effectiveness reduced to 50 percent of the unheated value, as shown in Table 5.1. The average maximum loads reduced to 40 percent of the unheated values in all specimens heated at 500°C (932°F), and 40 to 30 percent of the unheated value was observed in specimens heated at 600°C (1112°F). Even with exposure to 200°C (392ºF) heat for two hours, 60-percent retention in the bond effectiveness was observed when comparing the maximum load achieved during the pull-out testing.

Table 5.1: Percentage losses and retentions of average maximum loads for bond tests.

Heating Regime	Percentage Loss	Percentage Retention
Control	NA	100
1h200C	17	83
2h200C	36	64
4h200C	39	61
0.5h400C	46	54
1h400C	50	50
2h400C	53	47
4h400C	57	43
0.5h500C	63	37
1h500C	63	37
2h500C	60	40
4h500C	61	39
0.5h600C	59	41
1h600C	61	39
2h600C	72	28
4h600C	71	29

The effect of duration was also evaluated and shown to affect the bond specimens. At lower temperatures, such as 200°C (392°F), the duration at which the heat was held had a fairly significant effect on the bond losses, with a maximum difference of 22

percent between the 1 hour and 4 hour heating regimes. The 400°C (752ºF) specimens displayed a difference in the maximum load percent loss of only 7 percent between the 1- and 4-hour durations, and the 600°C (1112°F) specimens had a difference in percent loss of 11 percent between the 1- and 4-hour durations. These losses indicate that the duration did affect the effectiveness of the bond, especially temperature exposures below 500ºC (932ºF).

Maximum Bond Stress

The maximum bond stress reached during loading was analyzed as another measurement to determine the changes in bond effectiveness between prestressing steel and concrete after exposure to elevated temperatures. The decreasing trend in the average bond stress values shown in Figure 5.16 reveal that the maximum air temperature had more affect on the bond than the duration of heat exposure.

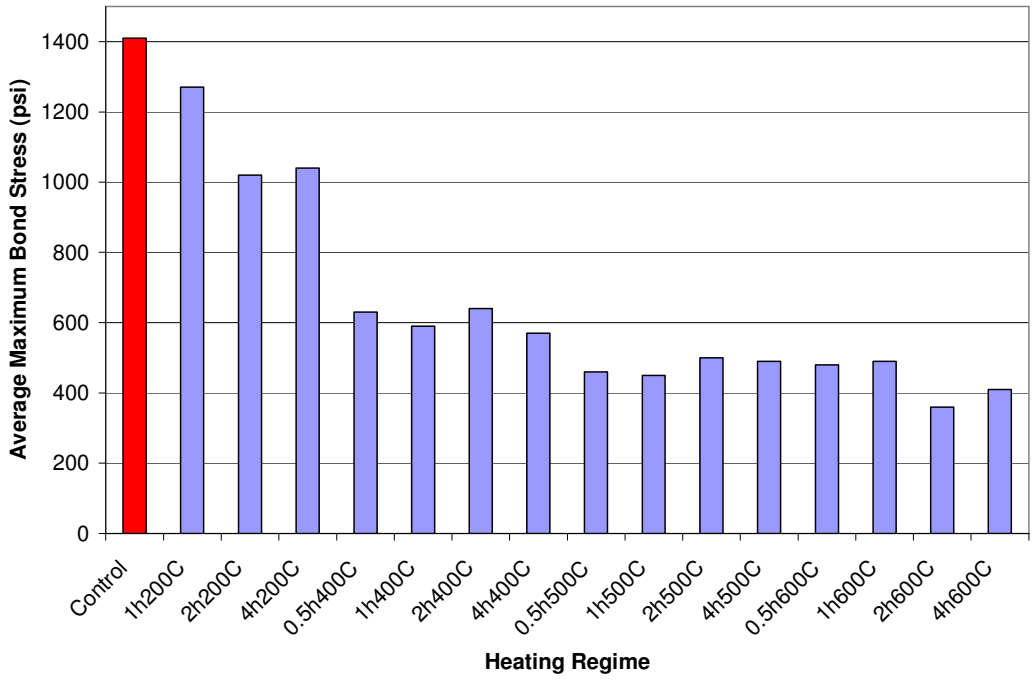

Figure 5.16: Average maximum bond stresses for all heating regimes.

The effect of maximum air temperature was evaluated by comparing the 1-hour durations for each maximum temperature. After an exposure of 1 hour at 200°C (392ºF), the maximum bond stresses reduced to 90 percent of the unheated value, as shown in Table 5.2. Comparatively, a short 1 hour exposure at 400°C (752ºF) resulted in 40-percent retention of the original value, indicating that the bond was affected by increasing the temperature from 200 to 400°C (392 to 752°F). Subsequently, approximately 30 percent of the unheated maximum bond stress value was retained following 1-hour exposures at 500 and 600°C (932 and 1110°F).

Table 5.2: Percent losses and retentions of bond stresses for all heating regimes.

Heating Regime	Percentage Loss	Percentage Retention
Control	NA	100
1h200C	10	90
2h200C	28	72
4h200C	26	74
0.5h400C	55	45
1h400C	58	42
2h400C	55	45
4h400C	60	40
0.5h500C	67	33
1h500C	68	32
2h500C	64	36
4h500C	65	35
0.5h600C	66	34
1h600C	65	35
2h600C	74	26
4h600C	71	29

The bond effectiveness did not appear to be affected by the duration of an exposure with maximum temperatures above 200ºC (392ºF). For instance, a difference of nearly 20 percent was observed between the bond stress losses associated with the 1h200C and 4h200C heating regimes. A bond stress loss difference of only 5 percent occurred between the 0.5h400C and 4h400C heating regimes. Again, a difference in bond stress losses of 5 percent was observed between the 0.5h600C and 4h600C heating regimes. By considering these examples, the duration was shown to affect the bond at exposures of 200ºC (392ºF). However, the duration of an exposure was not a significant factor in the bond effectiveness at higher temperatures.

Bond Changes Based on Core Temperature

The maximum internal temperature for each cylinder, as measured by an embedded thermocouple, was compared to the maximum load and maximum bond stresses, as shown in Figures 5.17 and 5.18, respectively. A relatively linear trend existed between the maximum internal temperature and the changes in bond effectiveness. This suggested that the bond effectiveness degraded linearly as a function of the temperature at the concrete and steel interface as the concrete was heated.

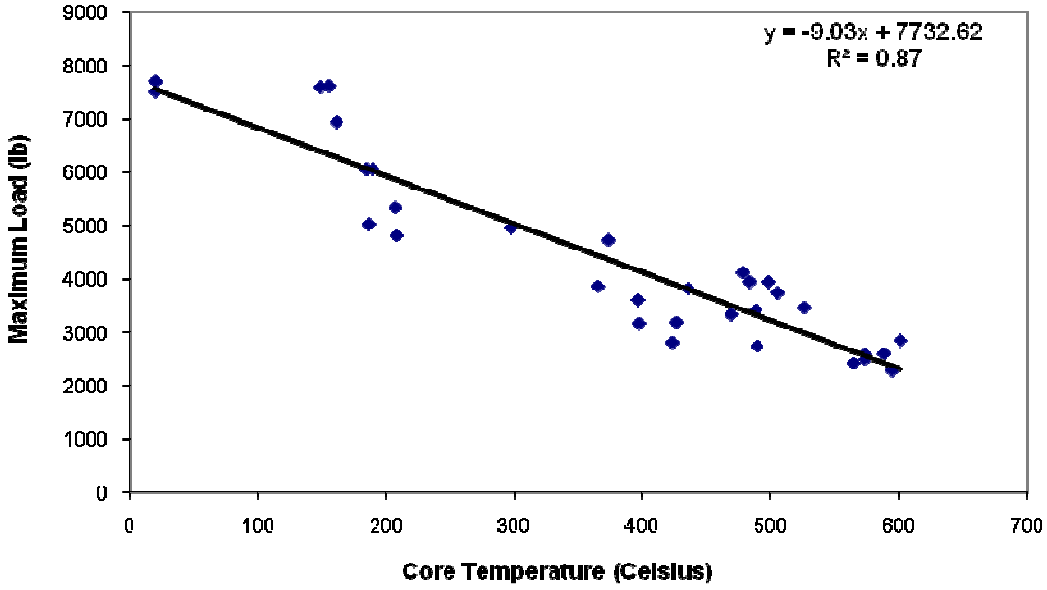

Figure 5.17: Graphical representation of relationship between maximum loads resisted by bond specimens and maximum internal temperature of bond specimens.

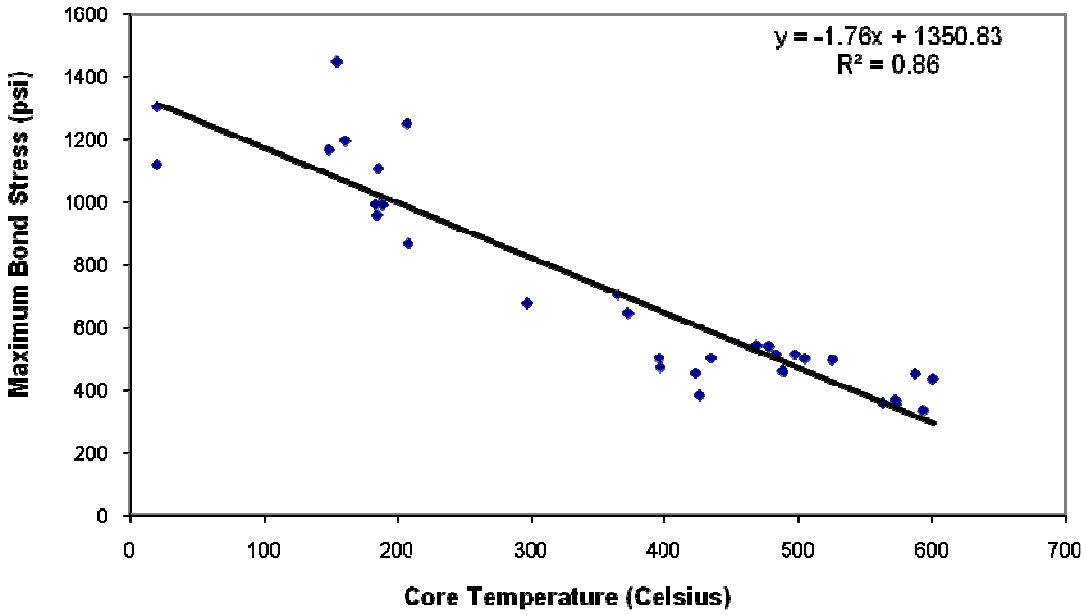

Figure 5.18: Graphical representation of relationship between maximum bond stress and maximum internal temperature of bond specimens.

Although the steel prestressing strands were wrapped in Kaowool during the heating process, some heat was assumed to have transferred to the concrete through the steel strand. The Kaowool aided in reducing the rate of heat transfer, but it was not completely heat resistant. The bond was likely affected by this parameter, because the heat transferred through the steel would have directly affected the bond interface between the steel and concrete.

The increasing losses are not surprising due to the physical changes that were observed after heating the concrete. As previously noted, the concrete surface cracking became more severe as the concrete was heated to increasing temperatures. An increase

in the number of cracks occurred, and crack widths enlarged. This cracking likely had an effect on the interface between the steel and the concrete in the bond specimens, causing this interface to become weaker as cracking occurred. Additionally, the differential thermal expansions of the steel and concrete during the heating process could have affected the bond effectiveness, causing the area at the interface to become partially damaged through these expansions.

5.7 Thermogravimetric Analysis

Cement Paste Samples

After performing a controlled experiment on cement paste samples, TGA was confirmed to be a useful tool in estimating the maximum temperature of cementitious materials. As shown previously in Figure 4.22, the heat treatment samples experienced little to no relative weight losses until exceeding the maximum temperature of the specified heat treatment. The results also showed that these curves followed the same general trend as the control samples upon reheating once they exceeded the maximum temperature of the specified heat treatment. The sudden drop in weight at approximately 450°C (800°F), was associated with the amount of calcium hydroxide (CH) in the cement paste (Alarcon-Ruiz et al. 2005). The 200°C (392°F) heat treatment also experienced this drop because it did not reach a peak temperature capable of eliminating the CH from the cement paste sample. Although the 400°C (752°F) heat treatment did not reach 450°C (800°F), the calcium hydroxide was not present in the cement following the heat

treatment at 400°C (752°F). Because the samples were held at the peak temperature for 15 minutes, the calcium hydroxide likely underwent dehydroxylation during this holding period. This suggests that CH can decompose at sustained temperatures of at least 400°C (752°F).

By taking the first derivative of TGA data to obtain the slopes along the TGA curves, the changes associated with the heat treatment curves in comparison to the unheated control sample were more recognizable. For instance, the 200°C (392°F) heat treatment curve began to coincide with the slopes of the control cement paste curve at approximately 250°C (480°F), as shown in Figure 5.19. Although the sample was only heated to 200°C (392°F), it did not follow the control curve until approximately 250°C (480°F). For other heat treatments, a similar trend was noticeable. For each of the 400, 500, and 600°C (752, 932, and 1112°F) heat treatments, the derivative curves did not intersect until after the peak temperature of the heat treatment was exceeded by approximately 50°C (120°F). This can be seen in Figures 5.20, 5.21, and 5.22. Although there was an apparent error in determining the exact maximum exposure temperature of a cement paste sample, the results show that TGA was effective in determining an estimated maximum temperature of exposure by analyzing the first derivative of a TGA data curve. This process is known as the first derivative analysis.

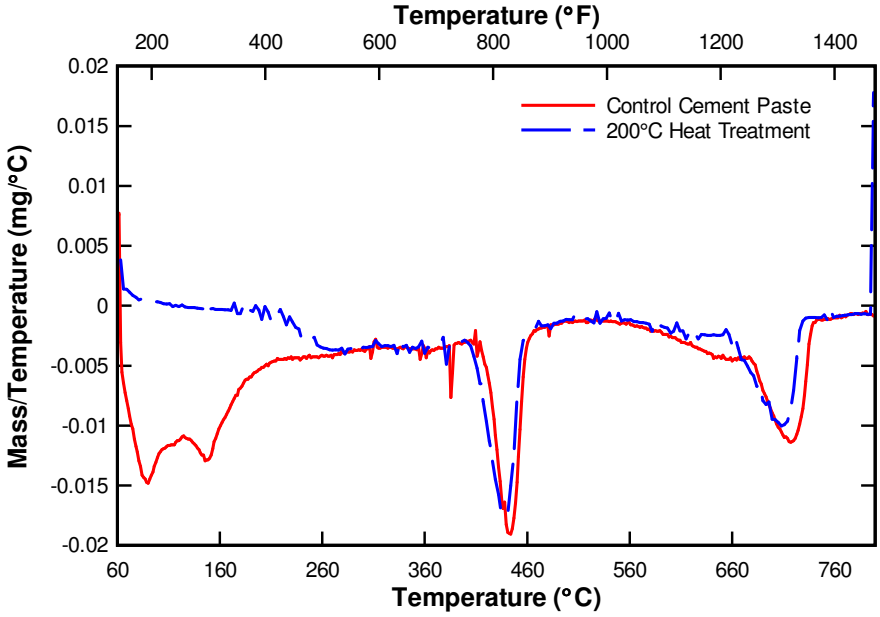

Figure 5.19: First derivative analysis of 200°C (392°F) heat treatment and control cement paste TGA results.

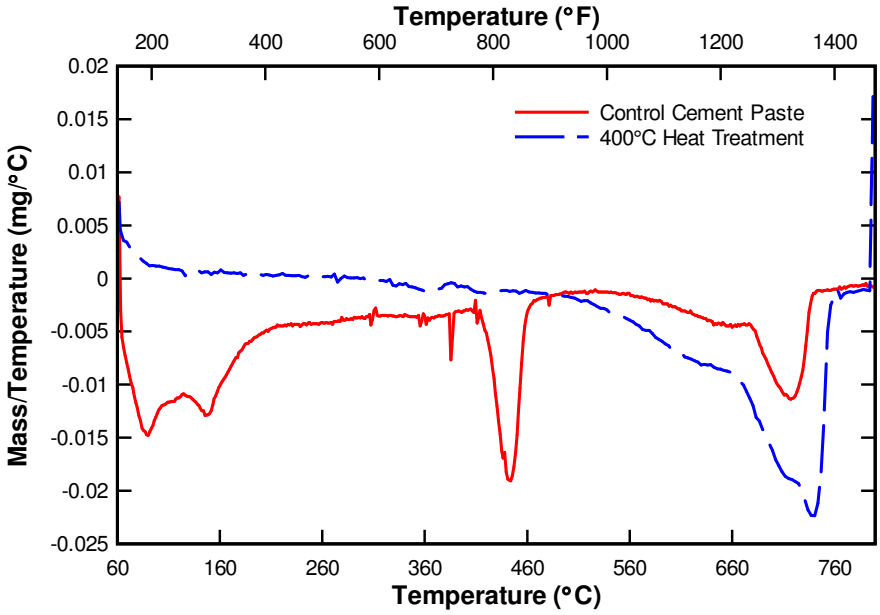

Figure 5.20: First derivative analysis of 400°C (752°F) heat treatment and control cement paste TGA results.

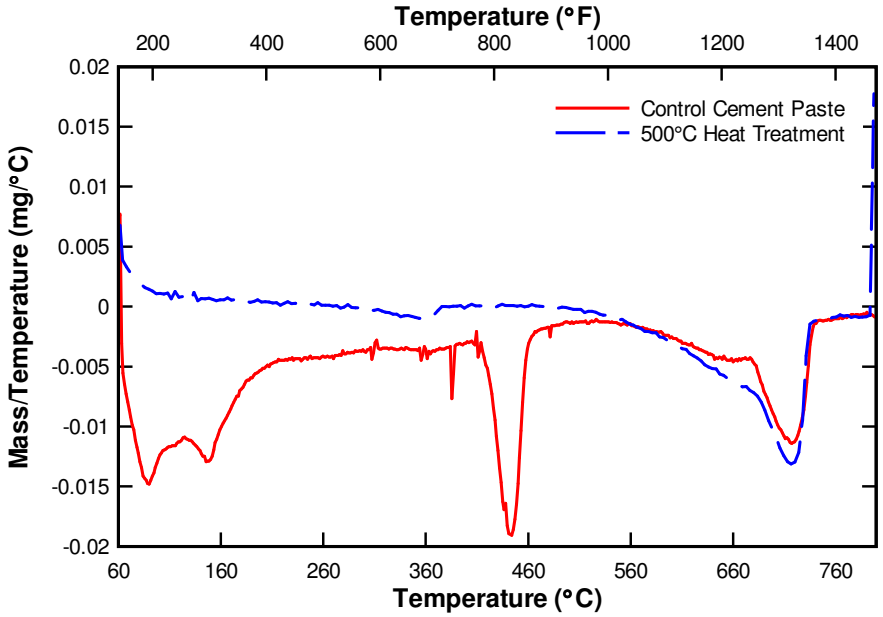

Figure 5.21: First derivative analysis of 500°C (932°F) heat treatment and control cement paste TGA results.

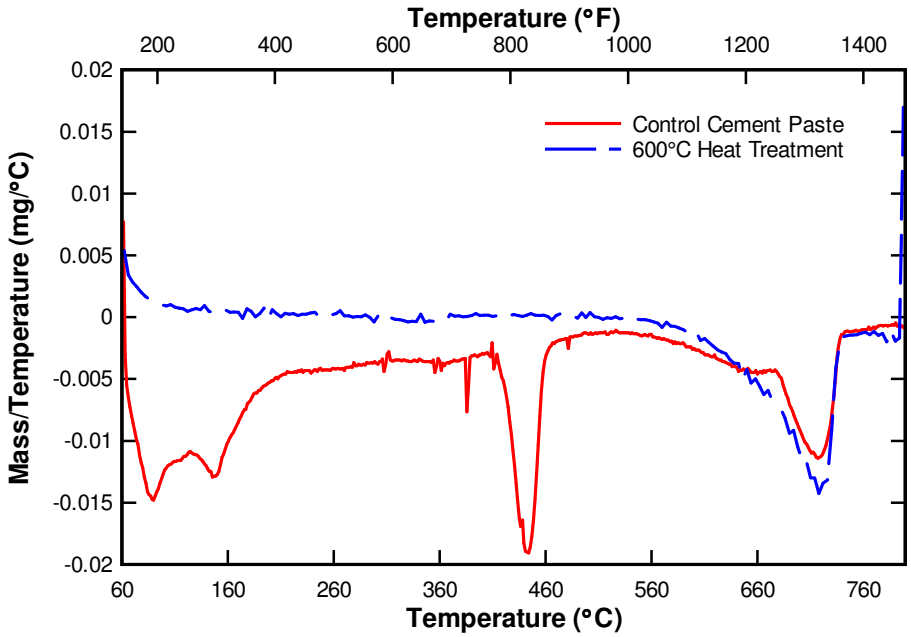

Figure 5.22: First derivative analysis of 600°C (1112°F) heat treatment and control cement paste TGA results.

Mortar Samples

Thermogravimetric analysis curves of cement paste have been analyzed in the past by previous researchers (Harmathy 1968, Alarcon-Ruiz et al. 2004), but little is known on the use of TGA for analyzing heat affected mortar. Therefore, mortar samples were tested in a similar controlled laboratory experiment to analyze the effectiveness of TGA.

A lower percentage of weight was lost in the mortar samples compared to the cement paste samples as a result of the addition of sand. Despite these differences, the same general trends existed by testing mortar samples, as shown previously in Figure 4.24. These curves also displayed that minimal weight loss occurred until exceeding the maximum temperature of the previously performed heat treatment.

Comparisons using the first derivative of the TGA data curve, or the first derivative analysis, suggested that TGA was capable of determining an approximate maximum exposure temperature of a mortar sample. The derivative curves, shown in Figures 5.23, 5.24, 5.25, and 5.26, reveal that TGA could be used to evaluate heat affected mortar. As in the cement paste samples, the mortar heat treatments did not intersect with control samples until heated to approximately 50°C (120°F) above the maximum temperature of a specific heat treatment. The amount of calcium hydroxide present in the sample was also noticeably less than that observed in cement paste samples, which was expected because of the dilution effect of the sand in the mortar mixture.

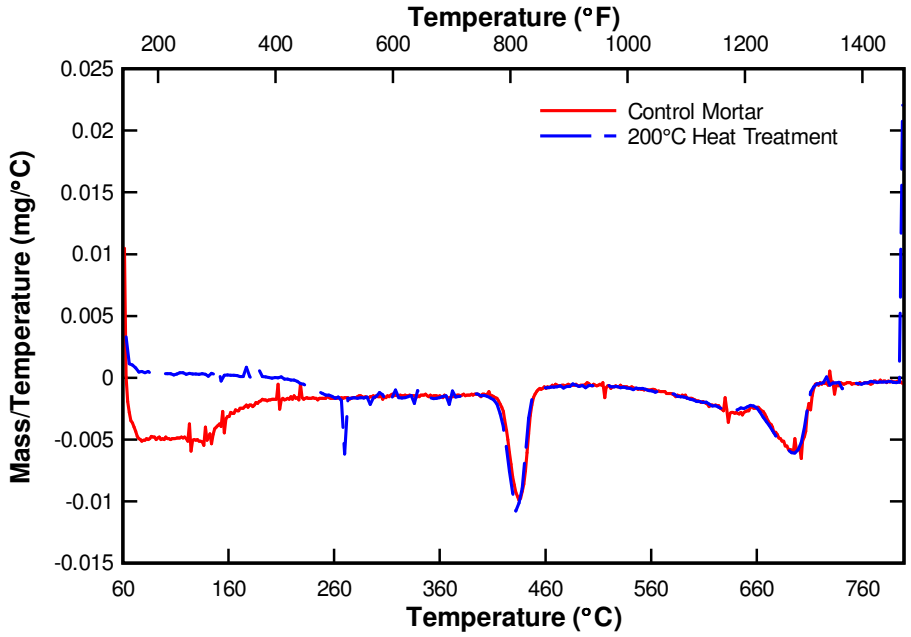

Figure 5.23: First derivative analysis of 200°C (392°F) heat treatment and control mortar TGA results.

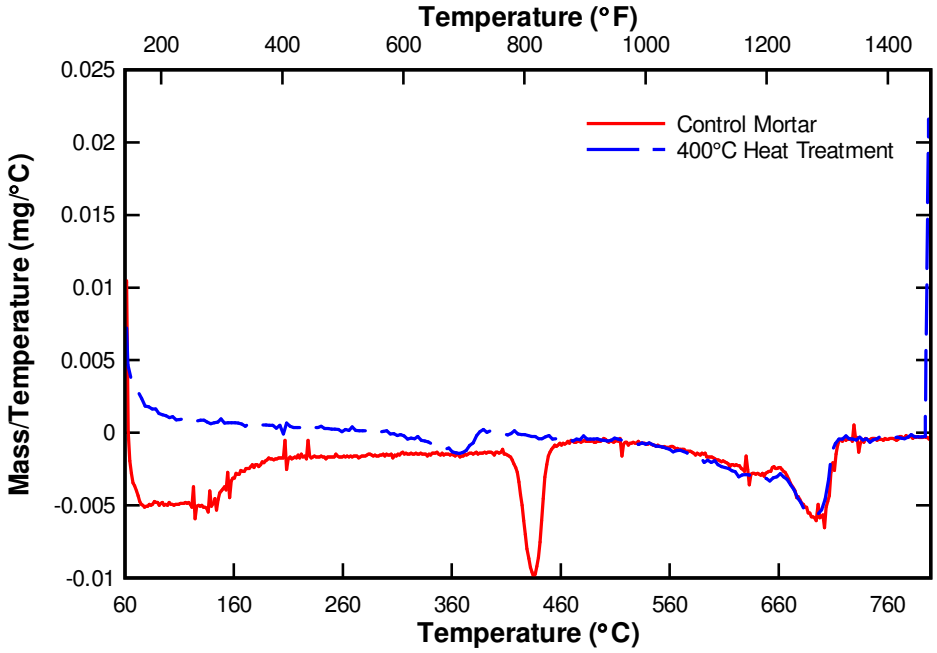

Figure 5.24: First derivative analysis of 400°C (752°F) heat treatment and control mortar TGA results.

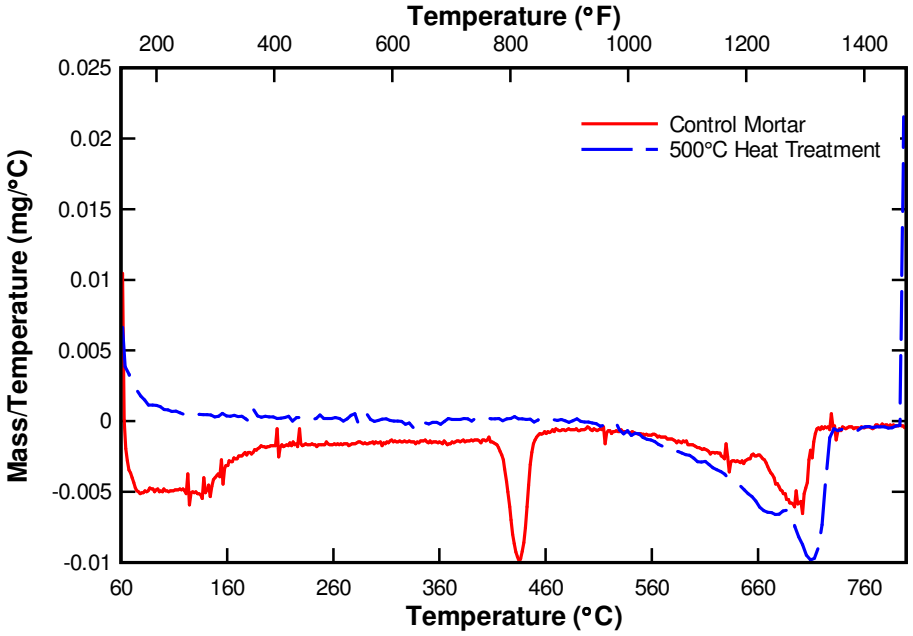

Figure 5.25: First derivative analysis of 500°C (932°F) heat treatment and control mortar TGA results.

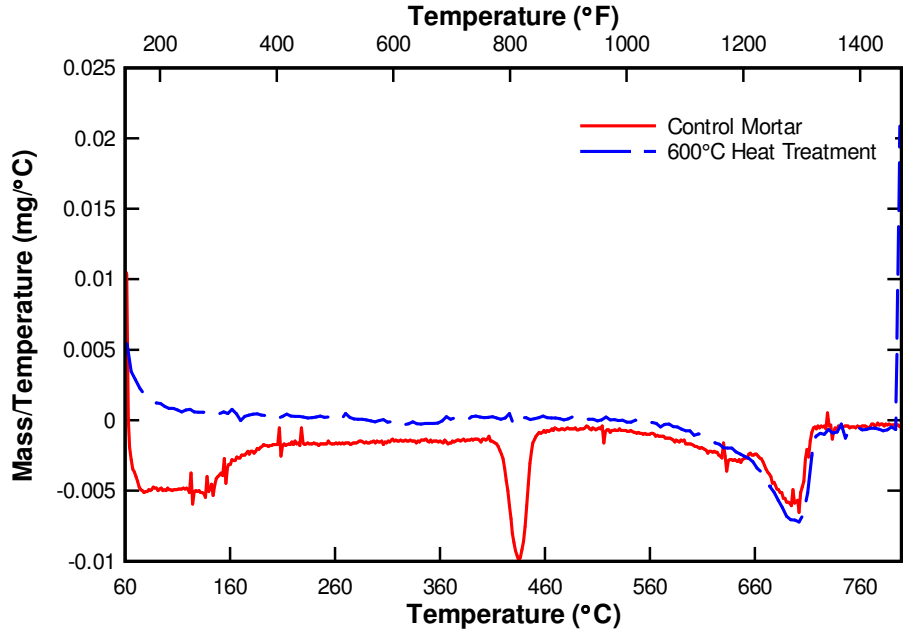

Figure 5.26: First derivative analysis of 600°C (1112°F) heat treatment and control mortar TGA results.

Concrete Samples

After confirming TGA to be a reasonable method for estimating the maximum temperature exposure of heat affected cement paste and mortar samples, TGA was performed on a concrete cylinder with known temperatures at the center and exterior surfaces. A heat profile within the concrete cylinder was generated based on samples taken in one inch increments through the cross-section at mid-height of the 6-inch diameter by 12-inch high cylinder. The 1h500C-S2 specimen was chosen for analysis because the embedded thermocouple generated a reasonable heat exposure curve at the interior, supporting the measurement of maximum internal temperature of the concrete at this point is accurate. The exterior of the concrete was assumed to be the ambient kiln temperature.

Consistent with previous research, the CH did not completely disappear after the concrete was heated (Alarcon-Ruiz et al. 2005). The reason for this, as suggested by Alarcon-Ruiz et al., is that the dehydroxylation of calcium hydroxide (CH) is a reversible reaction which begins during the cooling process, making it necessary to test samples quickly following heat exposure (Harmathy 1968, Alarcon-Ruiz et al. 2004). The effects of this reversible reaction were present in the concrete samples based on the TGA results.

For each sample, the calcium hydroxide (CH) content as a percentage was calculated using the Mettler Toledo software for evaluating TGA results. As shown in Figure 5.27, little CH was present on the heat exposed exterior of the cylinder, although there was a relatively significant amount of calcium carbonate present, as shown by the sharp decrease in the relative weight beginning at approximately 600°C (1112°F).

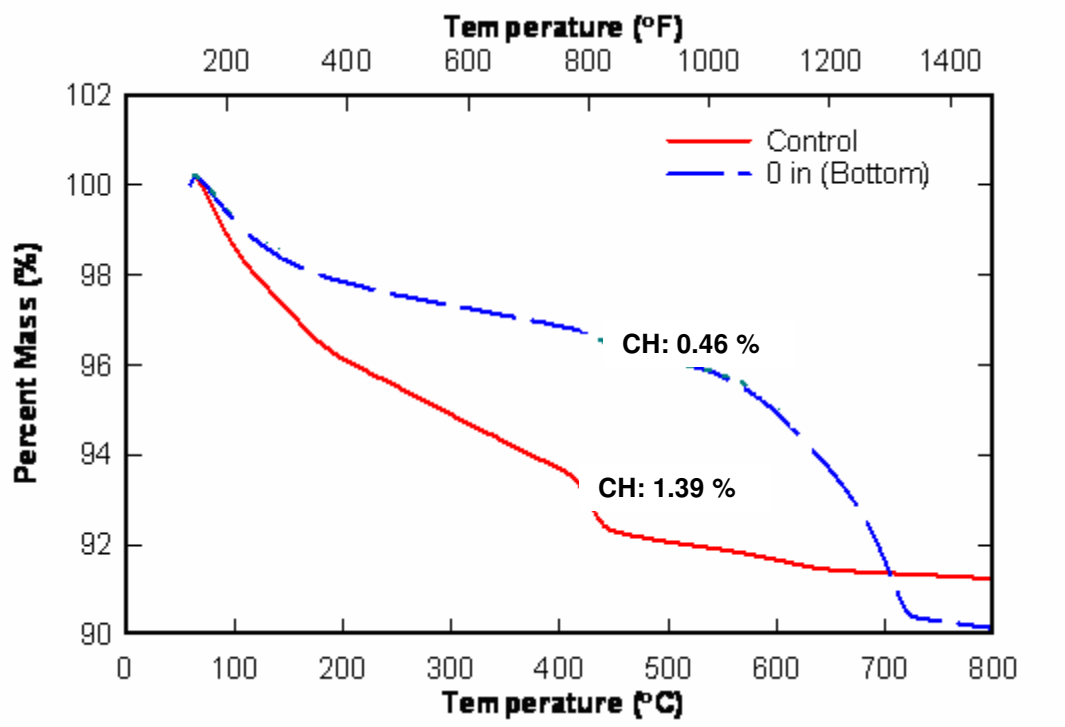

Figure 5.27: Relative mass and calcium hydroxide content of a control concrete sample and the bottom exterior of 1h500C-S2.

By taking the derivative of the TGA data curves to determine the slope changes, an intersection is observed between 450 and 550°C (800 and 1022°F), as shown in Figure 5.28. Based on the results of the cement paste and mortar heat treatment samples, this behavior was to be expected. An intersection typically occurred between the control and a heat affected sample near the maximum temperature of the heat treatment. This intersection was typically 50°C (120°F) above the specified heat treatment temperature for both the cement paste and mortar samples. By evaluating the differences between the derivative curves of the exterior surface sample and the control sample, the first point of intersection between the curves occurs at approximately 450°C (840°F). Following this

point, the differences between the slopes were relatively smaller for a short range of temperatures until the calcium carbonate content present in the exterior sample resulted in larger differences between the derivative curves. Based on these findings, the TGA results suggested that the concrete on the exterior was heated to approximately 450°C. This temperature was lower than the assumed temperature of the exterior of the concrete cylinder. Although not completely precise, TGA was shown to be a relatively reliable indicator for determining an approximate temperature exposure of the heat affected concrete sample.

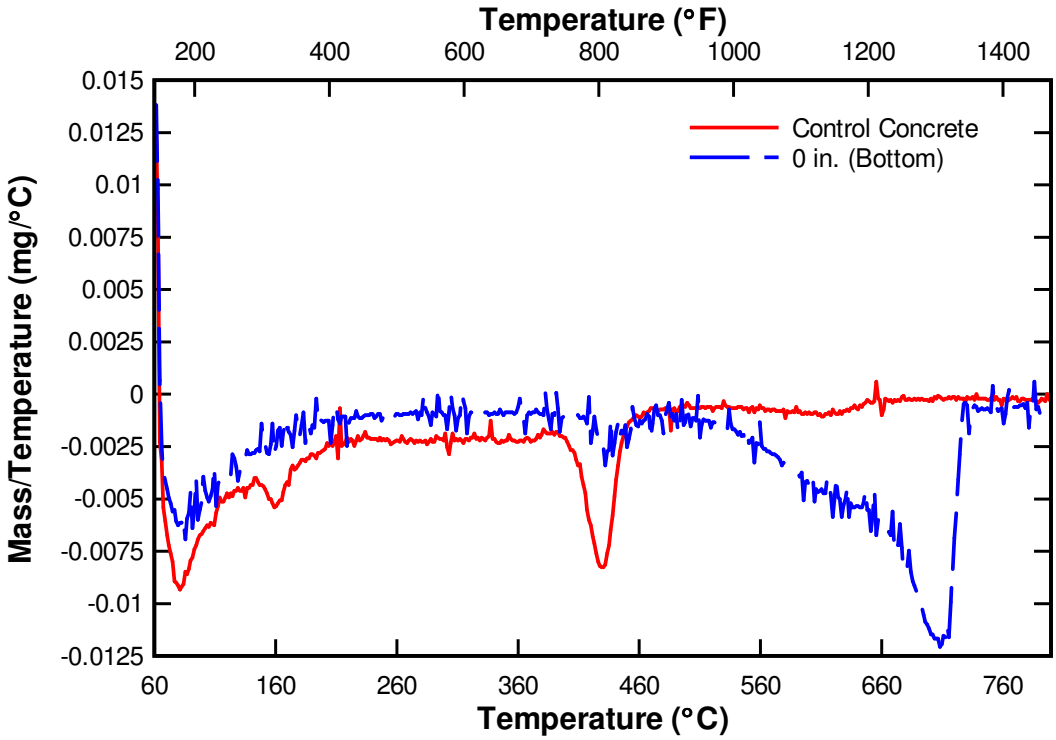

Figure 5.28: First derivative analysis of the Control and 0 in (Bottom) TGA result curves of 1h500C-S2.

The center of the concrete cylinder, located 3 inches from the heat exposed face, was also a point of known temperature. The temperature at the center, measured by an embedded thermocouple, reached a maximum of approximately 430°C (800°F). Based on the TGA results, the calcium hydroxide content was higher at the center of the cylinder than on the exterior surface, and little to no calcium carbonate was present in the center sample, as shown in Figure 5.29. A higher content of calcium hydroxide suggests that the sample at the center was heated to a lower temperature as compared to the exterior of the concrete cylinder. This was expected based on the temperature monitored by the embedded thermocouple. Since carbon-dioxide in air affects the carbonation levels of concrete, the reduction in calcium carbonate content of the center sample compared to the external surface sample is not surprising. This center sample had not been directly exposed to air prior to the TGA, unlike the sample taken from the exterior surface of the concrete cylinder.

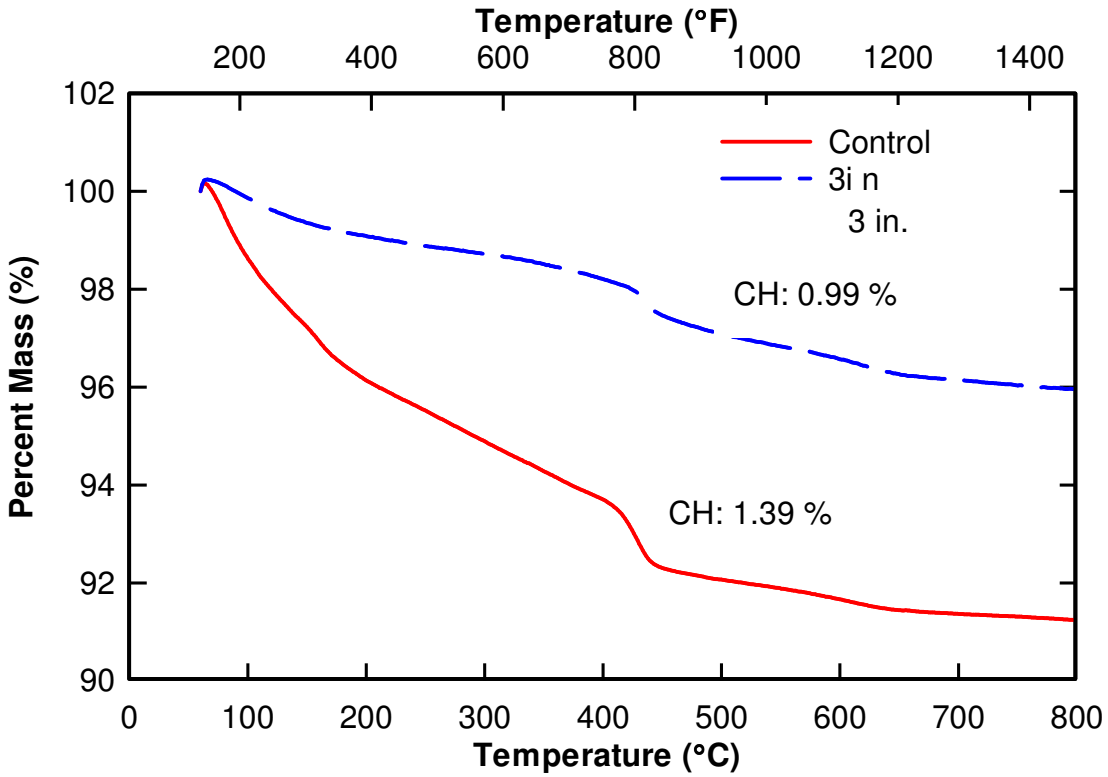

Figure 5.29: Percent mass of a control concrete sample and the center of 1h500C-S2.

By taking the derivative of the TGA result curves, the curves were shown to intersect at approximately 450°C (780°F), as shown in Figure 5.30. By calculating the differences between the derivative curves, the first intersection of the curves occurs at approximately 440°C (760°F). From this point forward, additional heating of the sample resulted in lower differences between the two derivative curves. Based on these results, the TGA suggests that the concrete was heated to approximately 440°C (760°F). This value is approximately 10°C (50°F) lower than the maximum temperature monitored by the thermocouple.

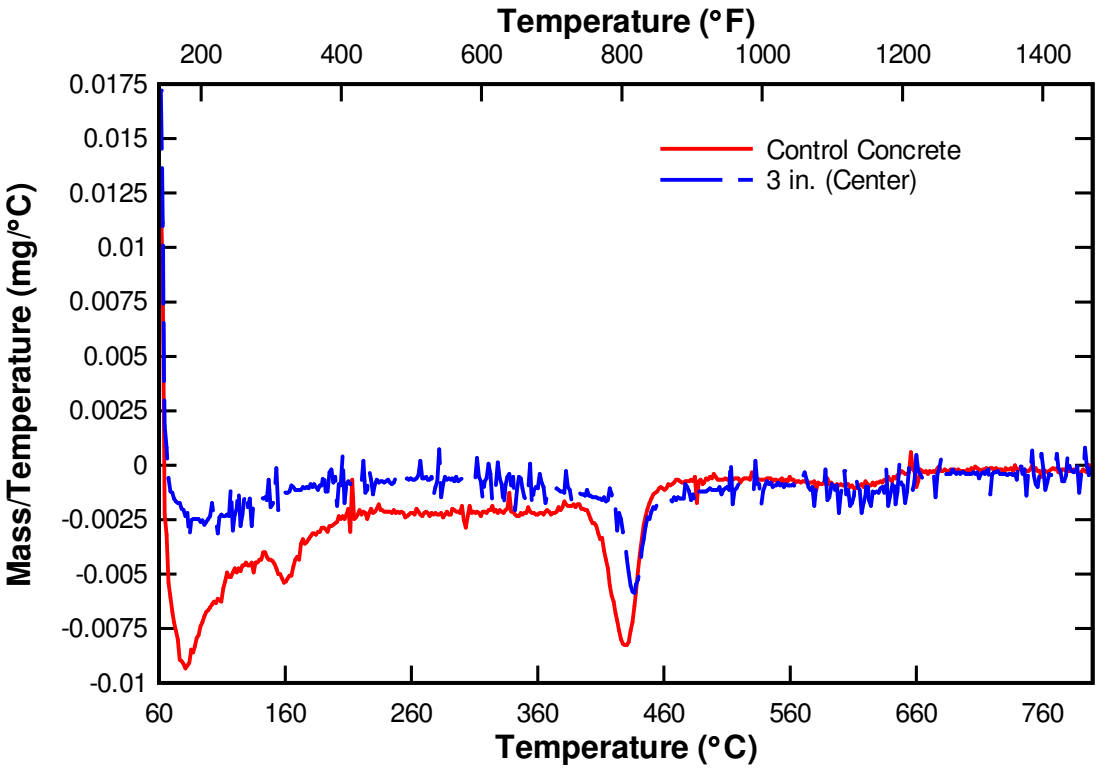

Figure 5.30: First derivative analysis of the Control and 3 in (Center) TGA result curves of 1h500C-S2.

By comparing the results of the center and exterior samples, TGA was shown to be a reliable method for determining an approximate maximum temperature exposure concrete. The heat affected concrete did appear to experience a reversal of the dehydroxylation reaction, resulting in CH present in the samples. A substantial amount of calcium carbonate was also present on the exterior of the concrete cylinder. This showed that a better storage method should be implemented in future work for samples evaluated using TGA at a time well after heat exposure.

Temperature Gradient of Concrete

By performing similar analyses on intermediate points of the cylinder, a temperature gradient was estimated based on approximate intersection points of the derivative curves. As shown in Table 5.2, the results illustrate a reasonable heat gradient, especially present within two inches of the center. The exterior samples at 0 and 6 inches resulted in lower temperature predictions based on the intersections of the derivative curves. Both samples indicated a substantial amount of calcium carbonate was present in the concrete, as previously shown in Figure 4.25 by the large drop in percent mass at approximately 600°C (1110°F). This presence of calcium carbonate likely affected the temperature prediction capabilities of TGA for the exterior samples, further indicating the need to collect and test samples quickly following heat exposure. Although the temperatures do not accurately reflect the actual temperatures at each point, TGA was a reliable indicator in predicting an approximate temperature of exposure.

Table 5.3: Temperatures of exposure throughout concrete cylinder by comparison of the slopes of TGA result curves.

Distance from Heat Exposure Face of Cylinder (in)	**Predicted Exposure Temperature (°C)**
6 (Top)	447
5	453
4	449
3	440
2	449
1	450
0 (Bottom)	450

CHAPTER SIX

CONCLUSIONS AND RECOMMENDATIONS

Based on the experimental results, conclusions are formulated and summarized in this Chapter. Future research is an important aspect of advancing the knowledge and understanding of heat-affected prestressed concrete structural elements. Because of this, several recommendations are also made for using these results in future research applications.

6.1 Property Changes of Concrete with Elevated Temperatures

Concrete material properties were shown to change following heat exposure. The compressive strength of concrete was shown to progressively decrease with an increase in temperature. A progressive decline in the modulus of elasticity of concrete was also shown to exist. Both compressive strength and modulus of elasticity of concrete were influenced by the duration at which the maximum temperature was held constant in the kiln. As the duration increased, the maximum internal temperature of the concrete increased. Based on the maximum internal temperature of the concrete, the compressive strength and modulus of elasticity of concrete degraded with increasing temperature; however, material properties of concrete do not degrade at the same rate.

6.2 Property Changes of Prestressing Steel with Elevated Temperatures

As prestressing steel was heated to elevated temperatures, an evident loss in tensile stress occurred at temperatures as low as 400°C (752°F). Exposures of 200°C (392°F) heat did not significantly affect the tensile stress of steel. The duration at which an elevated temperature was held constant may have affected the stress changes, but this was inconclusive based on the limited amount of data available.

The modulus of elasticity of steel appeared to decrease slightly with temperatures above 500°C (932°F), but results indicated that this decrease in the modulus was much smaller in comparison to the tensile stress changes associated with high temperatures.

6.3 Concrete and Prestressing Steel Bond

The bond stresses between concrete and prestressing steel were shown to decrease in a fairly linear trend with exposure to increasing temperatures. The main constituent in the degree of bond stress losses was the maximum temperature of exposure, with few changes in bond behavior occurring due to sustained exposures of elevated temperatures. This indicated that the bond was influenced primarily by the maximum temperature of the exposure of the concrete.

6.4 Thermogravimetric Analysis Techniques

Thermogravimetric analysis (TGA) was shown to be a useful tool in determining an approximate temperature range of heat affected concrete. This was indicated based on analyzing the first-derivative curves of TGA data. The intersection of the curve of a heat affected concrete sample and an unheated concrete sample, indicating similar slope behavior, was shown to be a reasonable approximation of the maximum temperature of heat affected concrete. Future research is encouraged in this area to fully understand and confirm this methodology as a reliable means of detecting temperature gradients through heat exposed concrete.

For more reliable results in future work, it is encouraged to extract and test samples using TGA within the first few days after heat exposure. This would serve as a preventative action to reduce the affects of carbonation of the concrete on results. If samples cannot be tested quickly, an improved storage method should be implemented in order to prevent air from penetrating to the concrete samples prior to performing TGA.

6.5 Recommendations for Future Research

Future research using structural elements, such as beams or columns, would be a logical step toward evaluating the effects of elevated temperatures on prestressed concrete fundamentals. Future researchers could potentially use the information provided by the results of this project to predict failures of prestressed concrete members. Further research could also be performed by using TGA techniques to predict the maximum

temperature exposure of concrete through the use of cored samples. These techniques could be used to further validate the use of TGA techniques in the analyses of heat affected concrete members.

Because few valid results were available for the ultimate stresses of prestressing steel, additional testing should be performed. An increased number of samples should be tested in order to be sure that an adequate number of samples produce valid test results based on the ASTM A370-05 specification. It may also be advantageous to perform additional tests on the modulus of elasticity of the steel to verify the presented results.

APPENDIX

Concrete Casting and Curing Information

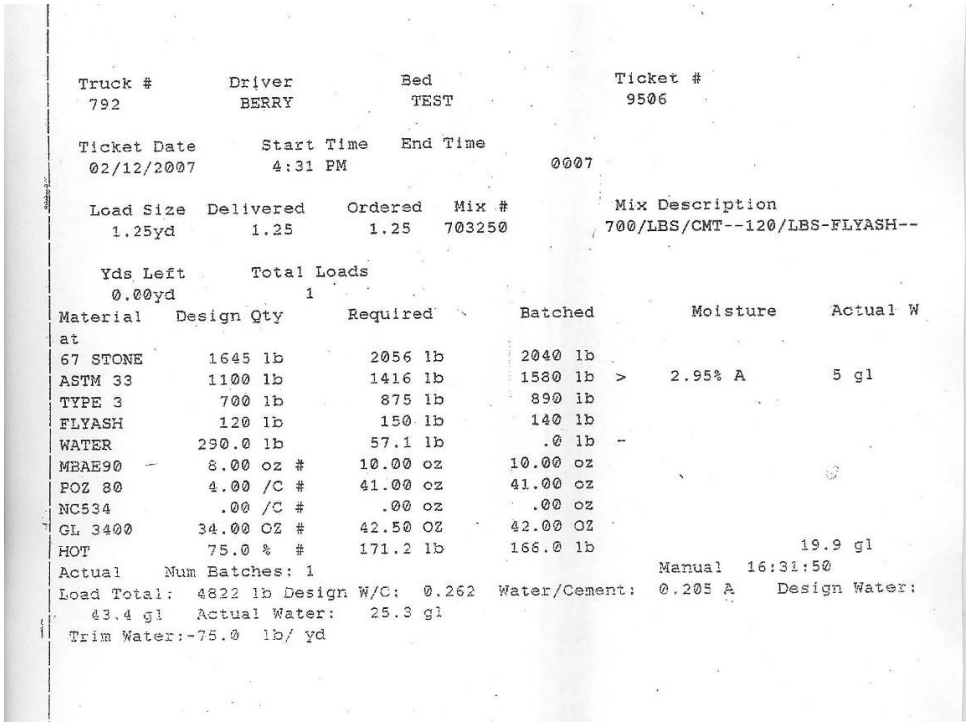

Truck # 792 | Driver BERRY | Bed TEST | Ticket # 9506

Ticket Date 02/12/2007 | Start Time 4:31 PM | End Time | 0007

Load Size 1.25yd | Delivered 1.25 | Ordered 1.25 | Mix # 703250 | Mix Description 700/LBS/CMT--120/LBS-FLYASH--

Yds Left 0.00yd | Total Loads 1

Material	Design Qty	Required	Batched		Moisture	Actual W at
67 STONE	1645 lb	2056 lb	2040 lb			
ASTM 33	1100 lb	1416 lb	1580 lb	>	2.95% A	5 gl
TYPE 3	700 lb	875 lb	890 lb			
FLYASH	120 lb	150 lb	140 lb			
WATER	290.0 lb	57.1 lb	.0 lb	-		
MBAE90	8.00 oz #	10.00 oz	10.00 oz			
POZ 80	4.00 /C #	41.00 oz	41.00 oz			
NC534	.00 /C #	.00 oz	.00 oz			
GL 3400	34.00 OZ #	42.50 OZ	42.00 OZ			
HOT	75.0 % #	171.2 lb	166.0 lb			19.9 gl

Actual Num Batches: 1 | Manual 16:31:50

Load Total: 4822 lb | Design W/C: 0.262 | Water/Cement: 0.205 A | Design Water: 43.4 gl | Actual Water: 25.3 gl

Trim Water:-75.0 lb/ yd

Figure A.1: Copy of mix design ticket from Metromont Corporation.

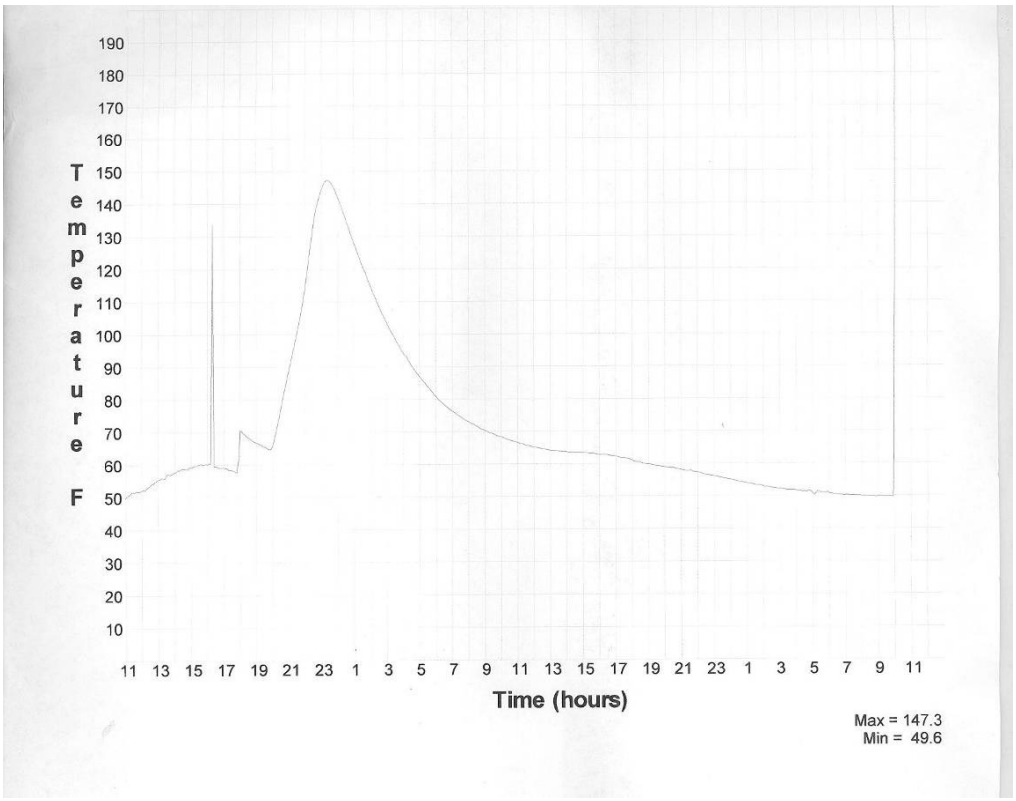

Figure A.2: Internal temperature of concrete cylinder during steam curing process.

REFERENCES

Abrams, M. "Compressive Strength of Concrete at Temperatures of 1600ºF." ACI Publication SP25-2. 1971.

Alarcon-Ruiz, L., G. Platret, E. Massieu, and A. Ehrlacher. "The use of thermal analysis in assessing the effect of temperature on a cement paste." Cement and Concrete Research 35, 2005.

ASTM A370-05. Standard Test Method and Definitions for Mechanical Testing of Steel Products.

ASTM C39/39M -03e1 Standard Test Method for Compressive Strength of Cylindrical Concrete Specimens.

ASTM C469-02e1 Standard Test Method for Static Modulus of Elasticity and Poisson's Ratio of Concrete in Compression.

Castillo, C. and A. Durrani. "Effect of Transient High Temperatures on High-Strength Concrete." ACI Materials Journal. Jan.-Feb. 1990.

Chang, Y., Y. Chen, M. Sheu, and G. Yao. "Residual stress-strain relationship for concrete after exposure to high temperatures." Cement and Concrete Research 36, 2006.

Diederichs, U. and U. Scheider. "Changes in Bond Behavior due to Elevated Temperatures." Bond in Concrete. 1982.

Georgali, B. and P. Tsakiridis. "Microstructure of fire-damaged concrete. A case study." Cement and Concrete Composites 27, 2004.

Harmathy, T. "Determining the Temperature History of Concrete Constructions Following Figure Exposure." ACI Journal. Nov. 1968.

Holmes, M., R. Anchor, G. Cook, and R. Crook. “The effects of elevated temperatures on the strength properties of reinforcing and prestressing steels.” The Structural Engineer. Vol 60B. Mar. 1982.

Khoury, G. “Effect of fire on concrete and concrete structures.” Proj. Struc. Eng. Mater. 2000.

Kose, M., H. Temiz, and H. Binici. “Effects of fire on precast members: A case study.” Engineering Failure Analysis 13, 2006.

Kosmatka, S., B. Kerkhoff, and W. Panarese. Design and Control of Concrete Mixtures, 14th Ed. PCA, 2002.

Matesova, D., D. Bonen, and S. Shah. “Factors affecting the resistance of cementitious materials at high temperatures and medium heating rates.” Materials and Structures. Oct. 2006.

Nawy, E. Prestressed Concrete: A Fundamental Approach, 5th Ed. Upper Saddle River, NJ: 2006.

Neves, I., J. Rodrigues, and A. Loureiro. “Mechanical Properties of Reinforcing and Prestressing Steels after Heating.” Journal of Materials in Civil Engineering. Nov. 1996.

PCI Design Handbook, 6th Ed. 2004.

Phan, L., and N. Carino. “Effects of Test Conditions and Mixture Proportions on Behavior of High-Strength Concrete Exposed to High Temperatures.” ACI Materials Journal. Jan.-Feb. 2002.

Ramachandran, V., R. Paroli, J. Beaudoin, and A. Delgado. Handbook of Thermal Analysis of Construction Materials. Norwich, NY: 2002.

Sagar, H. and F. Rostasy. “The Effects of Elevated Temperatures on the Bond Behavior of Embedded Reinforcing Bars.” Bond in Concrete. 1982.

Shutt, Craig A. “Precast’s Durability Helps Bridges Resist Fire Damage.” PCI ASCENT Spring 2006.

St John, D, A. Poole, and I. Sims. Concrete Petrography, A handbook of investigative techniques. London: 1998.

Royles, R., P. Morley, and M. Khan. “The Behavior of Reinforced Concrete at Elevated Temperatures with Particular Reference to Bond Strength.” Bond in Concrete. 1982.

Villain, G. and G. Platret. “Two Experimental Methods to Determine Carbonation Profiles in Concrete.” ACI Materials Journal. July-Aug. 2006.